UNIVERSITÀ DI PARMA

UNIVERSITA' DEGLI STUDI DI PARMA

DOTTORATO DI RICERCA IN
"Scienze della Terra"

CICLO XXXVII

Modeling transient vegetation effects in slope stability analysis for rainfall-induced shallow landslides: CRITERIA-1D and CRITERIA-3D

Coordinatore:
Chiar.mo Prof. Fabrizio Balsamo

Tutore:
Chiar.mo Prof. Roberto Valentino
Chiar.mo Prof. Marco Bittelli

Dottoranda: Giada Sannino

Anni Accademici 2021/2022 – 2023/2024

UNIVERSITÀ
DI PARMA

Department of Chemistry, Life Sciences and Environmental Sustainability

PhD in Earth Sciences

Modeling transient vegetation effects in slope stability analysis for rainfall-induced shallow landslides: CRITERIA-1D and CRITERIA-3D

Dissertation for the title of Doctor of Philosophy

Candidate:
Giada Sannino

Advisor:
Prof. Roberto Valentino

Coadvisor:
Prof. Marco Bittelli

Cycle XXXVII 2021-2022/2023-2024

Contents

Nomenclature

Abbreviations

AFBM	Analytical Fiber Bundle Model
AUC	Area Under the Curve (ROC curve)
AW	Available Water
CLC	Corine Land Cover
DEM	Digital Elevation Model
ET	Evapotranspiration
FBM	Fiber Bundle Model
FC	SWC at Field Capacity
FoS	Factor of Safety
GDD	Growing Degree Days
GIS	Geographical Information System
HCF	Hydraulic Conductivity Function
HD	Heat Dissipation sensor
IDW	Inverse Distance Weighted
ISM	Infinite Slope Method
ISS	Infinite Slope Scheme
LAI	Leaf Area Index
LEWS	Landslides Early Warning System
LIDAR	Laser Imaging Detection and Ranging
NBS	Nature Based Solution(s)
PBDDM	Physically-Based Deterministic Distributed Model(s)
PBDM	Physically-Based Distributed Model(s)
RBM	Root Bundle Model
RBMw	Root Bundle Model with root-failure Weibull survival function
RMSE	Root Mean Square Error
ROC	Receiver Operating Characteristic
RWU	Root Water Uptake
SAT	SWC at saturation
SQL	Structured Query Language
SWB	Soil Water Balance
SWC	Soil Water Content

SWCC	Soil Water Characteristic Curve
SWRC	Soil Water Retention Curve
TIN	Triangular Irregular Network
TDR	Time-Domain Reflectometer
USCS	Unified Soil Classification System
USDA	United States Department of Agriculture
VWC	Volumetric Water Content
WP	Water Potential
WWM	Wu and Waldron model

Roman letters

a, b	Coefficients of the linear regression between log(LAI) and GDD (LAI curve)
c'	Soil effective cohesion
$\mathbf{C_{4LAI}}$	Specific crop coefficient
$\mathbf{c_r}$	Root cohesion
$\mathbf{C_{tot}}$	Total soil cohesion
E	Actual evaporation
$\mathbf{e_a}$	Average pressure of vapor
$\mathbf{E_{max}}$	Maximum evaporation
$\mathbf{e_s}$	Average pressure of vapor in air saturation
$\mathbf{ET_0}$	Daily/hourly reference evapotranspiration
G	Net heat flow from the ground
$\mathbf{GDD_3}$	Sum of the GDD of the first 3 development phases
$\mathbf{GDD_4}$	Sum of the GDD of the phase 3 and 4 of the vegetation development
$\mathbf{h_e}$	Air-entry value
$\mathbf{H_i}$	Hydraulic potential at the node i
$\mathbf{H_j}$	Hydraulic potential at the node j
$\mathbf{H_{ss}}$	Depth of FoS computation
K, K(H)	Hydraulic Conductivity
$\mathbf{k_c}$	Crop coefficient
$\mathbf{K_{cmax}}$	Maximum crop coefficient
$\mathbf{k_e}$	Extinction factor
$\mathbf{K_{sat}}$	Saturated hydraulic conductivity
KT	Constant for the Hagreaves-Samani equation based on the geographical area
$\mathbf{LAI_{max}}$	Maximum LAI over the year of the considered vegetation
$\mathbf{LAI_{min}}$	Minimum LAI over the year of the considered vegetation
$\mathbf{L_{ij}}$	Distance
n	SWRC fitting parameter
$\mathbf{N_{4LAI}}$	Specific crop coefficient

$\mathbf{m}$	SWRC fitting parameter
$\mathbf{q}$	Water input or output
$\mathbf{q_i}$	Input flux at the i-th node
$\mathbf{R_a}$	Mean extraterrestrial radiation depending on latitude
$\mathbf{RD_0}$	Depth of the shallow soil without roots
$\mathbf{RD_{max}}$	Maximum root depth
$\mathbf{R_n}$	Net hourly solar radiation
$\mathbf{S_c}$	Degree of saturation at air-entry value
$\mathbf{S_e}$	Equivalent degree of saturation
$\mathbf{S_{ij}}$	Interface area between nodes i and j
$\mathbf{T}$	Actual transpiration
$\mathbf{T_{avg}}$	Average hourly air temperature
$\mathbf{TC}$	Turbulence coefficient
$\mathbf{Transp_{max}}$	Maximum transpiration
$\mathbf{T_{max}}$	Maximum daily temperature
$\mathbf{T_{min}}$	Minimum daily temperature
$\mathbf{u}$	Flux density
$\mathbf{(u_a - u_w)}$	Soil water potential (soil suction)
$\mathbf{u_{wind}}$	Hourly average wind speed at 2 meters height
$\mathbf{V_i}$	Amount of stored water in the volume surrounding the node i
$\mathbf{W}$	Total available computational soil volume at a point
$\mathbf{z}$	Computation depth with respect to the slope surface

Greek symbols

α	SWRC fitting parameter
β	Slope angle
γ	Soil unit weight
γ_p	Psychrometric constant
Δ	Slope of the function of saturated vapor
θ	Volumetric Water Content
θ_r	Residual water content at the wilting point
θ_s	Saturated water content
σ^s	Suction stress
τ	SWRC fitting parameter
ϕ'	Soil friction angle
ψ_{leaf}	Leaves suction

List of Figures

List of Tables

Abstract

Instability of natural slopes is a worldwide problem, with an increasing trend in the occurrence of landslides and the associated aggravation of socioeconomic losses. With regard to shallow landslides, phenomena exacerbation is due to extreme rainfall events, which are becoming more frequent because of the global temperature arise. Several attempts to model landslides' occurrence over the years have been done, involving probabilistic, deterministic or hybrid approaches. Statistical-based models need to be trained upon past landslide events for detecting new future occurrences. However, many shallow landslides were recently observed to occur as new activation, and thus their triggering conditions are mainly experienced for the first time. Physically-based models have the potentiality of quantifying the different processes involved during the landslide formation. Therefore, they are particularly suitable for addressing consequences of extreme climatic events. When involving transient hydrological phenomena, these models can reach high levels of accuracy, although they are forced to make simplifications in order to be practically applied. The interest in modeling vegetation effects on both unsaturated soil mechanics and hydrology is relatively recent. Yet, only few models consider the transient reinforcement effects exerted by plants on slopes, as the most common approach in slope stability models is to consider them as static components in the analyses. The aim of this thesis is to explore the effectiveness of modeling transient stability effects induced by vegetation growth and evapotranspiration activity in physically-based deterministic models for shallow landslides. The proposed models, CRITERIA-1D and CRITERIA-3D, are agro-hydrological models developed by the Regional Agency for the Environmental Protection and Energy of Emilia-Romagna region (Arpae-SIMC). In both models a simplified slope stability analysis, based on the infinite slope assumption and on the Factor of Safety computation, has been added. Results show that the proposed methodology is effective in reproducing real case studies at different application scales, and that neglecting vegetation effects in transient hydrology computation can lead to unsatisfactory results.

Chapter 1

Introduction

1.1 General problem

Shallow landslides, although involving relatively small volumes of soil compared with other types of landslides, constitute an hazard because they don't show premonitory signs over territories [1]. Because of these characteristics, it is difficult to develop a proper early warning system for this kind of phenomena [2–4]. On the contrary, for some big landslides that move slower in time, although challenging, techniques based on the field observation of the soil mass movement can be adopted [5–7]. When designing a proper tool for the early detection of shallow landslides, it should be kept in mind that the sliding occurrence is the last step of several hydrological processes [8]. However, landslide hydrology is often simplified in its components, with the aim of deriving alert thresholds that, if overcome, are likely to trigger new landslides [9]. Through this approach, which is widely used for applications on large areas, detailed information about local triggering conditions are inevitably lost. More particularly, although classic soil mechanics has been based on saturated condition since its early starts, nowadays it is accepted that unsaturated conditions are of interest, especially if non-stationary landslide processes need to be assessed at high spatial detail [10–12]. In relation to dynamic modeling of landslide occurrences, physically-based modeling has achieved the ability of comprising several processes maintaining acceptable running times. The potentiality of involving physically-based approach instead of statistical based models in landslides' detection is that the singular processes can be quantified, so that when a certain rainfall amount is expected, it can be detected when and where the landslides are about to occur [13]. The detail level reached by these models depends on the input resolution, especially on the Digital Elevation Model, as the computational

mesh is normally defined through it [14].
Under climate change forcing, extreme meteorological conditions are been experiencing more frequently with respect to the last decades [15]. Some recently occurred rainfall events have a very high returning period, far surpassing hundreds of years [16]. In these conditions, physically-based models still represent valuable tools, as they don't need observed conditions to be trained. Although in the last years the scientific community attention seemed to be more focused on probabilistic approaches [17], especially because of the spread of Artificial Intelligence techniques used for treating the unavoidable uncertainties of applications over large areas, the development of models based on classic physics approaches should not be abandoned. More particularly, some aspects have still been only partially explored in shallow landslides' prediction, so it is worthy to advance further.
As an example, even when adopting the most common simplified approach for stability analyses, which is the infinite slope scheme [18–20], the effects of vegetation on slope stability, especially under unsaturated regime, are still controversial and rarely considered [21, 22]. Dealing with vegetation modeling is highly complex as most of our knowledge is based on empirical modeling of, for example, roots behavior and canopies development [23]. Having field measurement in near-real time of vegetation aspects is complex, and, in fact, most of the actual physically-based models involving vegetation reinforcement effects adopt stationary quantities. Nonetheless, vegetation is a dynamic being and its effect on the surroundings is highly variable, both in space and time, and at the actual knowledge, accounting for its variability is quite complicated [24]. However, with the appropriate simplifications, the transient modeling of vegetation effects is accountable for in slope stability analyses. This thesis intends to explore the effectiveness of including transient vegetation effects on slope stability analysis for rainfall-induced shallow landslides.

1.2 Aim of the work

The overall aim of the project is exploring the potentiality of involving transient modeling of vegetation effects on slope stability analysis at different scales. In fact, through an agro-hydrological model, the possibility of linking the development of canopies and evapotranspiration activity to real meteorological data was used within the infinite slope framework for deriving the factor of safety. The implicit assumption is that plants modify the soil water balance in terms of water potential - hereinafter intended as physically equivalent to soil suction -, which in turn affects the soil shear strength in

partially saturated conditions. The scope of the work has been divided into three main objectives:

- Developing and applying the complete agro-hydro-mechanical model in the unidimensional domain (CRITERIA-1D). Through the validation of the model on one representative point of a test slope where soil moisture and water potential sensors are installed, the potentiality of considering hydrological effects exerted by vegetation with respect to a bare soil has been assessed (Chapter 3);

- Developing the complete model in the three-dimensional domain (CRITERIA-3D) and validating it at the same test slope considered in the previous step (CRITERIA-1D) but using data of the entire slope, in order to assess if the proposed approach is effective for predicting shallow landslide occurrences in time and space (Chapter 4);

- Applying the CRITERIA-3D model to a large area, selected among those hit by an extreme climatic event occurred in Emilia-Romagna region in May 2023, in order to explore the potentiality of the model as a territorial predictive tool based on available data (Chapter 5).

The test site used for the validation of both CRITERIA-1D and CRITERIA-3D is located in Oltrepò Pavese, Northern Apennines, in an area particularly susceptible to rainfall-induced shallow landslides. The test area is called Montuè, and comprises an experimental slope where a monitoring station and sensors to measure soil moisture and water potential are installed. Instead, the large test area has been selected around the town of Monteleone, Roncofreddo municipality (FC), in the Romagna area.

1.3 Organization of the dissertation

The dissertation has the following organization. In Chapter 2 the state of the art about deterministic physically-based modeling of shallow landslides is presented. The chapter is constituted by a review paper published in an international scientific journal. In the chapter, the focus is on deterministic models that include approaches for considering the vegetation effects on slope stability. In Chapter 3 the development and validation of CRITERIA-1D is presented, followed by Chapter 4, where the CRITERIA-3D model is presented. Both chapters are constituted by research papers, although only the one related to CRITERIA-1D has been already published. In Chapter 5 results related to the application of the CRITERIA-3D model on a wide area

is shown. Finally, Chapter 6 provides final considerations and comments on limitations and future developments of the proposed models.

Chapter 2

Deterministic Physically Based Distributed Models for Rainfall-Induced Shallow Landslides

This paper has been published in *Geosciences* journal on 27 September 2024.
Reference: **Sannino, G.**, Bordoni, M., Bittelli, M., Meisina, C., Tomei, F., & Valentino, R. (2024). Deterministic Physically Based Distributed Models for Rainfall-Induced Shallow Landslides. Geosciences, 14(10), 255.
doi: https://doi.org/10.3390/geosciences14100255 [17]

Abstract Facing global warming's consequences is a major issue in the present times. Regarding the climate, projections say that heavy rainfalls are going to increase with high probability together with temperature rise; thus, the hazard related to rainfall-induced shallow landslides will likely increase in density over susceptible territories. Different modeling approaches exist, and many of them are forced to make simplifications in order to reproduce landslide occurrences over space and time. Process-based models can help in quantifying the consequences of heavy rainfall in terms of slope instability at a territory scale. In this study, a narrative review of physically based deterministic distributed models (PBDDMs) is presented. Models were selected based on the adoption of the infinite slope scheme (ISS), the use of a deterministic approach (i.e., input and output are treated as absolute values), and the inclusion of new approaches in modeling slope stability through the ISS. The models are presented in chronological order with the aim of drawing a timeline of the evolution of PBDDMs and providing researchers and practitioners with basic knowledge of what scholars have proposed so far.

The results indicate that including vegetation's effects on slope stability has raised in importance over time but that there is still a need to find an efficient way to include them. In recent years, the literature production seems to be more focused on probabilistic approaches.

2.1 Introduction

Among landslides, those involving shallow soil (up to a 2–3 m depth) are most frequently induced by rainfall and are highly dangerous, as no premonitory signs are present over territories [1]. The landslide occurrence is the final step of a chain of processes that starts with rainfall infiltration and leads to slope collapse [25]. Therefore, a tool including process quantification to prepare for potential landslide hazards is necessary, especially under climate change conditions; in fact, the temperature rise will allow the atmosphere to hold more moisture so that a greater magnitude of heavy rainfall will likely occur [26]. However, little is known about the effects of climate and its variation on slope stability, landslides, landslide hazards, and the related risk of climate change [27]. Rainfall is recognized as the major shallow landslide triggering factor [28], and over time, different techniques have been employed to predict rainfall-induced shallow landslides in order to constitute Landslide Early Warning System (LEWS) tools [3]. To model landslide occurrences, two main approaches are recognized: physically based modeling and statistical modeling. These models can help in assessing not only the landslide susceptibility of large areas but also the related hazard, which is defined as the detection of the triggering time of a landslide (i.e., "when" or "how frequently" will occur) [29]. Physically based models are also referred to as process-based models, while statistical approaches are further named "data-driven models" as they use past events data based on the assumption that environmental conditions leading to landslides in the past are likely to provoke new instability phenomena in the future [30]. Although they represent interesting techniques for large scale susceptibility analysis, they highly depend on the resolution of past landslides inventories, which can propagate high levels of uncertainty to the outputs if they are not sufficiently detailed. Moreover, under climate change conditions, data-driven approaches have to be undertaken carefully since new environmental and meteorological conditions may not be represented by the past [31]. The use of physical–mathematical models has recently gained large consensus among engineers and the scientific community, not only for applications at the local or slope scale but also at larger extensions, as they can take into account the dynamic variability of the system [32]. Physically based model applications

over large areas are also supported by remote sensing, which allows extensive observation of landslides, especially where it would not be possible with ground-based techniques, thus providing robust landslide inventories upon which model output accuracy can be assessed [33–36]. Whether the aim is to design emergency plans to warn people or inform policy makers about the consequences of extreme climatic events, physically based distributed models represent valid tools as they can detect landslide occurrences in advance. When dealing with future landslide prediction and climate change impacts on slope stability, this modeling approach is considerably noteworthy, especially when vegetation presence is considered [37], thanks to the possibility of assessing single aspects' contribution to the overall stability. Physically based deterministic distributed models (PBDDMs) adopt deterministic approaches for both input and output and can be used to back-analyze real landslides in order to derive soil hydraulic and geotechnical parameters. Deterministic models can be highly sensitive to the input parameters' variability. To reduce uncertainty in assigning unknown soil parameters, some physical models include probabilistic treatments of input data or are coupled with other approaches to obtain probability maps of failure as outputs, e.g., [38]. When developing new models for shallow landslide detection, the processes to consider must be decided. Normally, PBDDMs for shallow landslide prediction are composed of a hydrological module interfaced with a geotechnical module, typically based on the estimation of the slope safety factor through the limit equilibrium method, as it is less computationally demanding than finite element numerical methods, which are often not practically useable over large areas [39]. At the same time, the hydrological processes involved in landslide initiation are many, and including all of them in a single model would make it impossible to run in a reasonable computational time. Because of this complexity, the majority of the existing models that consider hydrological aspects in detail tend to simplify the mechanical aspects. The simplified approach based on the infinite slope scheme (ISS) is adopted in the majority of PBDDMs for rainfall-induced shallow landslides. In this approach, the assumption of a planar failure geometry is considered consistent with the shape, size, and failure mechanisms of rainfall-induced shallow landslides, although this assumption has some applicability limitations [19]. In recent years, models including antecedent hydrological information have raised importance in landslide hazard assessment [40], and including vegetation-related processes has become fundamental in shallow landslides' prediction. This is because canopies and roots modify the stability condition of slopes under both hydrological and mechanical viewpoints [22, 41, 42]. The rooted portion of soil has peculiar characteristics, and its behavior, together with proper consideration of unsaturated soil mechanics, should be taken into account in shallow land-

slide prediction. Furthermore, the interest in nature-based solutions (NBSs) and bioengineering techniques has raised the importance of preventing landslides over territories, not only because of environmental purposes but also because of economic aspects [21, 43, 44]. Quantitatively assessing the role of vegetation on slope stability is of importance, although a comprehensive methodology is still lacking [23]. In this work, a non-systematic narrative review of the main physically based deterministic distributed models developed over time is presented, highlighting which aspects or techniques were used and introduced over time by the different models. The review is restricted to the models that adopt the infinite slope scheme and are based on the limit equilibrium method. The aim is to draw a chronological memory of rainfall-induced shallow landslides deterministic modeling and also to address new research efforts in directions that have not yet been explored. This paper is organized as follows. In the second section, a brief discussion of shallow landslide modeling methods is presented, stretching some conceptual aspects of hydrology and plants' contribution. The third section presents the materials and methods adopted for this work, while the fourth section describes the selected models in detail. It was chosen to include only models that do not use any kind of probabilistic approach. This choice is meant to be helpful for practitioners and non-academic, but also for new researchers, in order to classify physically based models for rainfall-induced shallow landslides into two different groups: "purely" physically based deterministic distributed models (PBDDMs), i.e., the specific topic of this review, and hybrid forms. In the end, a conclusive section considers aspects that still have to be properly explored in PBDDMs. Some suggestions are also provided.

2.2 Shallow Landslide Modeling Methods

2.2.1 Hydrology

As already mentioned, the majority of the existing PBDDMs for rainfall-induced shallow landslides prediction are composed of two interfaced modules: one computes the hydrological phenomena, and the other computes the slope stability. A recognized mechanism for shallow landslide activation is the rapid formation of nil or positive pore water pressure because of soil saturation [10, 45, 46]. Saturated lenses develop in response to rainfall events because of infiltration and seepage processes, and they can trigger landslides when enlarged enough. Water can accumulate in the soil because of the presence of an impermeable or low-permeability layer, either during vertical downward seepage or upward movements [47]. Some landslides can

then completely or partially mobilize into destructive earth flows because of liquefaction [48–51] while others only translate the detached material up to a certain distance. Because of these observations, the first slope stability models were developed based on saturated soil conditions [52]. Under saturation conditions, soil properties and hydrological parameters can be assumed as constant, and the role of matric suction (i.e., negative pore water pressure) is neglected. Real meteorological conditions can even be ignored in models based on saturated soil mechanics. In the most simplified cases where the soil is considered to be partially saturated, real rainfall amounts are considered as contributing to the uprising of a pre-existing groundwater table. Some limitations of these simplified approaches have been recognized, and practical applications related to slope stability problems also involve unsaturated soil mechanics [53]. In fact, since shallow landslides have been observed to occur even under negative pore water pressure, i.e., when the soil is in partially saturated condition [54, 55], it is important to consider the evolution in time of pore-water pressures and unsaturated soil mechanics in PBDDMs. Unsaturated soil mechanics are normally based on non-linear soil property functions, including the constitutive relationship between soil water content and soil suction (also defined as the water potential or hydraulic head), namely, the Soil Water Retention Curve (SWRC, or Soil Water Characteristic Curve, SWCC), and the one that relates soil suction or soil water content to soil hydraulic conductivity, namely, the Hydraulic Conductivity Function (HCF) [56, 57]. The relationships are unique for a certain pore size distribution of soil and are empirically defined. However, because of hysteretic behavior, these properties follow different patterns during wetting or drying phases [58]. Also, the presence of vegetation was demonstrated to alter the pore size distribution because of root growth, leading to an evolution of the SWRC and of the soil permeability over time with respect to SWRC or HCF of bare soil [59]. When considering unsaturated conditions, transient or stationary input rainfall can be assumed for hydrological balance computation, and water movements can be assessed through a transient analysis. The most commonly used approach to determine the transient values of soil water content is the use of partial differential equations—in particular, numerical solutions of Richards' equation for unsaturated seepage process [60, 61] at different spatial domains (i.e., 1-D, 2-D, or 3-D). This approach allows to consideration of different hydrological processes into a single balance equation, although in the 3-D domain, its computation over large areas can be consuming both in terms of energy and time [62]. When dealing with rainfall-induced landslide hydrology, several processes should be quantified. In any case, the major water input is represented by rainfall infiltration, which enters the soil matrix and undergoes gradient and gravity-driven movements.

Then, subsurface flows and redistribution processes take place, and soil hydraulic conductivity anisotropy should be considered [63]. In most cases, different hydraulic behaviors are only considered along soil vertical directions [64]. When a numerical problem is involved, it is essential to properly define boundary conditions, that is, defining how the considered physical system acts at the borders of its spatial and temporal domains [65]. As already mentioned, defining the antecedent condition of soil moisture prior to rainfall is fundamental to correctly simulate water movements during a precipitation event [66]. The global soil water balance equation should be solved for a certain time span, which should be antecedent with respect to the period of interest, in order to assess consistent soil moisture as an initial condition. In this sense, as a key hydrological process, plant growth and evapotranspiration activity should not be neglected [67]. In fact, vegetation alters the soil water content through different mechanisms, including the absorption of water over the rooted portion of the soil; the modification of SWRC; and parameters such as the saturated hydraulic conductivity, canopy rainfall interception, and the creation of preferential flow patterns through roots and stems. This latter aspect is very difficult to consider simultaneously with matrix flow equations if the model allows the consideration of two different domains at the same time [68]. Although preferential flow paths can have different natures and can originate in different ways, any of them is replicable by models based on matrix flow equations only if approaches such as dual-permeability (or double porosity) are adopted [69, 70]. Notwithstanding the effectiveness of Richards' equation in soil water balance computation, this approach may not be the most efficient in specific cases. For example, when a landslide is triggered because of an in-depth wetting front propagation, the hydrological mechanisms can be approximated through simplified approaches for infiltration (e.g., [71, 72].

2.2.2 Slope Stability

With regard to the geotechnical modules of PBDDMs, the most commonly used approach for slope stability is the computation of a Factor of Safety (FoS). This approach is based on the limit equilibrium method and considers the relation between stabilizing and destabilizing actions on a slope. When the FoS is equal to 1, the slope is in a critical equilibrium state; as the FoS drops below 1, the entire slope is estimated as unstable. Several methods to compute FoS exist [73]. In a general sense, FoS is computed over one or more potential failure surfaces in order to detect under which conditions and/or at which depth the landslide is triggered. PBDDMs should adopt an automatic procedure for analyzing different slip surfaces, especially when

the soil strength and pressure profiles differ along with depth and the model can consider multi-layered soils with different parametrization. Since shallow landslides are normally translational and their length/depth ratio is generally low, the infinite slope method (ISM), which assumes a ground-parallel planar failure surface, represents the most commonly used approach, although it has limitations [19]. Among others, Lu and Godt developed an equation for FoS that allows the classic saturated soil mechanics theory based on the effective stress concept to be easily extended to the unsaturated regime [74]. However, models that aim to simulate rotational movement also exist, as well as models that can approximate the landslide runout [75]. It is known that vegetation contributes to soil reinforcement in different ways and at different spatial scales [76,77]. With regard to plant roots, it is known that the rooting system can extend the soil shear strength either through water absorption or mechanical reinforcement, normally quantified as an additional cohesive term extending the soil's effective cohesion [78] and normally applied on the sliding surface. The mechanical reinforcement seems to be more effective in the shallower portion of the soil with respect to the hydrological reinforcement, which is effective down to a 1–2 m depth [79]. More in detail, the mechanical improvement in soil shear strength is exerted through the root network tensile strength and its interaction with soil and bedrock anchoring, as well as the ability of roots to cross the slip surface [80]. Both large and fine roots contribute to the global exerted reinforcement [81]. The overall root cohesion can be derived through different methods, namely, the Wu and Waldron model (WWM), the Fiber Bundle Model (FBM), the Analytical Fiber Bundle Model (AFBM), the Root Bundle Model (RBM), and the root bundle model with root-failure Weibull survival function (RBMw) [21, 82–87]. The root reinforcement can be either basal or lateral when applied at the base of a failure plane or on the lateral sides of the landslide body, respectively. Nevertheless, in soil conditions close to saturation, it is not totally clear if these effects are still present or not [76, 77]. Few of the existing models consider the real spatial variability of root distribution to assess the root reinforcement [88], even if the vegetation stand characteristics affect the magnitude of stabilization effects, especially if gaps are present [89]. PBDDMs can be applied at the slope scale, basin scale, or regional scale. In the first case, it may be possible to carry on field campaigns to obtain specific soil hydraulic and geotechnical parameters. In the second case, especially when the analyzed area is larger than a single slope or a small catchment, field work can become very expensive, and assigning reliable soil parameters can be challenging. For models that do not involve probabilistic approaches, parameters can be assigned based on texture or pedotransfer functions applied to geological units if extended field campaign data are not available [90].

2.3 Materials and Methods

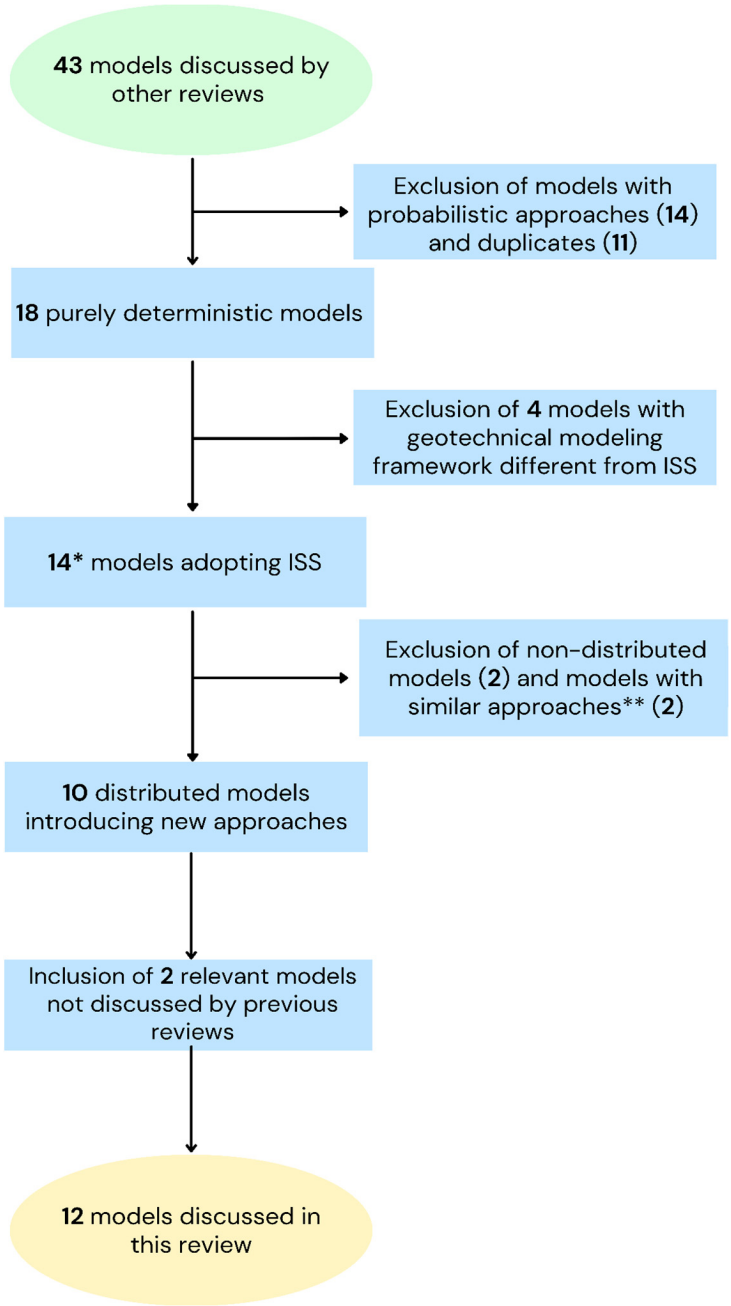

Figure 2.1: Flow chart of the methodology. * One of the reviewed models, SOSlope, uses the Discrete Element Method, but the ISS was adopted for the geometry definition. ** With "similar approaches", it is intended that the model was extending its previous version.

This study builds upon previous review papers such as [21,22,91] and follows a non-systematic approach, mainly focusing on chronology and some specific aspects of different models. The flow chart of the methodology is represented in Figure 1. A total of 43 models considered by other reviews were screened, and only 18 were detected as "purely deterministic". A total of 11 duplicates considered by more than one review were removed, while other 13 models presented some probabilistic approaches, and then they were removed. The resulting 18 deterministic models were analyzed, and 4 of them were discarded as they do not use the infinite slope scheme (ISS) as geotechnical model. In the last screening step, 2 models were removed because they were originally presented as non-distributed models, and 2 models considered by other reviews were an extension of a pre-existing model. The models which constitute extension of their previous version were, however, cited in the following section.

2.4 Discussion on Models

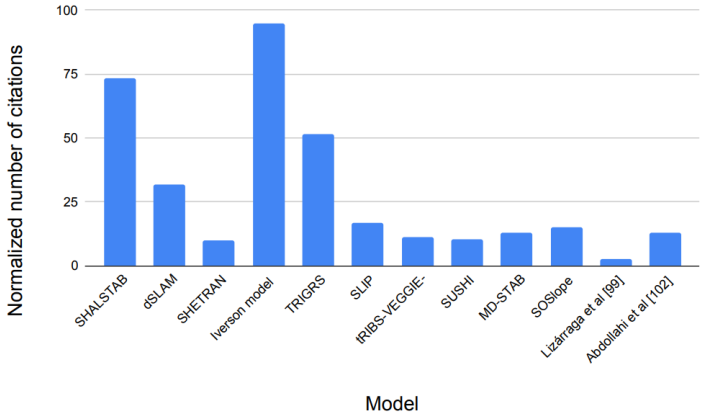

Figure 2.2: PBDDMs' normalized number of citations obtained (derived by Google Scholar). Models are in chronological order.

The 12 selected models are discussed in detail. SHALSTAB [92] is one of the first GIS-based PBDDMs published in 1994. It computes slope stability for cohesionless soils over an infinite slope under a steady-state flow condition, and it is intended to be used with ESRI-ArcGIS. By assuming a steady saturated flow, the model is able to calculate the rainfall amount that is necessary to trigger a landslide over a specified area using a contour-based Digital Elevation Model (DEM) methodology. Its output is an estimation of the critical saturated soil height computed through a hydrological model

called TOPOG [93]. The model neglects the effects of the degree of saturation in the vadose zone. Because of its structure and mathematical formulations, SHALSTAB is not suitable to forecast the timing of landslide triggering. In 1995, the dSLAM model was published [94]. The model aims to quantify the slope instability in steep and forested areas. With dSLAM, the mechanical root reinforcement is introduced in PBDDMs for shallow landslides, while hydraulic vegetation effects are ignored. The model is designed for translational slide overlying a lithic contact. dSLAM is a contour-based model and does not account for rainfall spatial distribution. The mechanical root reinforcement is considered a constant additive term to the overall soil cohesion. Hydrology is based on a kinematic wave groundwater model [95], and it can be run either with actual hyetographs or long-term sequences of precipitation. The authors demonstrate that the spatial distribution of slope instability is controlled by topography and forest harvesting. During major rainstorms, groundwater flow greately affects the factor of safety. In 1998, the SHETRAN model was extended with a shallow landslide erosion and sediment yield component [96, 97]. It is a basin-scale model that considers spatial variability of rainfall input and hydrological responses. It considers snowmelt as a triggering factor as well. The model computes the landslides' impact on sediment yields at the basin outlet, deriving the volume of dislocated material. Two levels of resolution are comprised: first, a finer spatial assessment of shallow landslide susceptibility is carried out, and a critical soil saturation condition is obtained through GISLIP, a GIS analysis tool; subsequently, a time-varying simulation based on the hydrological grid-based physical SHE model [98] is conducted at a coarser resolution, at which the geotechnical stability analysis also is conducted Therefore, the model can be computationally sustainable for basin-scale simulations (areas around 500 km2). The SHE model comprises evapotranspiration activity and canopy interception. In 2000, Iverson proposed a model intending to assess the effects of transient rainfall on the timing, rates, and locations of landslides [99]. The hydrology is computed considering the soil infiltration capacity equal to the saturated hydraulic conductivity in order to derive analytical values of the pressure head, assuming a pre-existing steady-state pore pressure. The aim of the model is to derive rainfall thresholds for triggering shallow landslides, corresponding to the peak value of pore pressure, by deriving transient pore pressure distributions that are added to the pre-existing one. Although a simplified transient analysis is included, Iverson's model is better suitable for shallow landslides related to short-duration rainfall (from approximately 1 h to 70 h), as the model neglects lateral water flow [100]. The model also derives post-failure motion. TRIGRS [101] is a grid-based PBDDM that aims at locating the timing and size of landslides. At the time, most of the

landslide prediction models were producing only susceptibility maps, not involving a complete transient and distributed analysis. In its first version, TRIGRS solves on a pixel-by-pixel basis the one-dimensional vertical version of Richards' equation by [102], assuming differentiated bare soil areas, which are characterized by a unique homogeneous isotropic layer. In general, TRIGRS is the most commonly used PBDDM for shallow landslides at the regional scale, even if no graphical interface is provided. Its use is linked to a Geographical Information System (GIS), where input data can be prepared and outputs can be visualized. Many versions of TRIGRS have been developed over time, including the unsaturated version, the accounting of a vegetation effect [103], and a parallelized version [104]. TRIGRS provides the minimum Factor of Safety (FoS) calculated at selected time steps of a rainstorm, the pore water pressures, and the depth of the minimum FoS at a certain time step. The soil is described by a SWRC. The unique consideration of 1-D water movements, although accurate under certain conditions, is not appropriate when complex topography is present over a large area. Moreover, the input DEM spatial resolution seems to strongly affect the results [14]. In the same year, 2008, the SLIP model was developed [105, 106]. It is a PBDDM that adopts a simplified hydrological approach to simulate soil water balance, assuming that the saturated portion of the soil increases because of infiltrating rainfall. At the same time, the soil desaturates through a percolation process. To be quickly applied to large areas with low computational effort, the model avoids the need to be provided with complex hydrological formulation and approximates a transient seepage computation. In its recent version, the SLIP model also includes a simplified approach for plant interception and root cohesion, changing the model into G-SLIP [107]. SLIP represents a valid example of a simplified although effective solution for Early Warning Systems over large areas, which is an urgent need due to climate change. In 2011, the SUSHI model was proposed by Capparelli and Versace [108]. It describes water movements in a bi-dimensional domain, allowing the consideration of irregular soil stratigraphy and different soil parameters. A 2-D Richards' equation is involved in the model, following the assumption of isotropic soil through the adoption of a specific "capillarity coefficient". This coefficient represents the rate at which water is absorbed or released because of pressure head changes in the soil. A fully implicit method and the finite difference method are employed for hydrology computation in the SUSHI model. Evapotranspiration is accounted for by adopting a uniform root distribution and deriving a sink transpiration term. The vegetation is modeled considering a fixed Leaf Area Index value (LAI) throughout the year. In 2013, Lepore et al. [109] published a model called tRIBS-VEGGIE-Landslide, then modified by Arnone et al. [110] in 2016 to

include probabilistic treatment of uncertainties. The methodology is based on a Triangular Irregular Network (TIN) mesh and accounts for post-failure movement by considering selected slope angles as thresholds for determining whether the landslide body will move down to a run-out distance. Landslide movement is assumed to follow the same flow directions evaluated by the tRIBS hydrological component (the deepest descend), which is based on a transient computation of infiltration and redistribution processes. The basin morphology can be modified by landslide deposits, with consequent impact on most of the simulated processes. Concerning vegetation, the model considers root mechanical reinforcement together with general soil cohesion, while the transpiration is estimated through the methodology provided by [111], which is based on vapor pressure deficit, soil moisture levels, rooting profile, leaf area, and available energy. In 2014, Milledge et al. [112] pointed out that the existing models were highly computationally demanding and were not practically applicable across landscapes. The proposed model, called MD-STAB, simulates lateral resistances acting on landslide margins using earth pressure theory and the lateral root distribution, which is modeled as an exponential function of soil depth in a three-dimensional limit equilibrium force balance. This assumption allows the model to consider roots that laterally cross the shearing surfaces. The possibility of considering forces that act on the lateral sides of rigid blocks contradicts the infinite slope assumption, for which the inter-slice interactions are ignored. This model has also been extended, including the derivation of root reinforcement from field-measured forest stand characteristics [113]. The model ignores infiltration, soil suction, and capillary rises, and the groundwater level is steady and parallel to the slope surface. In 2017, SOSlope was published by Cohen and Schwarz [114]. The model focuses on the effect of root and soil strength on slope stability in forests, accounting for single-tree contribution. The hydrological aspects are considered through a simplified and empirical dual-porosity model. Through this approach, SOSlope can approximate the water dynamics in both the soil matrix and the preferential flow domains. The model is suitable for assessing fundamental aspects such as the role of the forest structure (e.g., tree size, tree spacing), root distribution, and root mechanical properties on the triggering mechanisms of shallow landslides. SOSlope considers both lateral and basal root reinforcement and is able to reproduce the self-organized redistribution of forces on a slope during rainfall triggered shallow landslides. The model is particularly suitable for highly detailed forest management purposes, and outputs can be used in GIS environments. Lizàrraga and Buscarnera, in 2018, developed a model that uses suction-dependent plasticity and limit equilibrium theories to derive the slope Factor of Safety (FoS) in unsaturated soils [115,116]. The model considers mechanical aspects usually not included

in other models, such as suction-hardening and liquefaction potential [117]. The aim is to simultaneously quantify the susceptibility to frictional slips and liquefaction-induced flow slides of shallow soil slopes in order to incorporate these considerations in regional-scale landslide hazard mapping. The underlying hydrology is a transient computation based on Richards' equation. Laboratory data are used to determine input parameters. The model application points out the strong interplay between infiltration mechanisms (i.e., slow or fast) and the mode and depth of slope instability. Vegetation effects are neglected. In 2023, Abdollhai et al. [118] proposed a model specifically designed for the estimation of hillslope post-wildfire stability against rainfall-induced landslides. The proposed model constitutes a physically based yet practical slope stability framework capable of capturing the interplay of key driving factors and wildfire-induced alterations. The aim is to derive post-wildfire temporal changes in the Factor of Safety in response to rainfall. The transient hydrological analysis is conducted through an analytical approximation of 1D Richards' equation. The soil is considered isotropic and homogeneous. Changes in saturated soil water content are determined as a function of the soil elastic modulus, and the method proposed by [119] is then used to derive saturated water content in deformable soils. The post-wildfire effects on vegetation are quantified as a reduction in the transpiration rate due to the decrease in the number of roots. The infiltration capacity is also affected by wildfire, although in the first application, the authors decided not to account for it. Figure 2 reports the normalized number of citations of the different considered models. The normalized number of citations is calculated as the ratio between the total number of citations (as derived by Google Scholar) and the number of years since publication (i.e., the difference between the current year—2024—and the year of publication). It can be seen that the most cited models are the Iverson model, SHALSTAB, and TRIGRS. Out of them, only the dSLAM model has a normalized citation number higher than 25. These four models can thus be considered as milestones of PBDDM knowledge and development over time. Table 2.1 summarizes some features of the 12 analyzed models. Notwithstanding the adoption of the infinite slope scheme, the hydrology modules, as highlighted, show that the use of the 1D Richards equation in deterministic models for shallow landslides is the most commonly used method.

Table 2.1: A summary of the 12 selected models. * The columns "Country of application" and "Real case study" refer to the related cited paper in this review. "WWM" stands for "Wu and Waldron root reinforcement model"; "AFBM" stands for "Analytical Fiber Bundle Model" for root reinforcement.

Model	Country of Application *	Real Case Study	Hydrology	Vegetation
SHALSTAB [92]	United States	Tennessee Valley (colluvial soils), Mettman Ridge (colluvial soils), Split Creek (silty sands)	Derivation of the critical saturated soil height through TOPOG [93]	-
dSLAM [94]	United States	Cedar Creek basin, Oregon Coast Range (real landslides not well documented)	Kinematic wave groundwater model [95]	Mechanical basal root reinforcement (WWM) as constant C_r
SHETRAN [96]	United Kingdom of Great Britain, Northern Ireland	Kirkton research catchment in Balquhidder, Scotland (real landslides not well documented)	Lateral flow: Boussinesq equation; Vertical flow: 1D Richards' equation; snowmelt	ET, interception, spatially variable land use
Iverson [99]	-	-	Reduced form of Richards' equation	-
TRIGRS [101]	-	-	Richards' equation per [102]	Extension by [103] comprises root cohesion and tree surcharge
SLIP [106]	Italy	Different areas of Italy	Increase in the saturated portion of the soil with rainfall	Extension by [107] comprises interception and root cohesion
SUSHI [108]	Italy	May 1998 Sarno landslides on pyroclastic soils from Campania (Italy)	1D Richards' equation (Hydro-SUSHI module)	ET as function of LAI, interception
tRIBS-VEGGIE-Landslide [109]	Puerto Rico	Luquillo forest (Puerto Rico)- no real landslides	Hydrological effects: transpiration [111], evaporation reduction by canopies; vegetation variable with time, space, and depth (root distribution and root water uptake); root cohesion	
MD-STAB [112]	United States	November 1996, Coos Bay, Mettnam ridge debris flow (gravelly sand)	Hydrostatic condition	Only mechanical reinforcement: basal and lateral, variable with depth
SOSlope [114]	-	-	Macropore water pressure and matrix suction	Mechanical lateral root reinforcement (RBM)
Lizárraga et al. [115]	Italy	May 1998 landslides on pyroclastic soils from Campania (Italy)	Authors used TRIGRS to compute hydrology	-
Abdollahi et al. [118]	United States	2019 Las Lomas watershed (California) shallow landslide (sandy loam and loam soils)	1D Richards' equation	ET Mechanical basal root reinforcement (AFBM)

2.5 Discussion and conclusions

Based on the publishing date, several models were described in this narrative review, trying to draw a comprehensive overview of physically based deterministic models for shallow landslides. By analyzing the literature, purely deterministic approaches appear to have recently become less explored than they were in recent decades. However, it appears clear that the attention given to the stabilizing effects of vegetation has grown over the years, as testified by the rising complexity involved when trying to assess these effects in a consistent way. Big challenges are still open about this topic since most of the root reinforcement models are based on variables and parameters not easily derivable such as root architecture or root diameters. Most of the root reinforcement models have a strong empirical basis that is not easily applicable at large scale, particularly when different kinds of plant species cohabit [120]. New paradigms and expedients should be explored for root effect quantification over large areas, and purely deterministic models can help in this task, as the processes and the related parameters can be quantified and studied singularly in a specific way. An example is provided by [121], where root-induced modifications of soil hydraulic properties (namely, the saturated hydraulic conductivity and the Soil Water Retention Curve) are included in a physically based model. From this point of view, involving vegetation as a dynamic variable, accounting for growing over time and the space of roots and canopy, based on real meteorological data and intraseasonal dynamic variability, can improve the performance of slope stability models [122, 123]. More studies based on remote sensing linking canopy development with root architectures, rooting depth, and root spatial extensions could help in applying root development and reinforcement models over large areas, as vegetation parameters can be more easily derived when related to aboveground biomass [78]. On the contrary, non-invasive techniques for estimating roots' morphometric characteristics are still difficult to use. An important aspect that constitutes a strong point since the first PBDMs were published is the interoperability with GIS environments. This aspect can help decision makers to cross different sources of information about territories. As it is difficult to have a unique, comprehensive PBDDM for all the processes that should be accounted for in landslide hazard assessment, overlaying different model outputs or different spatial information can provide more insights on a large scale. In fact, it should not be overlooked that PBDDMs pretend to give a single, specific output based on single, selected input parameters that may not represent reality, especially when large periods are considered. Comparing different sources of information through pre- or post-processing techniques and procedures may help raise the reliability

of landslide risk assessment analyses, maintaining an acceptable operational time. In distributed models, sensitivity analysis to different DEM (or mesh) spatial resolutions should be included. It is known that accuracy changes according to the considered spatial resolution, either when computing hydrological phenomena or slope stability, especially when this latter is based on the infinite slope method. This aspect appears not properly considered when new models are developed, although the problem is crucial for proper application of the model itself. In fact, spatial discretization of the domain can lead to different results. Although rarely discussed when new models are developed, an important aspect for practical applications is the required running time of the different algorithms at the scale of interest. This problem is crucial, especially if the model should be used in early warning systems for civil protection purposes at the regional scale. It is worth remembering that a very important expedient to overcome the spatial uncertainty of parameters is including probabilistic approaches in PBDMs, thus leading to hybrid solutions. There are several valid examples in the literature, such as SINMAP [124], GEOTOP-Fs [125], HIRESSS [126], SlideForMap [127], and FSLAM [128]. These models include probabilistic assessments at different complexity rates, but in this paper, it was preferred to focus on physically based distributed models characterized by only deterministic input parameters and deterministic output results.

Chapter 3

Implementation of a slope stability method in the CRITERIA-1D agro-hydrological modeling scheme

This paper has been published in *Landslides* journal on 24 July 2024.
Reference: **Sannino, G.**, Tomei, F., Bittelli, M., Bordoni, M., Meisina, C., & Valentino, R. (2024). Implementation of a slope stability method in the CRITERIA-1D agro-hydrological modeling scheme. Landslides, 1-20.
doi: https://doi.org/10.1007/s10346-024-02313-w [123]

Abstract This paper presents the implementation of a slope stability method for rainfall-induced shallow landslides in CRITERIA-1D, which is an agro-hydrological model based on Richards' equation for transient infiltration and redistribution processes. CRITERIA-1D can simulate the presence and development of roots and canopies over space and time, the regulation of transpiration activity based on real meteorological data, and the evaporation reduction caused by canopies. The slope can be considered composed of a multi-layered soil, leading to the possibility of simulating the bedrock and of setting an initial water table level. CRITERIA-1D can consider different soil horizons characterized by different hydraulic conductivities and soil water retention curves, thus allowing the simulation of capillarity barriers. The validation of the proposed physically based slope stability model was conducted through the simulation of the collected water content and water potential data of an experimental slope. The monitored slope is located

close to Montuè, in the north-eastern sector of Oltrepò Pavese (northern Apennines—Italy). Just close to the monitoring station, a shallow landslide occurred in 2014 at a depth of around 100 cm. The results show the utility of agro-hydrological modeling schemes in modeling the antecedent soil moisture condition and in reducing the overestimation of landslides events detection, which is an issue for early warning systems and slope management related to rainfall-induced shallow landslides. The presented model can be used also to test different bioengineering solutions for slope stabilization, especially when data about rooting systems and plant physiology are known.

3.1 Introduction

The characterization of the mechanisms that trigger landslides is a complex although necessary task for civil protection purposes. A difficult aspect is the choice of the criteria and methods for identifying a triggering event, as these can change the amount of landslides detected [129]. Among dangerous landslides, rainfall-induced ones are by far the most frequent, triggered during or following periods of intense and persistent rainfall [40]. In particular, rainfall-induced shallow landslides represent one of the most catastrophic natural hazards because they occur suddenly and can potentially travel a long distance and at high velocity [130]. The hydrological processes in and around a shallow landslide area are fundamental to assess changes in the soil water potential. Decreasing the water potential (in absolute value) reduces the soil shear strength [131] and thus the slope stability. Moreover, including antecedent hydrological information in landslide hazard assessment is still a challenging issue for landslide hydrology research [40]. The prediction of landslide occurrence has been conducted in many different ways over the years, including data-driven and process-based approaches. Data-driven approaches have been widely utilized in the last decades to derive landslide susceptibility maps, especially in large areas where hydrological and geotechnical data are limited [132,133]. These models, which include machine learning techniques, are based on the treatment of past landslide data. Statistical, data-driven approaches assume that, if conditions remain the same, landslides will be triggered again [134]. However, under climate change, past conditions may not represent valid predictors, and these methods need to be used with care. On the other hand, physically based models are appropriate tools not only for susceptibility mapping but also for hazard and risk assessment of rainfall-induced shallow landslides because they can appropriately quantify the processes that trigger failures [135]. These kinds of models have the advantage of taking directly measurable quantities as input parameters, and, although

they provide more accurate results the more data are measured, they can nevertheless be used even where the data on geotechnical and hydraulic properties, as well as temporal changes in topography or subsurface conditions, are relatively scarce [136, 137]. Moreover, physically based models appear rather suitable for use also under climate change conditions [37], especially at the local/slope or small catchment scale, as they are not based on past landslide events. Conducting a quantitative landslide assessment analysis can have different purposes. In the literature, a distinction is made between landslide "susceptibility" and landslide "hazard" [29]: susceptibility mapping aims at detecting only the spatial potential occurrence of landslides, and it is based on physical, geological, and slope conditions such as the land use, referred to a specific moment. Instead, hazard assessments analyses involve evaluating also the temporal occurrence of a landslide. To achieve this goal, a time-dependent soil water balance (SWB) computation is useful to assess the soil condition at, and prior to, the moment of landslide occurrence in response to rainfall events. At the slope scale, physically based models that involve transient hydrological analyses are an advanced solution for determining soil water content and soil water potential, especially on vegetated areas, where the water content computation should be coupled with a proper modeling of the vegetation. It is well-known that plants contribute to the water dynamics on slopes. The action of plants on the overall water budget and specifically on unsaturated soil properties is rather strong [76]. Among other parameters, the saturated hydraulic conductivity and the soil water retention curve are modified by the activity of vegetation [41, 42]. Quantifying these aspects is of particular interest when evaluating the soil condition prior to precipitation in rainfall-induced shallow landslide hazard assessment. Two families of physically based models for rainfall-induced shallow landslides exist, namely probabilistic and deterministic models [22]. The first category involves statistical techniques for treating uncertainty of the input parameters. Slope stability outputs are given as a probability of failure. The second category adopts specific values of parameters that can be either field-measured or literature-derived, making these models suitable to be used also for future rainfall scenarios, permitting an adequate quantification of several processes, especially at the slope scale. Over time, many different hydrological physically based deterministic models have been developed to solve the soil water quantification problem in the vadose zone, accounting for the activity and development of plants for agronomic applications (e.g., [138–140]). These models are named agro-hydrological as they are mainly designed for crop irrigation control and water use efficiency purposes. These models can account for the growth over time of both the aboveground and belowground mass of vegetation, considering the phenology, the harvesting period, and

seeding time for crops, based on the thermal time, which drives roots and canopies development. In agro-hydrological models, the presence of roots can be considered variable with depth, and the transpiration activity can be dynamically assessed. These models accept meteorological data as a dynamic input, at different temporal resolutions. A well-established method to conduct landslide hazard assessment is by adopting stability models coupled with water balance analyses in different spatial domains (e.g., [101,105,141]). However, these investigations largely consider that vegetation improves the accuracy of slope stability analyses [107–109,125,142–147]. Traditionally, the effects of vegetation on slope stability are classified as hydraulic and mechanical effects: the first comprising the transpiration-induced increase of suction, modification of soil hydraulic properties (i.e., changes in pore distributions, the soil water retention curve, and saturated hydraulic conductivity), the effect of canopy evaporation reduction, and preferential roots channel flow; the second comprising processes such as the mechanical reinforcement by roots, both basal and lateral, and the root soil anchoring. Few of the current widely used models account for the impact of vegetation on soil hydraulic properties [22, 42, 148], while the mechanical stabilizing effect of vegetation is more easily included in slope stability as a unique additive term for the whole soil profile, especially in those models that adopt the factor of safety computation within the infinite slope method framework. However, the major mechanical reinforcement effect has been observed to be effective only over the shallowest portion of the soil; conversely, hydrological reinforcement effects seem to be more significant at major depths [79]. In general, vegetation effects are considered static input data, rarely taken into account as transient and depth-variable amounts [37], although considering the vertical variability of both soil properties and the distribution of roots better represents the reality. Even though the soil depth involved in shallow landslides is relatively small (i.e., normally less than 2–3 m), in this shallow layer, water can encounter lenses of different permeability, both while infiltrating and during upward capillarity movements. Thus, the proper characterization of soil horizons, including the rooted portions of soils, is important to detect events such as the formation of nil or positive pore pressures, which are recognized as the main factor triggering shallow landslides. In this paper, a slope stability model is implemented into a physically based, deterministic agro-hydrological model named CRITERIA-1D [149, 150]. The model was developed by the Hydrometeorological and Climate Service (SIMC) of the Public Agency for Environmental Prevention and Energy of the Emilia-Romagna Region (ARPAE) and is freely available online. CRITERIA-1D computes the daily soil water balance by solving a unidimensional version of Richards' equation for the transient infiltration process. The equation ac-

counts for the following hydrological processes: water infiltration, deep and lateral drainage, capillary rise, surface runoff, soil evaporation, plant transpiration, canopy evaporation reduction, water irrigation inputs, and water table oscillations. As an agro-hydrological model, CRITERIA-1D is coupled with conceptual models that simulate the development over time of both aboveground (through the leaf area index) and belowground (through root depth and density) vegetation biomass. The model accounts for a multilayered soil, including the hydrological and geotechnical characterization of each horizon, a depth and time-variable root density distribution, and root mechanical reinforcement. The soil water content, water potential, and slope stability can be computed at any selected depth. The novelty of the proposed model is that it simultaneously accounts for all the abovementioned aspects and that it considers both canopies and roots as daily dynamic inputs based on real meteorological data. The model is then suitable for testing slope stability even under future meteorological conditions and climate scenarios, because of its physically based simulation of plant evolution. Moreover, the model assumes the initial vegetation condition and a portion of meteorological input data for the spin-up process, deriving the soil water balance on a daily basis. In this way, a consistent suction initial boundary condition for the complete hydrology–stability simulation is provided. Although the direct effect of vegetation on the soil water retention curve and saturated conductivity over time are not directly assessed in CRITERIA-1D like in other models (e.g., [42, 148, 151, 152]), the model considers the evapotranspiration-induced water potential besides the pre-wetting suction condition induced by root water uptake. The water uptake is modeled through a macroscopic approach, considering the water removed by the rooted portion of the soil as a term in the general soil water balance equation. Few of the existing physically based models for landslide hazard assessment involving transient hydrology computation comprise all of the cited aspects simultaneously [22, 37, 91]. Based on field hydrological and geotechnical data, the model is applied and validated at the Montuè test site, where a shallow landslide occurred in 2014. The model results showed good agreement with field water content and water potential data with low input parameter calibration when the hydrological effects of vegetation on the soil water content are included. In fact, the results were obtained for two different scenarios: the first considers a bare soil, and the second assumes the presence of developed vegetation. The comparison of the two scenarios' results shows that an agro-hydrological model such as CRITERIA-1D is a reliable tool for the quantitative assessment of hydrological aspects in a landslide phenomenon and also in natural environments. In fact, when the transpiration-induced suction increase, derived from rooted layers and the leaf area index (LAI) development over time, is

considered, the field data are better approximated and landslide occurrence is not overestimated.

3.2 The model

3.2.1 Hydrological computation

CRITERIA-1D is an open-source numerical code that simulates the main hydrological processes in the soil–plant system. The code comprises a numerical solution based on a one-dimensional restriction of the agro-hydrological model CRITERIA-3D [153], which implements Richards' equation. CRITERIA-1D and CRITERIA-3D were developed by the Hydro-Meteorological Service of the Emilia-Romagna Region (ARPAE SIMC, Italy) to model the main phenomena related to soil water balance. These phenomena are described through the coupling of surface and subsurface flows and the coupling of soil water fluxes computation with conceptual models for crop development, solar radiation, evapotranspiration, and snowmelt [153]. The mono-dimensional CRITERIA-1D model solves a general soil water balance by accounting for processes related to infiltration, plant water uptake, capillarity, and evaporation, while the surface runoff is considered through a simplified approach (Fig. 3.1). The surface and subsurface flows are coupled, and an approximation of lateral drainage is included. As concerns the delaying effect of vegetation on the infiltration rate, a pond depth can be assigned to the soil surface depending on the land use. When this pond is full of water and new water inputs are added at a rate higher than the infiltration rate of the shallowest layer, the surplus exits the soil water balance. The input data are represented by the daily air temperature (minimum and maximum), daily total precipitation, crop, and soil parameters. The main computed outputs are the soil water content (SWC), the water potential, the leaf area index (LAI), the daily evapotranspiration (ET), and its components (crop transpiration and soil evaporation). CRITERIA-1D comprises a detailed description of the root density with depth, which is one of the main key factors in soil water balance computation and also in slope stability analysis [77]. The most important hydrological properties in CRITERIA-1D are as follows: the soil saturation (SAT), which indicates the volume of the fraction of voids that can be occupied by water; the field capacity (FC), which is the presumed water content at which internal drainage stops; and the wilting point, which is considered the residual amount of water that plants are not able to take up due to the high water potential. These three properties depend on the soil texture, as the soil particle size and voids influence the

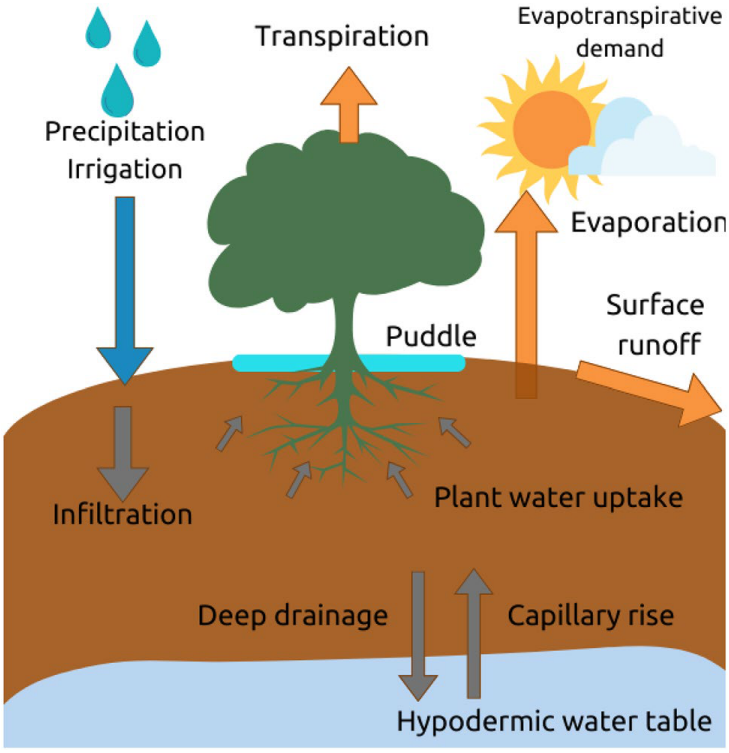

Figure 3.1: CRITERIA soil water balance general scheme

soil behavior in retaining water under a certain water potential rate. The infiltration process of rainfall in the soil is controlled by the surface conditions and the hydraulic conductivity (K) of the different soil layers. The numerical model in CRITERIA-1D solves a global continuity equation through an integrated finite difference formulation for a homogeneous reference volume:

$$\int div(u)dx + \int \frac{\delta(W\theta)}{\delta t}dz = \int qdz \tag{3.1}$$

where:
u is the flux density,
W is the total available volume at a point,
θ is the fraction of W occupied by water (volumetric water content),
q is the water input or output, and
z is the computation depth.

In CRITERIA-1D, the domain is approximated by a one dimensional grid of nodes. Thus, the equation is equivalent to the mass balance equation for the volume surrounding each node:

$$\frac{\delta V_i}{\delta t} = \Sigma_{j=1}^{n} Q_{ij} + q_i \;\; \forall\, i \neq j \tag{3.2}$$

where:
V_i is the amount of stored water in the volume surrounding the node i;
Q_{ij} is the flux between the i-th and the j-th node;
q_i is the input flux at the i-th node.

The flux Q_{ij} is described by Darcy's Law in the finite difference form:

$$Q_{ij} = -K_{ij} S_{ij} \frac{H_i - H_j}{L_{ij}} \tag{3.3}$$

where S_{ij} is the interfacial area between nodes i and j; L_{ij} is the distance between the two nodes; H_i and H_j are the hydraulic potentials at the nodes i and j, respectively; and K_{ij} is the internode conductivity, derived as a geometric mean of nodal conductivities K_i (H_i) and K_j (H_j). The water balance is solved assuming that each soil layer is homogeneous and that the soil skeleton is not deformable. Each soil layer is represented by a single node, characterized by hydrological and soil texture parameters derived from the field soil horizons. Outputs can be obtained at any selected depth between the surface and the bottom soil boundary. The model comprises an automatic time step quantification algorithm, and the mass balance error is computed with reference to the results of the previous time step through a tolerance threshold. In order to get values of water potential and hydraulic conductivities at each node, CRITERIA-1D uses the modified van Genuchten–Mualem formulation proposed by Ippisch et al. (2006) [154] to calculate the equivalent degree of saturation (S_e) (3.4). The hydraulic conductivity function (K) is calculated through the approach presented by Mualem (1976) (3.5):

$$S_e = \begin{cases} \frac{1}{S_c}[1 + (\alpha h)^n]^{-m} & if(h > h_e) \\ 1 & if(h \leq h_e) \end{cases} . \tag{3.4}$$

$$K = \begin{cases} K_{sat} S_e^t [\frac{1-(1-(S_e S_c)^{\frac{1}{m}})^m}{1-(1-S_c^{\frac{1}{m}})^m}] & if(S_e < 1) \\ K_{sat} & if(S_e \geq 1) \end{cases} . \tag{3.5}$$

where:
h_e is the air-entry value (depending on the soil texture) [kPa];
$S_c = [1 + (\alpha h_e)^n]^{-m}$ is the degree of saturation at air-entry value h_e;

S_e is the degree of saturation [−];
α, τ, n, and m are the fitting parameters;
K_{sat} is the saturated hydraulic conductivity [m/s].

Experimental fitting parameters for both the van Genuchten curve and the saturated hydraulic conductivity curve can be used in the model. If there is a lack of experimental data, the model estimates the necessary parameters based on the soil texture through appropriate pedotransfer functions. This latter choice is useful in study cases where data collection may not be possible. More details and mathematical formulations about the hydrology of CRITERIA-3D can be found in Bittelli et al. (2010) [153], while for technical details of CRITERIA-1D, refer to Tomei et al. (2024) [150].

3.2.2 Boundary conditions

As concerns the initial hydraulic state, CRITERIA-1D adopts a Neumann boundary condition imposing that the water content at the surface is equal to zero, while at the bottom of the domain, a free drainage condition is imposed. The other layers are initially assigned with an available water (AW) of 0.8, close to field capacity (FC). The initial fluxes are set equal to zero for all the soil layers. Generally, CRITERIA-1D starts with thermal summations equal to zero (corresponding to January 1st in the northern hemisphere and July 1st in the southern hemisphere) and uses a certain period of meteorological data for the spin-up process, in order to assess the soil water content and soil water potential condition prior to the target simulation period, comprising daily evapotranspiration and crop evolution. If a water table is present, CRITERIA-1D automatically sets the corresponding prescribed water potential and water content as the initial state, and these data are used to assess the capillary rise process. If the water table is not considered in the numerical simulation, the only bottom boundary condition is free drainage. As concerns the upper spatial boundary, the hydraulic condition is modeled through a ponding depth based on the type of crop present. Initially, the surface flux is set to zero, and the pond is filled up with rainfall or irrigation until saturation. If the pond is completely full, runoff starts. Simultaneously with the filling, water infiltrates at a rate equal to the hydraulic conductivity of the first shallow layer.

3.2.3 Crop modeling

The presence of a crop is modeled in CRITERIA-1D through coupled conceptual models that contribute to soil water balance computation. From the

hydrological point of view, plants modify the soil water balance in the root zone because of root water uptake (RWU). Water removed from rooted layers increases the slope stability [77,110]. Another action exerted by plants is the reduction of the evaporation rate in the shallow layers because of canopies, whose development is modeled in CRITERIA-1D through temperatures. In fact, according to the so-called thermal time, quantified in growing degree days (GDD), four life cycle stages (five for herbaceous crops) can be assessed in CRITERIA-1D. In more detail, with the above-specific GDD thresholds based on the considered species, plants can accumulate heat, and the heat accumulation will result in a certain number of growing degree days:

$$GDD = \frac{(T_{min} + T_{max})}{2} - Threshold \tag{3.6}$$

The sum of the GDD, in turn, defines the time-variable leaf area index (LAI) over the year based on two functions. The first describes the growing phase of the vegetation, comprising (i) the sprouting phase (if the crop is herbaceous), (ii) the exponential growth of the LAI, and (iii) the linear growth of the LAI:

$$LAI = \frac{LAI_{max} - LAI_{min}}{1 + e^{a+b*GDD}} + LAI_{min} \tag{3.7}$$

where:
LAI_{max} and LAI_{min} are the maximum and minimum LAI of the considered vegetation;
a and b are the coefficients of the linear regression between log(LAI) and GDD.

The second LAI function in CRITERIA-1D characterizes, for herbaceous and horticultural crops, the decreasing phase of the LAI, thus comprising (i) the decreasing growth rate of the LAI and (ii) the decrease of the LAI:

$$LAI = \frac{LAI_{max} - LAI_{min}}{1 + \frac{10*(GDD-GDD_3)^{N_{4LAI}}}{GDD_4*C_{4LAI}}} + LAI_{min} \tag{3.8}$$

where:
GDD_3 is the sum of the GDD of the first 3 phases;
GDD_4 is the sum of the GDD of phase 3 and phase 4;
$C_{4\ LAI}$ and $N_{4\ LAI}$ are specific coefficients for the crop.

When the LAI exceeds GDD_4, the herbaceous or horticultural crops undergo harvesting, and thus the LAI is automatically set equal to LAI_{min}.

Instead, trees exponentially decrease, reaching a minimum value in the mid-autumn season. For grass crops, mowing cycles are also simulated. On the other hand, if the land cover is fallow, phenological stages are not considered. In this latter case, the LAI reaches its maximum through heat accumulation and then remains stable until November 1st of each year. After this date, the LAI starts to decrease linearly until the last day of the year, when LAI_{min} is reached. The parameters needed to compute the evolution of the LAI over time can be set manually through a user-friendly interface; otherwise, CRITERIA-1D provides them for an implemented set of crops. Depending on the type of soil and the actual development of the crop, the infiltrated water may be more or less available to the vegetation, affecting its transpiration rate. Transpiration acts until the wilting point, represented by leaves suction (ψ_{leaf}), is attained (approximately 1500–1800 kPa, depending on the crop type). The potential evapotranspiration (ET_0) is modeled through the Hargreaves–Samani (1985) [155] equation, which uses only extraterrestrial radiation, and the maximum and minimum daily temperature to obtain daily values of ET_0:

$$ET_0 = 0.0023 \frac{R_a}{2.456} \left(\frac{T_{max} + T_{min}}{2} + 17.78\right)(T_{max} - T_{min})^{\frac{1}{2}} \tag{3.9}$$

where:
R_a is the mean extraterrestrial radiation depending on latitude [mm/day];
T_{max} is the maximum daily temperature;
T_{min} is the minimum daily temperature;
17.78 is the conversion factor for 0 degrees Fahrenheit;
0.0023 is an empirical coefficient, derived from 0.0135 × KT.
The constant 0.0135 was originally proposed by Hargreaves and Samani (1985) [155], while KT depends on the geographical area. For this application, KT=0.17 is assumed.

The reference evapotranspiration ET_0 obtained through 3.9 is divided into maximum soil evaporation and maximum crop transpiration in CRITERIA-1D on the basis of a crop coefficient, k_c, defined as a function of the LAI. The vegetation is involved also in the soil evaporation reduction. Then, the model estimates the actual soil evaporation and crop transpiration based on the soil water availability, and transpiration is computed only for the rooted layers of the soil, defined by a selected maximum root depth, driven by the wilting point of the crop. More detailed information about CRITERIA-1D vegetation modeling can be found in the manuals freely provided by Antolini et al. (2016) [156] and Tomei et al. (2024) [150].

3.2.4 Slope stability

Rainfall-induced shallow landslides involve a soil mantle that is much less thick than the slope failure length [74]. For this reason, the failure plane is assumed parallel to the slope surface and a planar infinite slope scheme has been implemented in CRITERIA-1D to analyze the slope stability. This choice is consistent with the hydrological computation, since the soil layers are considered rigid and homogeneous. Thus, the CRITERIA-1D model is suitable to predict planar slip surfaces [157] at different depths. The slope stability is estimated by the computation of a factor of safety (FoS) for each soil layer through the equation proposed by Lu and Godt (2008) [74], which is based on the suction stress concept (σ^s):

$$FoS = \frac{\tan\phi'}{\tan\beta} + \frac{2C_{tot}}{\gamma H_{ss}\sin 2\beta} - \frac{\sigma^s}{\gamma H_{ss}}(\tan\beta + \cot\beta)\tan\phi' \tag{3.10}$$

where:
$\sigma^s = -\frac{\theta-\theta_r}{\theta_s-\theta_r}(u_a - u_w)$;
(u_a-u_w) is the soil water potential [kPa];
C_{tot}=c'+ c_r;
c' is the effective soil cohesion [kPa];
c_r is the root mechanical contribution [kPa];
θ is the actual soil water content [m^3/m^3];
θ_r is the residual water content at the wilting point [m^3/m^3];
θ_s is the saturated water content [m^3/m^3];
ϕ' is the friction angle [°];
β is the slope angle [°];
H_{ss} is the depth of interest [m];
γ is the unit weight of the soil [kN/m^3]

In CRITERIA-1D, the contribution of the rooting system to the global soil shear strength is quantified as an additional cohesion (c_r), which can be added to c', obtaining a total cohesive term (c_{tot}). The mechanical contribution can be either field-measured or derived through different models that are present in the scientific literature. The most used root reinforcement models are the Wu and Waldron model (WWM), the Fiber Bundle Model (FBM), and the Root Bundle Model (RBM). All three models make it possible to calculate the maximum force that can be sustained by a root bundle [158]. The value derived from literature cases can be considered a maximum root strength contribution that will be assigned to the layer with the highest root density in CRITERIA-1D. The maximum value will be reduced for the effective root density at each layer of the soil profile. Through this approach, a variable

root strength contribution with depth is assumed by CRITERIA-1D in the root zone.

3.3 Test site

The experimental slope is located in Montuè village, Oltrepò Pavese, a hilly region in the northern Apennines, Italy (Fig. 3.2). A monitoring station installed on the slope has acquired meteorological and soil measurements data since 2012 (Fig. 3.3).

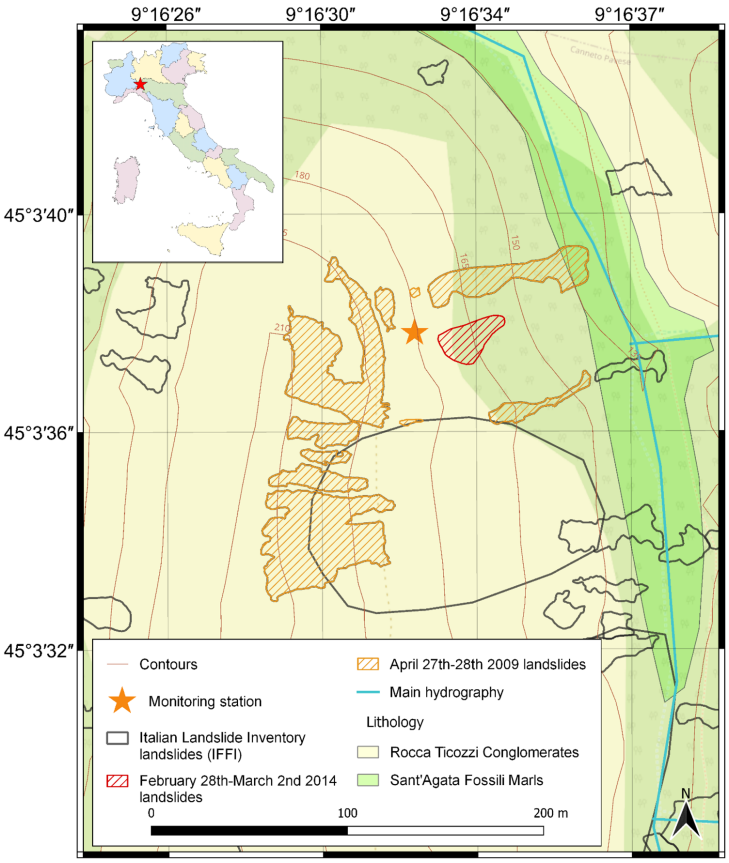

Figure 3.2: Study area

The area is prone to rainfall-induced shallow landslides, most of which are caused by intense or prolonged rainfall events. Since around 1950, the first documented rainfall-induced landslides in the north-eastern sector of Oltrepò Pavese occurred in 2009 as represented in Fig. 3.2. These landslides were caused by an extreme rainfall event of 620 mm in 62 h [58]. Between February 28 and March 2, 2014, a new landslide occurred a few meters from the

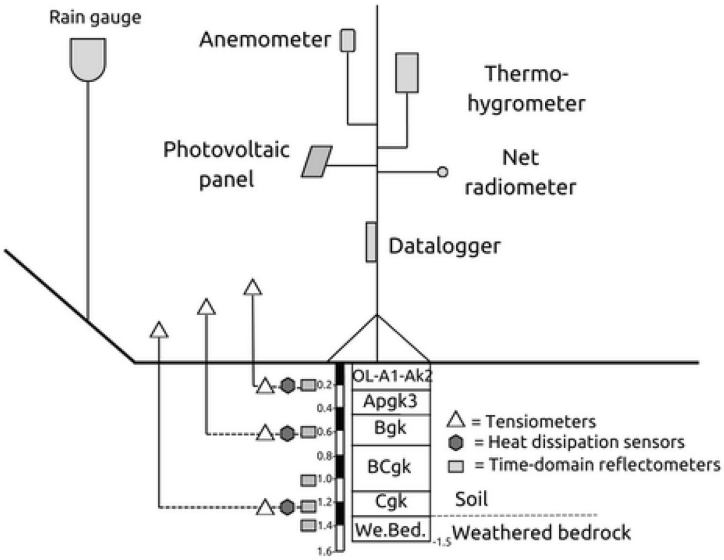

Figure 3.3: The monitoring station

monitoring station (Fig. 3.2 and Fig. 3.4) due to an amount of 68.9 mm of rainfall in 42 h, registered at the monitoring station. The sensors installed

Figure 3.4: The 2014 landslide (location and size are reported in Fig. 3.2)

at Montuè test site allow the acquisition of measurements of meteorological variables, such as precipitation, temperature, solar radiation, relative humidity, wind intensity, and direction, as well as soil variables, such as soil water content and pore water pressures (or water potential) at different depths (Fig. 3.3). More precisely, the integrated monitoring station at Montuè comprises a rain gauge (Model 52,203, Young Comp., Traverse City, MI), a thermo-hygrometer (Model HMP155A, Campbell Sci. Inc., Lo-

Table 3.1: Montuè field equipment

Variable	Device	Accuracy	Model	Range of measure
Soil water content, soil temperature, soil water electrical conductivity	TDR probes	0.01-0,02	CS610, Campbell Sci. Inc., Logan, UT	0-1
Soil water potential (<-10 J/kg)	Heat dissipation (HD)	1.5-2.0 J/kg	HD229, Campbell Sci., Logan, UT	-10,000/-10 J/kg
Soil water potential (>-10 J/kg)	Tensiometer	1.5-2.0 J/kg	Jet-Fill 2725, SoilMoisture Equipment Corp., Santa Barbara, CA	-80/15 J/kg
Rainfall	Rain gauge	0.01 mm	52,203, Young Comp., Traverse City, MI	0 mm
Air temperature, air humidity	Thermo-hygrometer	0.2 °C, 1%	HMP155A, Campbell Sci. Inc., Logan, UT	-80/60° C, 0-100%
Atmospheric pressure	Barometer	0.1 hPa	CS100, Campbell Sci. Inc., Logan, UT	600-1100 hPa
Wind speed, wind direction	Anemometer	0.01 m/s, 3°	WINDSONIC, Campbell Sci. Inc., Logan, UT	0-60 m/s, 0-359°
Net solar radiation	Net radiometer	3 W/m2	NR-LITE 2, Kipp & Zonen, Delft, Netherlands	-
Datalogger: No. 1 CR1000X (Campbell Scientific, Inc.)				

gan, UT), a barometer (Model CS100, Campbell Sci. Inc., Logan, UT), an anemometer (Model WINDSONIC, Campbell Sci. Inc., Logan, UT), and a net radiometer (Model NR-LITE 2, Kipp & Zonen, Delft, Netherlands) as meteorological sensors. Moreover, six time-domain reflectometer (TDR) probes (Model CS610, Campbell Sci. Inc., Logan, UT) equipped with a multiplexer (SDMX50, Campbell Sci. Inc., Logan, UT), installed at 20, 40, 60, 100, 120, and 140 cm from the ground level, measure the soil water content (Fig. 3.3). A combination of three tensiometers (Model Jet-Fill 2725, SoilMoisture Equipment Corp., Santa Barbara, CA) and three heat dissipation (HD) sensors (Model HD229, Campbell Sci., Logan, UT) are installed at 20, 60, and 120 cm from the ground level and measure the pore water pressure. The tensiometers measure the pore water pressure directly, while the HD sensors get the pore water pressure values through the use of the conversion equation from Flint et al. (2002) [159]. HD sensors can only acquire values lower than -10 kPa ([54], so the tensiometers are necessary to measure values higher than -10 kPa [58]. Table 3.1 summarizes the different sensors' characteristics, while in the Appendix, the calibration curve used for the heat dissipation sensors is provided (3.13).

From previous studies by Bordoni et al. (2015) [58], it is known that the slip surface depth for the 2014 landslide was around 100 cm, and the most likely triggering condition was the formation of a perched water table above the calcic horizon, located at a depth of 120 cm. The soil at Montuè is a calcic Gleysol [160]. A detailed description of the site pedology, not discussed here, is presented in the work of Bordoni et al. (2015) [58]. The horizons represented in Fig. 3.3 are classified as silt loam (I and V) and silty clay loam (II, III, and IV). The underlying lithology is constituted by Rocca Ticozzi conglomerates, a bedrock made up of gravel, sand, and poorly cemented conglomerates with a low percentage of marls. At a depth of 130 cm, contact

between the soil and the weathered bedrock has been observed. The soil coverage in 2014 was constituted by grass and shrubs with rooting at a maximum depth of 40 cm [58], while woodlands were present all around the monitoring station and the landslide area. The soil coverage on the landslide body was constituted by sparse, young woodland (Fig. 3.4). Since 2012, hysteretic processes and variability of the field-measured saturated hydraulic conductivity (K_{sat}) in different periods of the year have also been observed (Bordoni et al. 2015, 2017, 2021b), but in the present application, no hysteretic behavior was directly considered.

3.4 Model application

To apply CRITERIA-1D at the test site, soil horizons with similar properties were grouped together on the basis of the research by Bordoni et al. (2015) [58]. The soil stratigraphy and relative horizon parameters listed in Tables 3.2 and 3.3 were used in this application.

Table 3.2: CRITERIA-1D soil parameters for Montuè application

Horizon	Depth range (cm)	Coarse fraction (%)	Organic matter (%)	Sand (%)	Silt (%)	Clay (%)	Bulk density (g/cm^3)	c' (kPa)	ϕ' (°)
I	0-22	0	1.44	16.6	58.0	25.4	1.733	0	31
II	22-42	0	1.36	11.9	59.9	28.2	1.703	0	31
III	42-70	0	1.03	16.0	53.9	30.1	1.703	0	33
IV	70-110	0	0.88	12.6	57.9	29.5	1.897	0	33
V	110-130	0	0.62	7.70	65.8	26.5	1.861	29	26
We. Bedr	130-150	50	0.30	75.0	25.0	0.00	1.841	29	26

Values of the texture, effective cohesion, friction angle, and bulk density were obtained from field measurements and from the previous research by Bordoni et al. (2015) [58]. Values for the saturated and residual water content were derived from field-measured time series for the period of interest [134, 161].

Table 3.3: CRITERIA-1D hydrological parameters for Montuè application

Horizon	θ_s (m^3/m^3)	θ_r (m^3/m^3)	h_e (kPa)	n (-)	m (-)	α (kPa^{-1})	K_{sat} (m/s)	Available water (m^3/m^3)
I	0.39	0.12	2.6	1.412	0.292	0.011	7.50E-07	0.263
II	0.40	0.13	3.1	1.392	0.282	0.011	2.00E-07	0.261
III	0.44	0.15	3.1	1.385	0.278	0.010	2.00E-07	0.261
IV	0.41	0.10	3.1	1.388	0.280	0.024	2.00E-07	0.284
V	0.48	0.16	2.6	1.326	0.246	0.018	7.50E-07	0.303
We. Bedr	0.41	0.12	1.0	1.361	0.265	0.019	1.00E-07	0.280

It must be specified that the root mechanical contribution (c_r) has been assumed equal to zero, differently from what has been done in recent research for similar sites [162]. The reason for this choice is that in a condition at or close to saturation, the bond between roots and soil may become very weak, eliminating additional cohesion [163]. Moreover, when the vegetation composition and the roots' distribution are unknown, values of additive cohesion taken from the literature may lead to non-precautionary values of FoS in saturated conditions. For this application, the simulation period spans from January 1 2012 to December 31 2015, in order to model two years of weather data to reproduce the soil moisture condition prior to the 2014 landslide (Fig. 3.5). Parameters for the van Genuchten soil water retention curve and hydraulic conductivity function were estimated based on the field water content and water potential time series; values were thus provided for the saturation (SAT), field capacity (FC), and permanent wilting point, considered for the fine grained horizons as the water content measured at a water potential of 0.1, 30, and 1600 kPa, respectively. For the last layer, namely the weathered bedrock, the SWRC was fitted adopting 10 kPa instead of 30 kPa as the field capacity value. However, as already mentioned, if no values are provided, the CRITERIA-1D model can derive them, assigning fitting parameters for the van Genuchten–Mualem model based on the horizon's texture. The soil permeability, which has been determined through field measurements of saturated hydraulic conductivity (K_{sat}), showed great variability over the years and in different seasons. As testified by previous research [58, 161, 164], the Montuè test site is constituted by a soil with hysteretic behavior. This hysteretic behavior is a typical phenomenon observed in the majority of soils. It consists in a difference between the wetting and drying phases of soils, resulting in a different observed water content–water potential relationship. At Montuè, field observation revealed that the soil presents a hysteretic behavior, and also a variable K_{sat} over time was measured. The K_{sat} variability can be induced by plants as well [42]. Through CRITERIA-1D, different simulations were carried out using the different measured values of hydraulic conductivity at saturation. Meanwhile, a reference value for each horizon, based on its texture, was used in this application (Tab. 3.3), according to field data that suggested an average value of the measured range of K_{sat} as the most consistent. This choice is also sustained by the fact that, for the years of interest, no values of K_{sat} were directly measured in the field. The different simulations showed that for water content values close to saturation, the results were similar even if K_{sat} differed by up to two orders of magnitude, while maintaining the other parameters. As the aim of this research is testing the use of CRITERIA-1D for landslide prediction and the condition of interest is in most cases represented by near saturation or complete sat-

uration, the results were considered satisfactory, and the average K_{sat} value based on soil texture [150, 165] was selected for simulations.

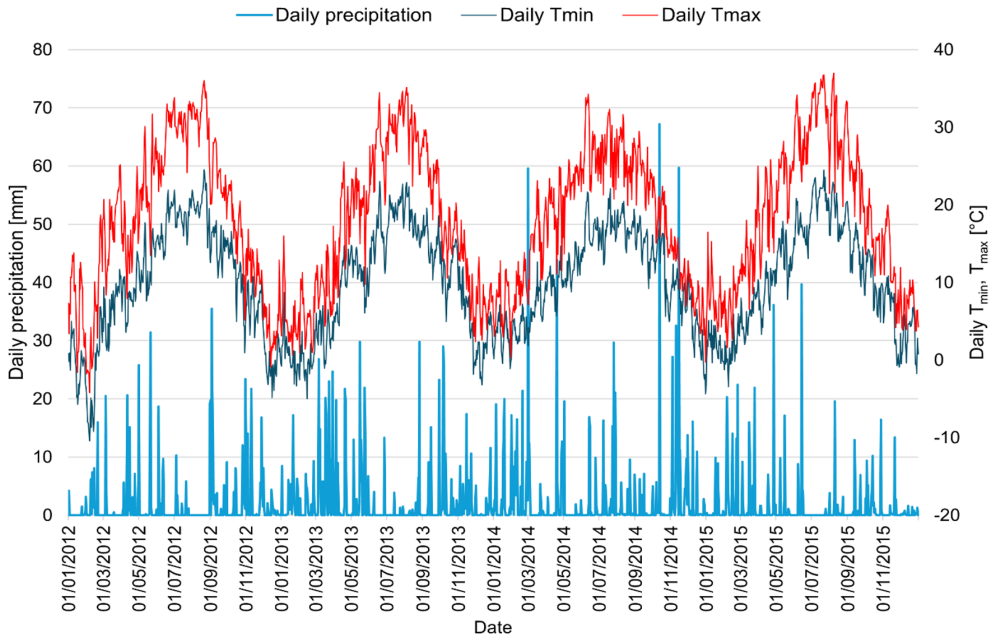

Figure 3.5: Input weather data for the simulation (dates in dd/mm/yyyy format)

At Montuè, the bottom layer, whose depth ranges from 130 to 150 cm, is classified as weathered bedrock. Its permeability was never measured, and in CRITERIA-1D, it was arbitrarily set in order to reproduce a less permeable layer with respect to the overlaid ones. As the only possible bottom boundary condition is free drainage, this artifact is necessary to reproduce the field case of the Montuè test site. In fact, the formation of a perched water table at a depth between 80 and 120 cm seems to have provoked the 2014 landslide [58]. A slope angle of 0.5 m/m was considered a representative of the whole slope in this application. Table 3.4 summarizes the vegetation parameters used by CRITERIA-1D for the Montuè case study. As already mentioned, for some kinds of crops, specific sets of parameters are provided with the model; however, in this application, the specific composition of the vegetation in each season at Montuè is unknown. Nevertheless, it is known that mainly herbaceous plants and some shrubs were covering the station when the landslide occurred. In the absence of more detailed data, the yearly vegetation coverage was simulated as fallow as concerns the LAI behavior, assigning a minimum LAI of 0.5 for the coldest months, passing rapidly (simulated through the GDD of the two phases) to a maximum LAI of 2.5,

Table 3.4: CRITERIA-1D vegetation parameters for Montuè application

LAI_{min} (m^2/m^2)	0.5
LAI_{max} (m^2/m^2)	2.5
Lower thermal threshold (°C)	0
Upper thermal threshold (°C)	35
GDD Phase 1 (°C)	3500
GDD Phase 2 (°C)	1000
LAI curve factor a (-)	4.1
LAI curve factor b (-)	-0.0014
Root depth RD_0 (cm)	5
Root depth RD_{max} (cm)	130
k_c max (-)	1
Root shape distribution	Cardioid
Root shape deformation factor (-)	0
Irrigation (mm)	0
ψ_{leaf} (kPa)	1569.02
c_r (kPa)	0

maintained from late March to late October (Fig. 3.6). The coverage periods were derived by satellite photographs that show live vegetation covering the test site in 2014 (Fig. 3.7).

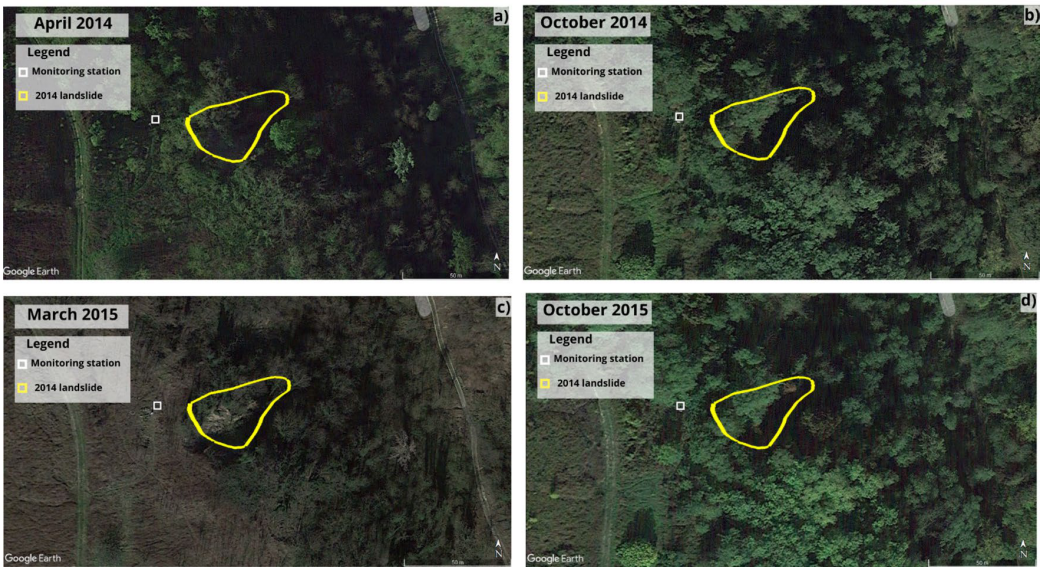

Figure 3.7: Vegetation cover condition derived from satellite photographs: April 2014 (a), October 2014 (b), March 2015 (c), and October 2015 (d)

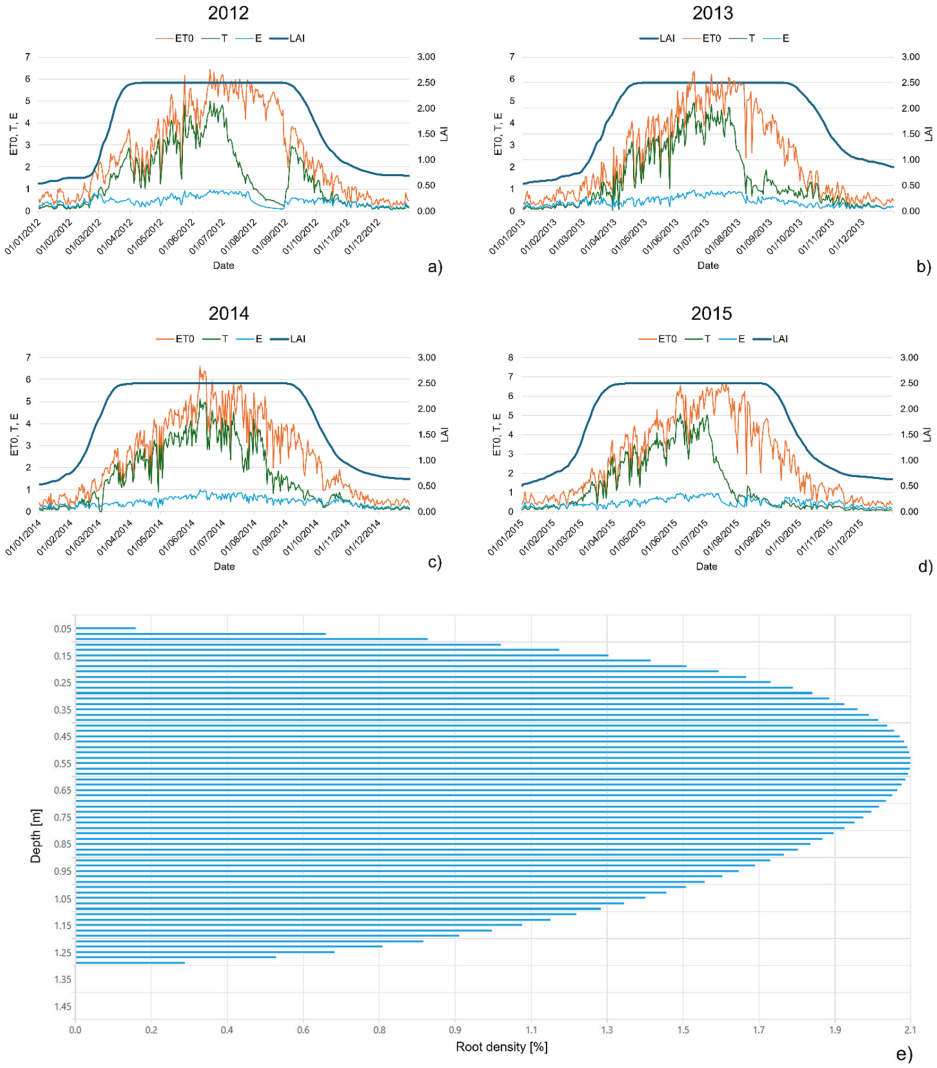

Figure 3.6: Vegetation development over the simulation periods: LAI, potential evapotranspiration (ET_0), actual evaporation (E), actual transpiration (T) in 2012 (a), 2013 (b), 2014 (c), 2015 (d), and the static root density with depth (e) (dates are provided in dd/mm/yyyy format)

The root density was considered static for the 4-year simulation period, because the transpiration-induced hydrological reinforcement effect is controlled in CRITERIA-1D by the leaf area index. The maximum root depth (RD_{max}) is set at the contact between the soil and the weathered bedrock (130 cm), because of the presence of shrubs and of Robinia pseudoacacia L. trees at the landslide site (Fig. 3.4), which is located a few meters from the monitoring station (Fig. 3.7). Roots are assumed to start at a depth of 5 cm to sim-

ulate a root collar (RD_0=5 cm). The root distribution is set as a standard cardioid with no shape deformation (Fig. 3.6e). The minimum LAI was set as diverse from zero to reproduce the evaporation reduction caused by vegetation also in the winter months; as in this site, the soil remains covered with dead vegetation. CRITERIA-1D was originally designed for agronomic applications, and this work represents the first attempt to apply it in more naturally vegetated environments; thus, in the absence of detailed measurements, vegetation parameters were calibrated according to the field water content and water potential data. The other model application shown in this work considers a bare soil covering the slope. The intention is to compare the results with those obtained by assuming the presence of vegetation. With regard to meteorological input data, precipitation and air temperature daily records were derived from the monitoring station at Montuè (Fig. 3.5). Missing temperature records were linearly interpolated. Missing precipitation records were replaced with data derived from a spatialization algorithm using neighboring monitoring stations. It is worth noting that the landslide of Fig. 3.4 is suitable for modeling with the infinite slope method because of the planar slip surface shape observed. Moreover, the soil volume involved had a thickness of around 1 m over a slope more than 110 m long. As the length was much larger than the height of the soil volume, the assumption of the infinite slope appears consistent with reality.

3.5 Results and discussion

3.5.1 Hydrology

The water budget was computed at different depths. In particular, outputs at 20, 40, 60, 100, 120, and 140 cm related to the two applications were derived. As already discussed, one case considers the presence of vegetation,

Table 3.5: Root mean square errors for the hydrological simulations

Depth - (m)	RMSE - bare soil (m^3/m^3)	RMSE - vegetation (m^3/m^3)
0.2	0.06	0.05
0.4	0.07	0.05
0.6	0.08	0.06
1.0	0.08	0.04
1.2	0.10	0.08
1.4	0.08	0.05
0-1.5	0.07	0.04

while the other considers a bare soil. The soil and weather data are the same in both applications and are derived from a monitoring station located a few meters away from the landslide scarp (Fig. 3.2). The results show that, in the upper layers (Fig. 3.8), plant transpiration and root water uptake allowed for a better description of the minimum water content values observed in the dry seasons than the bare soil. With regard to the maximum water content values observed in the wet seasons, the first two layers are better simulated through a bare soil assumption. However, with regard to the minimum water content amounts, a simulation that accounts for plant transpiration and root water uptake, even when a small portion of shallow soils is occupied by roots (i.e., a maximum of around 2 % in the first 40 cm, see Fig. 3.6e), better describes the measured data. Moreover, it should be considered that CRITERIA-1D assumes only horizontal ground surface and soil horizons, while at the Montuè test site, the monitoring station is located on a slope, and it is surrounded by vegetation. Since both the lateral water movements and the water taken up by neighboring plants are neglected, a bare soil does not approximate the actual decrease in soil water content, which is indeed better approximated in a simulation considering a vegetated slope. It can be noted that the fast water infiltration movements due to high daily rainfall amounts (see as an example the rainfall events of 01 September 2012 and 01 November 2014 in Fig. 3.8) are correctly simulated by CRITERIA-1D for both vegetated and bare soil. However, the consequent minimum water content, due to the combined effect of gravity movements, lateral flows, and the water uptake by roots, is better modeled by the simulation that assumes the presence of vegetation, at 20 cm, 40 cm, and 60 cm of depth.

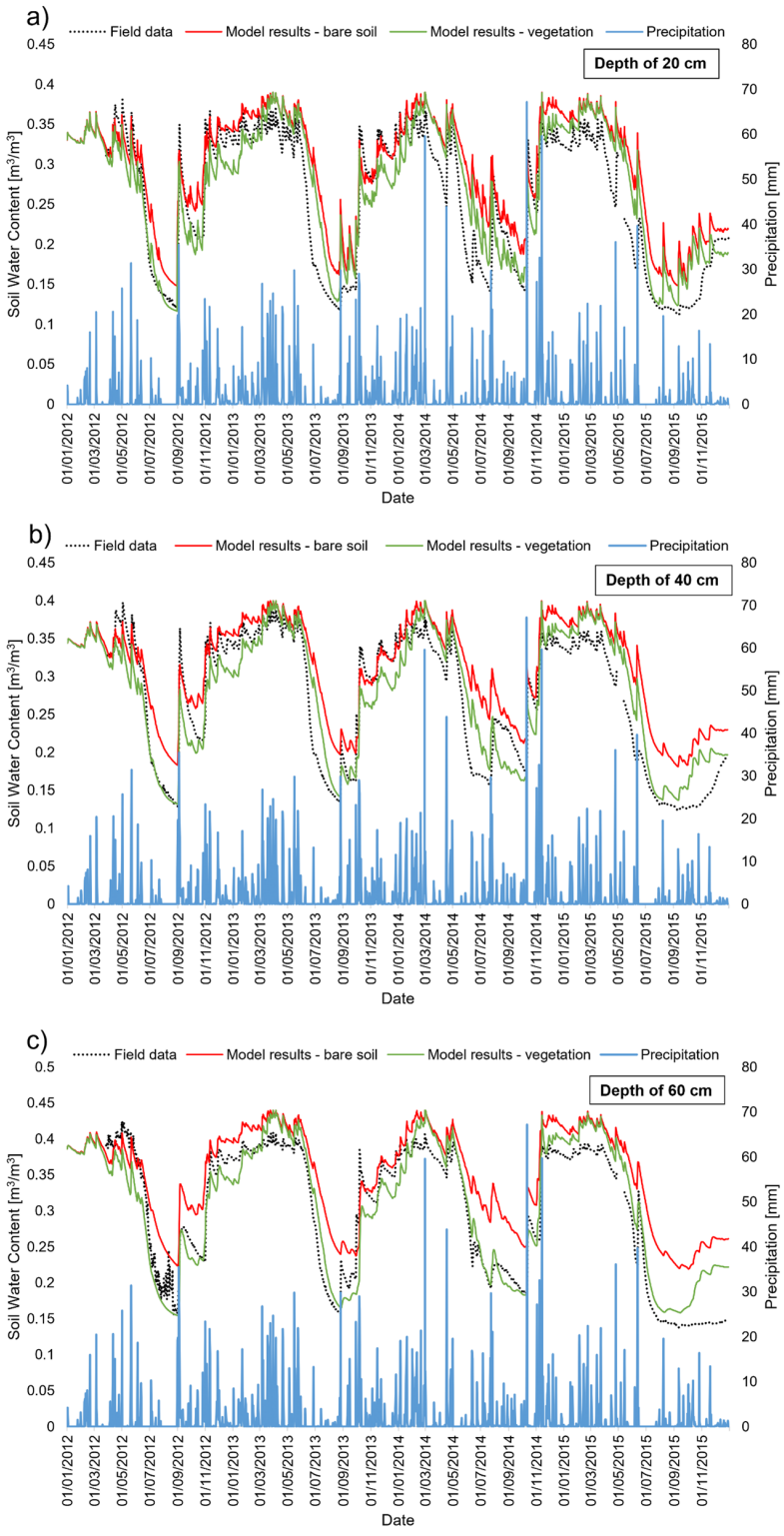

Figure 3.8: Water content simulation at depths of 20 (a), 40 (b), and 60 cm (c) (dates are provided in dd/mm/yyyy format)

A further aspect that needs to be emphasized is that the simulation covers a 4-year period, spanning from January 2012 to December 2015. It has been observed that throughout this period, the vegetation has grown, especially after the 2012 excavation works connected to the installation of the monitoring station. For this reason, the computed water content appears to be overestimated with respect to the field measurements in 2015, even around the maximum values, when bare soil is considered. The overestimation becomes larger moving down in depth (see Fig. 3.8) for values around the minimum water content. The results obtained at depths of 100 cm and 120 cm (Fig. 3.9a, b) show a different situation with respect to the upper layers. In fact, the field data are better approximated for both the maximum and minimum values if vegetation is included in the model (green curves). It appears clear that considering rooted deep layers allows a better modeling of the real hydrological phenomena occurring in this soil. At a depth of 140 cm (Fig. 3.9c), the field data suggest a different behavior. This layer, which was classified as weathered bedrock based on field observations, shows longer periods with water content values close to saturation compared with all the other depths. However, although roots are not present in this layer, the case of vegetated soil performs better than the bare soil. It has to be highlighted that the results for this layer refer solely to the soil matrix, while the presence of gravel and thus the related water movements are not simulated.

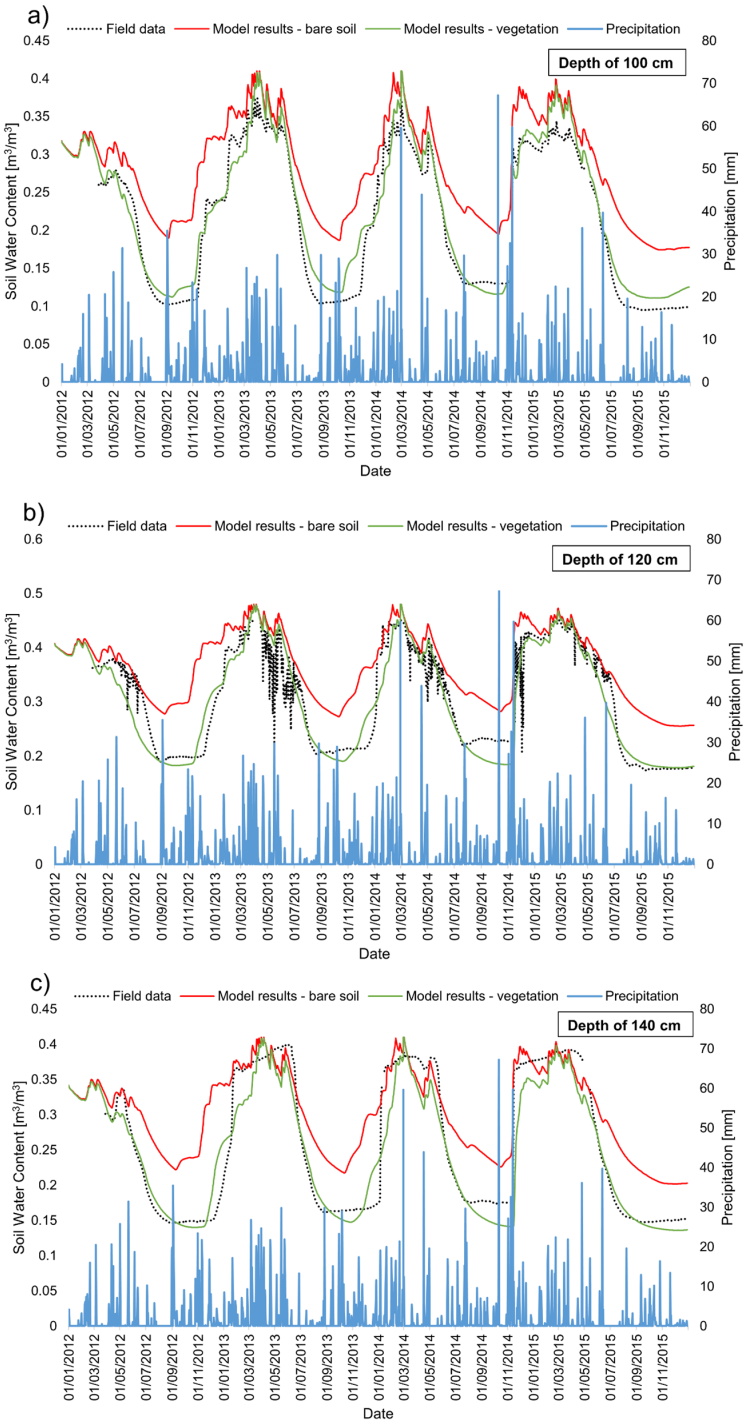

Figure 3.9: Water content simulation at depths of 100 (a), 120 (b), and 140 cm (c) (dates are provided in dd/mm/yyyy format)

Figure 3.10 shows the results obtained by calculating the average of both the measured and simulated water contents between the ground level and a depth of 150 cm. It can be seen that the overall hydrological behavior is better simulated if the presence of vegetation is considered. The root mean square error (RMSE) (Table 3.5) confirms a better performance for the vegetated slope simulation for all the considered depths. These results highlight the importance of including a detailed description of the vegetation dynamics and root development (in both space and time) to properly quantify the soil hydrological processes leading to shallow landslides.

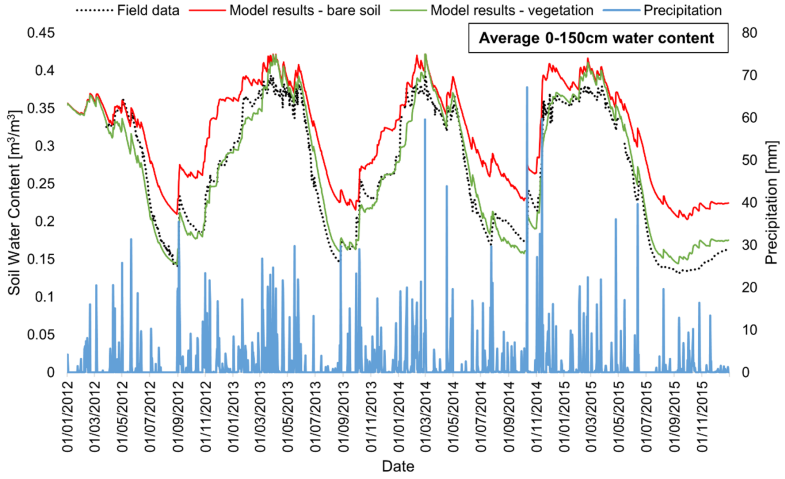

Figure 3.10: Average water content simulation for the whole profile from 0 to 150 cm (dates are provided in dd/mm/yyyy format))

3.5.2 Water potential

The difference in soil water potential between adjacent computational nodes is the leading physical variable for all water transport processes, storage, infiltration, and redistribution in CRITERIA-1D. Based on soil texture and field water potential data, if available, each homogeneous soil layer is characterized by its own soil water retention curve (SWRC), and water movement is driven by the water potential gradients. The water potential was computed at depths of 20, 60, and 120 cm corresponding to the sensor's installation depths at the Montuè site (Fig. 3.3). CRITERIA-1D can indicate some water content levels at chosen points of the SWRC. For this application, values for the saturation, field capacity, and wilting point were derived from field data for the different horizons. The modified Ippisch–van Genuchten model is employed as the SWRC in both CRITERIA-1D and CRITERIA-3D [54]. The results represented in Fig. 3.11 show that the condition close to sat-

uration or at complete saturation for prolonged periods starts at a depth of 60 cm, being more stable at 120 cm. This suggests the formation of a perched water table, probably at an intermediate depth. From field data, it is found that, between February 28th and March 2nd, i.e., when the landslide occurred, positive water potentials developed. These values were correctly detected for both the vegetated and bare soil simulations in CRITERIA-1D. The difference between the two scenarios is evident by observing the low values of the water potentials, similarly to the water content simulations. Considering the presence of vegetation (green lines in Fig. 3.11a–c) returns higher values of negative water potential during summer dry periods compared with the bare soil simulation, especially at the shallowest depth considered (Fig.3.11a). However, at deeper layers, the vegetated scenario outperforms that with bare soil (Fig. 3.11b, c). The water potential values appear to be simulated well with the vegetated soil especially in summer 2014, up to a depth of 60 cm (Fig. 3.11b). Actually, this was the only summer in the considered period in which the transpiration activity did not drop because of a high rainfall rate (Fig. 3.6c). The effect of considering evapotranspiration is evident at deeper layers. The water potential patterns are better captured particularly as concerns the minimum values and the rapid drying movements. An example is represented by the simulation at the depth of 60 cm, where the maximum root density occurs (Fig. 3.6e). At this layer, the simulated descending water potential trend in time is accurate in July, when the transpiration is still present (Fig. 3.11b). It is worth highlighting the effect of evapotranspiration-induced suction on the soil water potential in September 2012 (Fig. 3.11b), when the transpiration starts again because of a high amount of rainfall. Only the vegetated simulation simulates the subsequent drying phase. Generally, the wetting curve branches are better captured by the vegetated simulation over the whole of the considered time span, suggesting the importance of simulating the pre-wetting water potential due to evapotranspiration activity, as well as the evaporation reduction because of canopies.

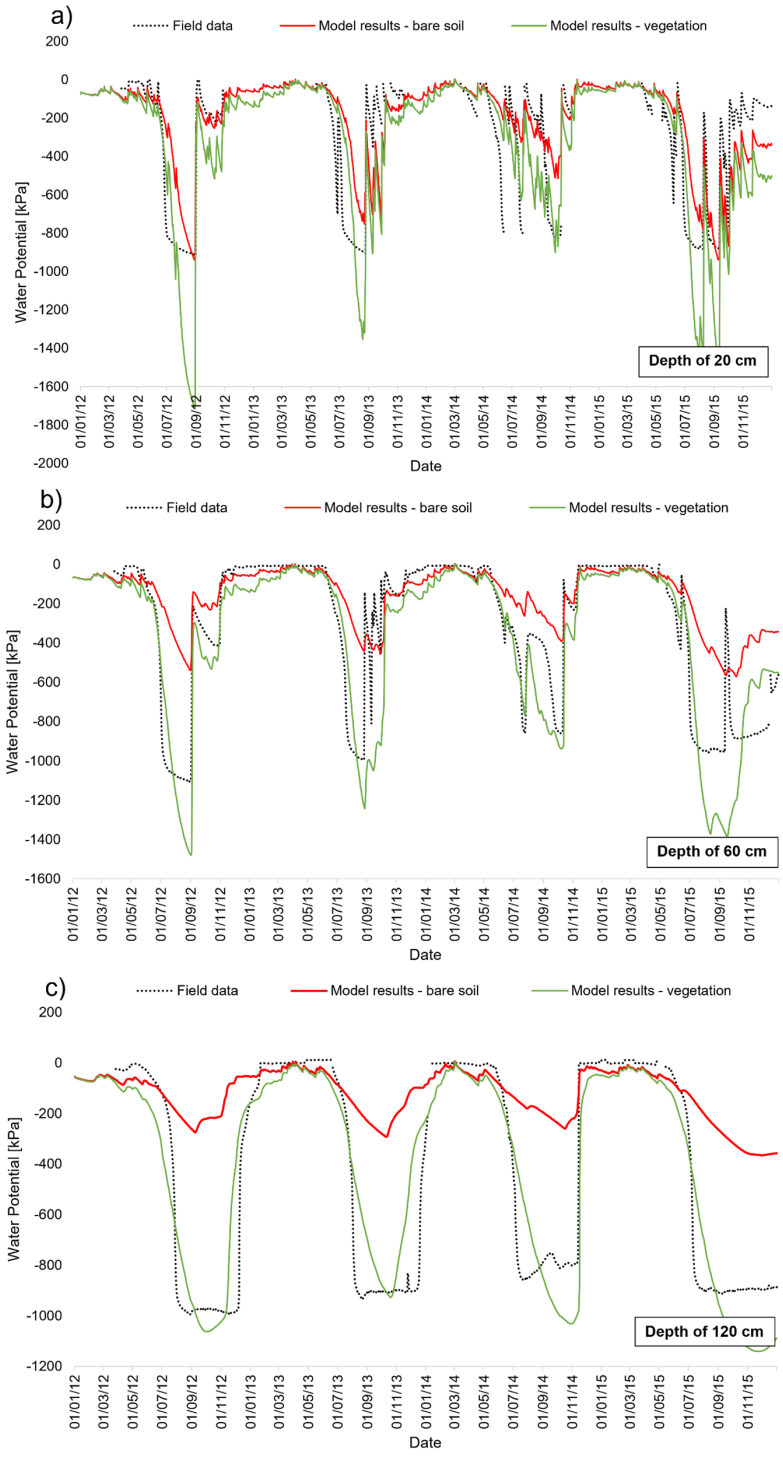

Figure 3.11: Water potential simulation at depths of 20 (a), 60 (b), and 120 cm (c) (dates are provided in dd/mm/yy format)

3.5.3 Slope stability analysis

Figure 3.12 shows the results of the slope stability analysis carried out through CRITERIA-1D in terms of variation of the factor of safety (FoS) in time at different depths. The trend of the FoS showed that considering a bare soil can lead to overestimations of landslide events detection (Fig.3.12a). In fact, during the simulation period, the FoS assumes a value lower than one, indicating instability, several times if no vegetation and evapotranspiration-induced stability effect is considered. This aspect must not be neglected when a tool is to be used for early warning purposes. When considering the presence

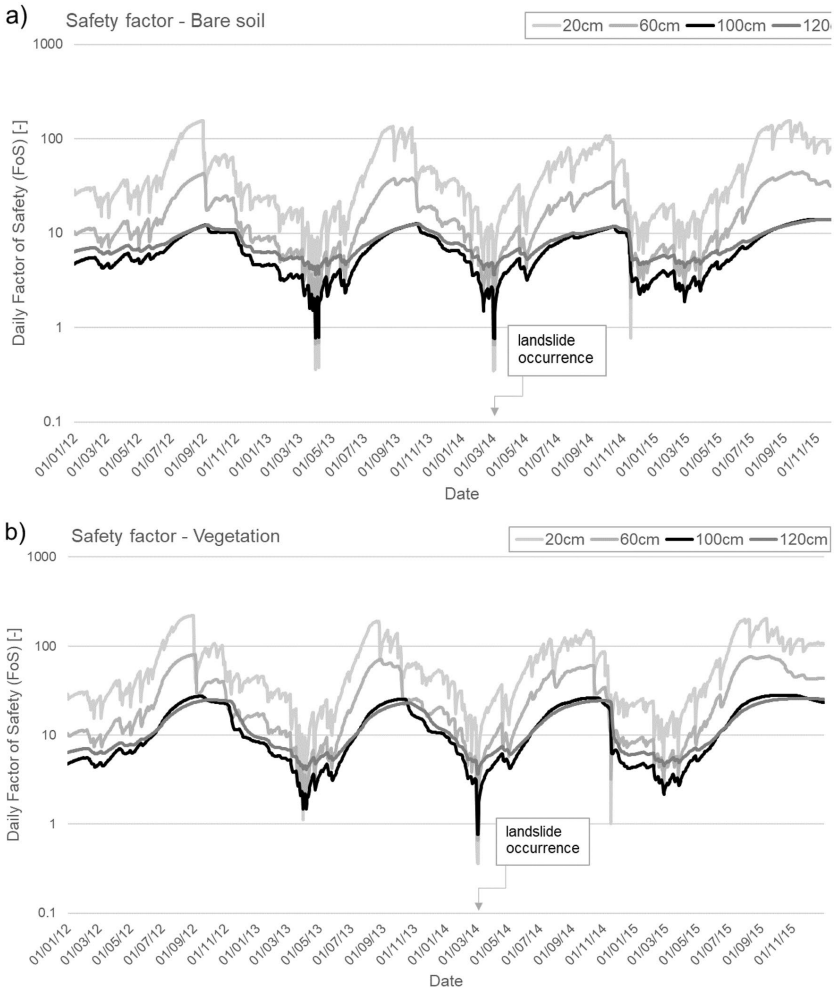

Figure 3.12: Simulation of daily factor of safety at different depths considering a bare soil (a) and the presence of vegetation (b) (dates are provided in dd/mm/yy format)

and the hydrological effect of vegetation, the situation is different, and the

unique landslide of 2014 is correctly predicted at a depth of 100 cm, i.e., the real depth of occurrence, as already detected by Bordoni et al. (2015) [58] (Fig. 3.12b). In CRITERIA-1D, the root water uptake activity is related to the leaf area index at every time step (Fig. 3.6). The LAI changes from its minimum to its maximum based on real meteorological data throughout the year, and from 1 year to another, together with evapotranspiration (see Fig. 3.6). Thus, the hydrological effect on the soil shear strength caused by plants modeled in CRITERIA-1D has a reliable physical basis, although a standard root distribution was used in this application. Furthermore, the transpiration activity in CRITERIA-1D is stopped when the soil is dry or saturated, on the basis of a water tolerance threshold that can be manually set. The year 2013 was characterized by a prolonged wet period with respect to the other considered years (Fig. 3.5), and many subsequent rainfall events occurred. Despite this, as the LAI was growing to its maximum level (the false detected landslide for the bare soil is between April and May 2013, see Figs. 3.6b and 3.12a), the transpiration activity continued, such that the factor of safety did not drop below one. On the contrary, in 2014, very high rainfall (approximately 70 mm in 42 h) occurred during a wet period, and the transpiration dropped to zero because of the stress condition due to soil saturation (Fig. 3.6c). These results suggest that the cause of the landslide occurrence was the interruption of the root water uptake and thus the hydraulic reinforcement effect. Like other physically based deterministic models, CRITERIA-1D does not comprise any statistical treatment of input parameters uncertainties. If parameters are not directly measured in the field, it is possible to calibrate the soil and crop parameters for a certain slope through the back analysis of past landslides and measured time series of soil water content and water potential. Moreover, although CRITERIA-1D cannot reproduce the volumetric changes due to the shrinking–swelling cycles and the consequent formation of macro-voids and preferential flows, it appears suitable for fine-grained silty soils even if texture-based parameters are used. The proper modeling of vegetation, enlarging the soil water balance components, helps the model to be consistent even when using calibrated values of the soil parameters.

3.6 Conclusions

The aim of this research was to implement a slope stability method into the agro-hydrological CRITERIA-1D model, due to its ability to consider the presence of vegetation as a dynamic, spatially, and time-variable input. Another objective was to test the reliability of the proposed approach for the

implementation of the same slope stability method in the three-dimensional CRITERIA-3D, which is an ongoing research activity. Modeling the root zone and the presence of canopies is recognized as an important aspect for landslide prediction, especially when computation of the soil water balance transient is included in the model. The main findings obtained by employing the CRITERIA-1D model can be summarized as follows:

- The implementation of a slope stability method in an agro-hydrological modeling scheme is a valid tool for rainfall-induced shallow landslide prediction. In particular, the possibility of dynamically modeling the transpiration-induced hydrological effects is of importance; although it is not the unique hydrological vegetation effect on unsaturated soil properties [79], it is rarely considered by the current widely adopted models.

- On soils with hysteretic behavior, the use of a unique soil water retention curve (SWRC) and the underlying assumption of homogeneous soil layers sometimes may not be appropriate. However, at the Montuè test site, thanks to the possibility of modeling vegetation dynamically, the choice of using texture-based values of K_{sat} showed its efficacy.

- With regard to slope stability analysis, the root density distribution and the presence of plants affect water movements and the water potential in soils, and this research underlined the importance of including this component in physically based deterministic models to avoid the overestimation of landslide event detection. Although designed for agronomical contexts, CRITERIA-1D shows good suitability also for a natural environment case.

- The pre-wetting condition due to the evapotranspiration-induced hydrological effect has an important impact on slope stability transient evaluation; moreover, in shallow landslide models, account should be taken of the fact that transpiration can become null when the soil undergoes saturated conditions. Accounting for this mechanism can improve the accuracy of models.

Further developments will include the implementation and validation of the slope stability model in the three-dimensional CRITERIA-3D code [153] on the same test site and the validation of CRITERIA-1D in other natural environments. Another research focus will be the possibility of implementing different soil hydrological parameters depending on the season. Also, the presence of any differences between considering only the hydrological or both

the hydrological and mechanical root effect in shallow landslide prediction through CRITERIA-1D where field data are available will be investigated. The possibility of simulating plants growing from 1 year to another when the simulations cover more than 1 year through the LAI will be also explored. As an open-source tool, CRITERIA-1D can help the design of nature-based solutions for slope instability mitigation purposes, as different scenarios can be designed and tested on past landslides events, especially if the mechanical contributions of roots are also properly considered [162, 166].

Appendix

Figure 3.13 shows the calibration curve of heat dissipation (HD) sensors used at the Montuè test site. The curve was derived from the sensor's instruction manual (Campbell Scientific, Inc. (2006). 229 Heat dissipation matric water potential sensor: Instruction manual. Campbell Scientific Inc.: Logan, Utah, USA).

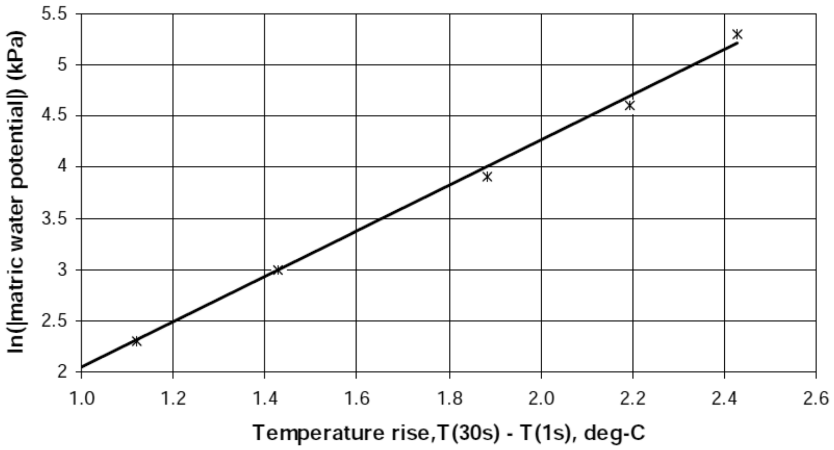

Figure 3.13: Calibration curve of heat dissipation sensors showing the matric water potential vs temperature rise

Chapter 4

A three-dimensional agro-hydro-mechanical model for predictive analysis of shallow landslides: CRITERIA-3D

This paper has been submitted to *Engineering Geology* journal on 19 November 2024 and it is currently under review.

Abstract In this paper a three-dimensional agro-hydrological model for shallow landslides' prediction is presented. The model is an extension of the CRITERIA-3D free-source model for crop development and soil hydrology, developed by the Hydrometeorological service of the Regional Agency for Environmental prevention and Energy of Emilia Romagna region (Arpae-simc). The soil-water balance is computed through the coupling of surface and subsurface flows in multi-layered soils over areas topographically characterized by Digital Elevation Model (DEM). The rainfall infiltration process is simulated through a three-dimensional version of Richards' equation. Surface runoff, lateral drainage, capillarity rise, soil evaporation and plant transpiration contribute to the computation of the soil hydrology on an hourly basis. The model accepts meteorological hourly records as input data and outputs can be obtained for any time step at any selected depth of the soil profile. Among the outputs, volumetric water content, soil-water potential and the factor of safety of the slope can be selected. The validation of the proposed model has been carried out considering a test slope in Montuè (northern Italy), where a shallow landslide occurred in 2014 a few meters away from a meteorological and soil moisture measurement station. The paper shows the accuracy of the model in predicting the landslide occurrence in response to rainfall both in time and space.

Although there are some model limitations, at the slope scale the model results are highly accurate with respect to field data even when the spatial resolution of the Digital Elevation Model is reduced.

4.1 Introduction

Rainfall-induced shallow landslides and erosion are widespread phenomena that affect people and territories. Future projections show that global warming, because of the rise in temperatures, will increase the extreme rainfall events worldwide [15]. Extreme events can provoke shallow landslides with high probability in those territories that already present a series of predisposing factors. Shallow landslides, although involving small volumes of soil, represent a hazard since they don't show premonitory signs over territories [1]. Sometimes the material involved provokes a rapid evolution in debris or earth flows moving at very high velocities. Beyond the specific evolution of the phenomenon, a single extreme rainfall event over landslide-prone territories may cause a dense distribution of landslides [58]. Tools that can detect in advance the location and timing of landslides occurrences are of high importance, especially in countries that are hotspots for landslide hazard in Europe. Italy is a particular country of interest, being the first country in Europe for the number of landslide events [30]. Although some confusion exists in literature, hazard landslide assessment is defined as the probability of instability occurring within a given area and in a given period of time. It means defining "when" or "how frequently" a certain kind of landslide will occur [29]. Extreme climatic events are arising, and some of them are very destructive. An example is supplied by the May 2023 flood occurred in Emilia-Romagna region, where 65'598 shallow landslides were triggered and 78.5 % of them occurred in areas that were not included in available landslide inventories [167]. In fact, although most of the landslide prediction techniques have been based on the assumption of the stationarity of rainfall events, (i.e., considering that "the past is a guide for the future" as discussed by [3]) this condition is not anymore guaranteed under climate change forcings. Moreover, it is difficult to precisely detect the triggering time of a landslide during a precipitation event. In this perspective, physically-based tools for modeling processes acting at both surface and subsurface levels are of importance [168]. More particularly, the landslide occurrence constitutes the final step of a chain of processes that starts from the rainfall event and leads to the loss of the strengthening effect exerted by soil suction, and early warning systems should take into account the singular components in order to be used as real-time analysis tools. Determining a-priori when the

triggering moment will be reached, especially at distributed scales, is an ambitious task that is only partially solved by empirical methods such as the adoption of rainfall thresholds [169–171]. Physically-based methods, at the cost of major consumption of computational time and energy, constitute a flexible tool. In fact, when applied at large scales, physically-based models can account for several different transient processes when representing reality. This ability is not guaranteed by statistical or empirical methods, and the literature reports different examples of merging these two complementary approaches [172–174]. Storically, landslide detection methods have been based on saturated soil conditions, adopting the Terzaghi's effective stress principle, in which suction is quantified through saturated seepage theories [49, 74]. Although these methods obtain conservative measures of slope stability as they mostly consider restrictive assumptions (i.e., the soil is saturated, the water potential is positive and thus the soil strength is at its minimum value) they may not be accurate for practical landslide hazard assessment. In fact, as they appear not suitable to be adopted for near-real time landslides' detection tools such as early warning systems, where the consideration of transient suction effects is of high importance [175, 176]. During some field monitoring campaigns, different landslides have been observed to occur even when the soil was still in partially saturated condition, that is more likely to occur meanwhile a rainfall event is ongoing, as water content and pore water pressure changes affect the soil strength [177]. Only through physically-based models that consider unsaturated soil mechanics the triggering of such landslides can be predicted. Anyhow, especially when the soil moisture is high due to antecedent precipitation events, the saturation condition may be reached during the triggering rainfall event. Thus, when assessing slope stability, including initial or antecedent moisture conditions can raise the prediction accuracy and be a valid tool for civil protection purposes [40]. For the same reasons, as vegetation affects the soil water conditions, the modeling of its effects on both soil hydrological behavior and stability is an aspect that should be considered [**?**, 178], although it is still under debate if after heavy storms these effects are exerted or not [77, 179]. Nonetheless, predictive slope stability analyses of shallow landslides often neglect vegetation reinforcement effects, which are not completely explored yet. It is known that physically-based models can account for the above-mentioned aspects in slope stability computation, as they can quantify specific effects and their relative importance [180]. Physically-based models for triggering mechanisms of shallow landslides can give insights in landslide formation, delivering decision-makers deeper points of view for taking action and prevention measurements. At a regional or watershed scale, the use of three-dimensional hydrological models provides realistic representation of

soil conditions prior and during rainfall events, leading to an improvement in both space and time forecasting capabilities [125]. This is due especially to the possibility of modeling lateral redistribution processes and not only the vertical upward or downward water movements, as one-dimensional models do [131]. Moreover, three-dimensional models can consider complex topography that in most cases constitutes an important predisposing factor for shallow landslides [181]. Normally, landslide hazard assessment models are composed by an hydrological module interconnected with a geotechnical one [21]. The landslide hazard assessment in three-dimensional distributed models can be computed either considering stationary or transient hydrology. In this latter case, rainfall input over the spatial domain is a dynamic variable, which represents the real temporal pattern of rainfall. When the distributed model is related to very large areas, rainfall inputs should also be spatially interpolated based on real rainfall gauge records; in fact, evidence showed that the landslide spatial patterns are linked to the precipitation spatio-temporal resolution [182]. In addition, a further component that affects shallow landslides and can be modelled based on real meteorological data is the vegetation growth [183]. Such an aspect can constitute an advisable tool in relation to climate change adaptation strategies [184]. In fact, under climate change forcing, environmental conditions and their effect on the vegetation could not be accurately represented if a stationary plant coverage is adopted, especially because vegetation responses to climate are non-static components of the hydrological balances. The possibility of simulating roots and canopies dynamically can raise the insights provided by a model simulation. As it is well known, vegetation effects on slope stability have been studied in detail in the last decades [22]. However, not only the vegetation should be modeled as changing with time, but also its properties should be able to change together with the soil moisture and rainfall conditions [185]. Most of the three-dimensional distributed models adopt a unique, comprehensive soil water balance (SWB) equation comprising selected hydrological processes, such as the infiltration, which is commonly simulated through Richards' equation [186]. The use of Richards' equation implies that the soil is considered as an homogeneous porous medium; indeed, soil properties and structure are not spatially homogeneous [187, 188]. A source of spatial heterogeneity related to soil water flow is the presence of macro voids and preferential paths, through which water bypasses a large part of the soil matrix [189]. When drying, fine-grained soils can undergo the formation of soil cracking of different depths and widths, which constitute a typology of macro voids [190]. Soil cracking process is a complex phenomenon, although the flow behavior through them and their evolution has been characterized by several studies (e.g. [191–194]. It is known that the

amount of clay content promotes the crack formation, but crack formation in vegetated soil structures is still only partially explored [195]. It was shown that capillary forces resulting from soil drying can cause shrinkage and suction in soil mass [196] and induce cracks formation as consequence [197,198]. Involving complex soil hydrological processes such as the macropores flow in shallow landslides models could help in landslide prediction. An aspect that is rarely addressed when hydrological models are developed is the effect that the spatial resolution of input data may have on the outputs. More particularly, the Digital Elevation Model (DEM), which usually defines the mesh of the model computation, has been demonstrated to have an effect on numerical models' performance [14,199,200]. Testing the model output accuracy in relation to the input spatial resolution can give insights about the practical application of a proposed distributed model. In this work, the first application of CRITERIA-3D for predicting landslides' occurrence in a seminatural environment is presented. CRITERIA-3D is a physically-based model including an agro-hydrological module that solves soil-water balance accounting for vegetation activity and evolution, snow accumulation and melting, solar radiation and soil cracking formation. The original agro-hydrological module of CRITERIA-3D [153] has been extended introducing a slope stability computation module based on the limit equilibrium theory within the infinite slope scheme framework. The model allows to obtain time-varying maps of the Factor of Safety (FoS), which is calculated at different depths. The model is able to consider the differences existing in space and time of both canopies development and root density. Based on the validation carried out only in one dimension (CRITERIA-1D, [123]) the complete 3-dimensional model has been validated back-analyzing a real landslide occurred during the monitoring period on a test slope. Results showed that CRITERIA-3D is able to reproduce with high accuracy the field water content, the soil water potential behavior and the aerial geometry of the landslide. The effect of different spatial resolutions of the input Digital Elevation Model (DEM) has been tested in terms of both hydrological parameters and FoS of the slope. Some differences due to the resolution have been observed on the FoS more than in hydrological parameters' computation.

4.2 Model description

The agro-hydrological CRITERIA-3D model [153], after being improved and extended to slope stability analyses in one-dimension [123], has been adopted to carry out a three-dimensional slope stability analysis on a test slope. This section describes the basic components of the model, highlighting the further

improvements developed in the present research. It is worth specifying that, in the following, the term "water potential" is used as equivalent to "soil suction".

4.2.1 Hydrology

The CRITERIA-3D model [153] is based on a numerical solution of the three-dimensional Richards' equation. The model solves a global soil-water balance equation, coupling surface and subsurface flows, computing soil water fluxes and embedding conceptual models for crop development, evapotranspiration, snow accumulation and melting, and solar radiation, based on hourly weather data (Fig. 4.1). The needed input data are: a Digital Elevation Model (DEM) of the area of interest; a hourly meteorological time series comprising air temperature, precipitation, solar radiation, wind intensity and relative humidity records; a soil map with the parametrization of the different soil layers; a land use/crop map with the related parameters.

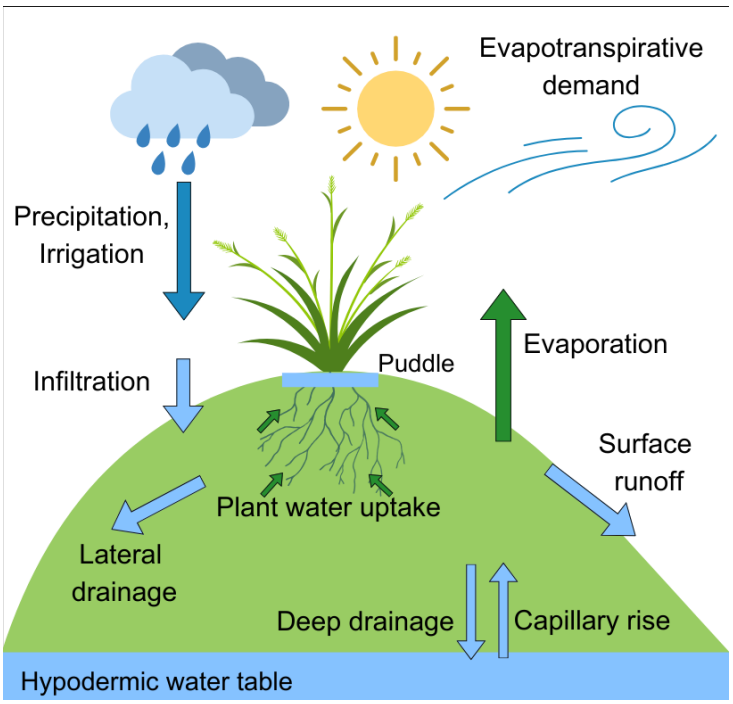

Figure 4.1: Representation of the CRITERIA-3D soil-water balance

CRITERIA-3D is able to consider multi-layered soil units, where each layer is characterized by different hydrological parameters and soil-water retention curves on the basis of the modified Van Genuchten-Mualem model proposed

by Ippisch et al. (2006) [154]. This latter can be either texture-based or field-derived, in the sense that fitting values for specific water potential values can be provided. The computation domain in CRITERIA-3D is discretized based on the Digital Elevation Model (DEM) used, which can be explored through a 3D interface. The DEM spatial resolution constitutes the 2D surface mesh. In plan, land use, soil and topographic maps are provided as Arcview Binary Raster format (.flt). Along the soil depth, computational layers with different thicknesses are set according to a geometric progression, which considers the shallow layers to be divided more finely with respect to the bottom ones. In fact, over the shallow portion of the soil, effects of evaporation, solar radiation and canopy coverage produce more complex soil-water fluxes that can be better represented when the vertical discretization is thinner. Soil information such as layer parameters are provided as SQL databases (.db). Results can be obtained in terms of maps (.flt) at specified hourly time steps for all the computational soil layers, and also in terms of hourly time series (.db) on selected output points. For both types of outcomes, the output variables can be referred to specific soil depths. Out of default results, the volumetric water content, the water potential and the degree of saturation can be required as model outcomes. The infiltration in the first layer is governed by its water content and its hydraulic conductivity, and by the surface boundary conditions. A pond depth connected to the presence of vegetation can be set, in order to simulate the effect of water accumulation. The pond is useful to simulate a delay in runoff process initiation, due to the presence of vegetation, during a rainfall event. The runoff is also regulated by the roughness parameter, which depends on the kind of vegetation. Canopies are also involved in the soil-water balance through the reduction of evaporation. Subsurface water movements across adjacent nodes are governed by hydraulic conductivity gradients, and develop as redistribution movements in all directions after the water infiltrates into the soil [153]. Although the one-dimensional approximation of water movements is normally referred to the vertical infiltration, in some cases the hydraulic conductivity along other directions may be different and higher than the vertical one, due to the soil pore structure [64]. The ratio between horizontal and vertical hydraulic conductivity, either saturated or unsaturated, is a measure of the hydraulic soil anisotropy, which depends on soil texture, on the current water potential, and on the variability range of hydraulic conductivity [201]. Although it is a complex phenomenon, for fine-textured soils some authors discussed how the unsaturated anisotropy ratio decreases toward a minimum value the more the soil dries [202]. A slight increase, after the minimum value is reached, is then observed until the soil approaches the minimum degree of saturation. In the CRITERIA-3D model it is possible to set a static horizontal/vertical

hydraulic conductivity ratio, although it was shown that it is a temporally variable parameter [203, 204]. The anisotropy ratio can help to increase the accuracy of the hydrological simulation in terms of numerical convergence. The required level of accuracy can be set by the user, on the basis of the desired model performance. Decreasing the required accuracy or using a wider DEM spatial resolution helps in the reduction of the computation time. The main output of the hydrology computation are the volumetric water content and the water potential for each soil layer.

4.2.2 Snow accumulation and melt

The snow melt is simulated in CRITERIA-3D based on the algorithm presented by Brooks (2003) and Brooks et al. (2007) [205, 206]. The method is based on mass and energy balance computed for the snow pack. Snow accumulation in drifts is derived through the Snow Tran-3D model [207], adjusted for the wind speed hourly measurements. The model, derived by Brooks (2003) [205], was modified in CRITERIA-3D by Bittelli et al. (2010) [153] introducing the effect of stream flow kinetic energy, the runoff liquid water temperature, the advective exchange between the runoff water and the snowpack. The snow accumulation and melting simulation allows the water infiltration to be delayed when the air temperature is at or below 0 °C. More details are provided in Bittelli et al. (2010) [153].

4.2.3 Soil cracking

An improvement with respect to the original version of CRITERIA-3D [153] is represented by the implementation of a conceptual model for soil cracking formation. In fact, as the hydrology is governed by matrix flow equations such as Darcy's law, the model was originally designed for undeformable and uniform soils. In order to appropriately simulate the hydrological behavior of fine soils, especially when there is a high percentage of fine particles, conceptual models were considered as possible solutions. In the updated version of CRITERIA-3D, it is assumed that cracks start to form when the void fraction overcomes a user-selected threshold. The void fraction is identified as the difference between the saturated soil water content and the current soil water content. After this threshold, cracks continue to enlarge until the void fraction reaches a user-defined upper boundary, where the soil cracking is at its maximum development. At this point, the soil is considered occupied by soil desiccation cracks for a certain percentage, which is set equal to 5% by default. Between the two boundaries, the soil cracking formation continues linearly [208] (Fig. 4.2).

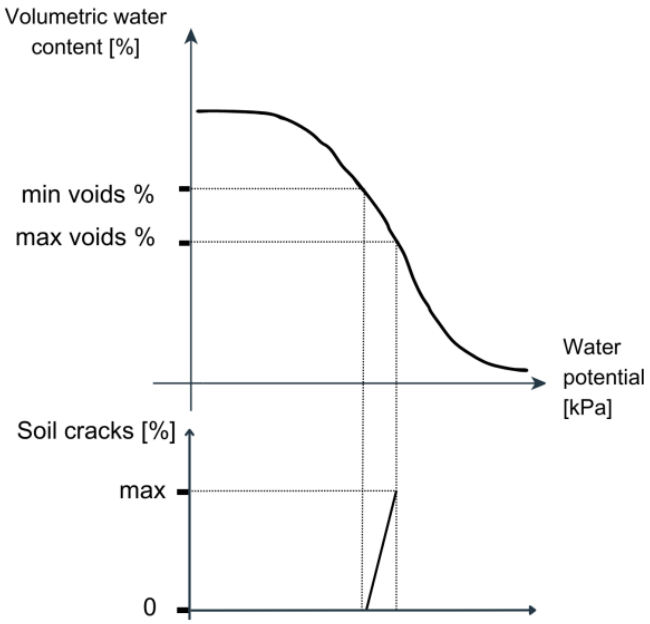

Figure 4.2: Schematic representation of the CRITERIA-3D soil cracking conceptual model

The soil percentage occupied by cracks is converted into an amount of infiltrating water that fills the soil layers from the bottom upwards. This water amount is calculated per each unit thickness of the soil (in centimeters), and starts from the maximum cracking depth, which is user defined. At this depth, a positive flux amount (mm/cm) is assigned. Depending on the rainfall amount falling, the crack will continue to be filled as long as voids and rainfall are present. This effect will occur only if the encountered soil layers, from the maximum cracking depth to the surface, have fine fraction content, defined as the sum of silt and clay content, higher than 50%, and in relation to the gravel percentage. In fact, as shown by Yesiller et al. (2000) [209], the percentage of fines in a soil is an important factor in causing desiccation cracking [198]. With this conceptual model, CRITERIA-3D approximates the first-order crack formation; in fact, these cracks are wider and longer compared to the second- and third-order cracks [64]. As only the soil permeability changes with the pore size distribution, maintaining the same SWCC [210] and assigning a positive flux to nodes interested by the cracks' formation can be considered an appropriate assumption.

4.2.4 Crop modeling

The crop modeling approach is the same adopted in the CRITERIA-1D model, which is described in Sannino et al. (2024) [123], and in the CRITERIA-1D/3D technical manuals [150, 156]. Growth and decay of both roots and canopies throughout the year are modeled based on real meteorological data through the growing thermal time of the crop [211, 212]. Depending on air temperatures, the vegetation stores specific amounts of heat based on a thermal threshold. These heat amounts are accumulated in growing degree days (GDD, Sannino et al., 2024 [123]). Specific thresholds are set in order to determine whether the plants accumulate heat and are in selected phenological stages. This scheme is adopted in CRITERIA-3D for both crops and natural environments, and the different growing phases can be modified to approximate the real phenology of the considered species, in a specific habitat. Moreover, CRITERIA-3D allows to consider different land uses, as input maps, in terms of vegetation type. Each vegetation type is characterized by specific parameters conceiving the plant species, the roots' architecture and depth, the evapotranspirative activity, the growing degree days that are necessary to change phenological stage, the canopy development over the year, and the crop coefficient k_c [213]. After the vegetation emergence, maximum evaporation and maximum transpiration are derived from the reference evapotranspiration (ET_0), following the approach of Driessen and Konjin (1992) [214] with some modifications. The maximum evaporation (E_{max}) is defined through Equation 4.1:

$$E_{max} = (1 - K_c) * ET_0 \tag{4.1}$$

While the maximum transpiration ($Transp_{max}$) is derived through Equation 4.2:

$$Transp_{max} = K_c * TC * ET_0 \tag{4.2}$$

Where $TC = 1 + (K_{cmax} - 1) * K_c$; TC is the turbulence coefficient [-], defined through the maximum value of k_c ($K_{c\ max}$) as proposed by Doorenbos and Kassam (1979) [215]. The crop coefficient k_c is a function of the leaf area index (LAI) (Eq. 4.3):

$$k_c = 1 - e^{-k_e * LAI} \tag{4.3}$$

Where:

k_c = crop coefficient [-];
k_e = extinction factor, equal to 0.5 [-];
LAI = Leaf Area Index [-].

Reference evapotranspiration (ET_0) is obtained on an hourly basis through the Penman-Monteith method as reviewed by Allen et al. (1994) [216]. ET_0 depends on solar radiation, wind intensity, air temperature, and relative humidity (Eq. 4.4). Potential evaporation and transpiration are then limited to their actual values by the effective soil water availability.

$$ET_0 = \frac{0.408\Delta * (R_n - G) + \gamma_p \frac{900}{T_{avg}+273} u(e_s - e_a)}{\Delta + \gamma_p(1 + 0.34u)} \tag{4.4}$$

Where:
ET_0 = reference evapotranspiration [mm];
R_n = net solar radiation [MJ/m^{2}d];
G = net heat flow from the ground [MJ/m^{2}d] ;
Δ = slope of the function of saturated vapor [kPa/°C];
γ_p= psychrometric constant [kPa/°C];
T_{avg} = average air temperature [°C];
u_{wind} = daily average wind speed at 2 meters height [m/s];
$e_s = 0.6108e^{\frac{17.27*T_{avg}}{T_{avg}+237.3}}$ is the average pressure of vapor in air saturation [kPa];
e_a = average pressure of vapor [kPa].

In these terms, the evapotranspiration is obtained on an hourly basis as a function of both meteorological data and vegetation condition, as the crop coefficient k_c is used to compute the actual hourly transpiration and evaporation from the reference evapotranspiration, passing through the maximum possible values. In fact, E_{max} and T_{max} (Eq. 4.1 and 4.2) are then reduced to the actual values based on the real soil moisture condition of the shallow layers and the rooted soil layers, respectively.
As already stated in the previous "hydrology" section, in CRITERIA-3D a pond depth can be set. This depth is used to assess the amount of water that is necessary to be accumulated before runoff starts and to compute the actual evaporation as well. It is a proxy for how much canopies can decelerate the rainfall infiltration. The maximum pond depth is reduced as a function of the actual leaf area index (that depends on the phenological stage of the plant) and the local slope, in order to approximate the effect of real morphology on the interception action of canopies.

4.2.5 Boundary conditions

The following default boundary conditions are set in CRITERIA-3D: free runoff at the surface nodes and free drainage at the bottom layer nodes. Atmospheric boundary conditions can be either positive flux (precipitation) assigned to the surface, or negative flux (potential evapotranspiration) assigned to the layers where roots are present. From a temporal point of view, CRITERIA-3D uses meteorological input data corresponding to at least one year to set up an accurate initial wetness state of the soil domain.

4.2.6 Slope stability

The slope stability is assessed through the calculation of the Factor of Safety (FoS) for each computational element. The computational elements are constituted by rigid soil blocks, with a cross section area corresponding to the DEM spatial resolution and a thickness corresponding to that of each soil layer 4.3. This allows the CRITERIA-3D model to calculate FoS at different depths. The limit equilibrium method within the infinite slope framework is adopted [123]. The soil is assumed as a rigid-plastic material and its shear strength is expressed through the Mohr-Coulomb criterion.
The equation used to calculate hourly values of FoS is derived from Lu and Godt (2008) [74] (Equation 4.5). Based on the suction stress concept (σ^s), the method takes into account the whole range of soil moisture conditions and their effect on soil strength:

$$FoS = \frac{\tan \phi'}{\tan \beta} + \frac{2c_{tot}}{\gamma H_{ss} sin2\beta} - \frac{\sigma^s}{\gamma H_{ss}}(\tan \beta + \cot \beta) \tan \phi' \qquad (4.5)$$

Where:
$\sigma^s = -\frac{\theta - \theta_r}{\theta_s - \theta_r}(u_a - u_w)$;
c_{tot} = c'+ c_r;
c' is the effective soil cohesion [kPa];
c_r is the root mechanical contribution [kPa];
θ is the actual soil water content [m^3/m^3];
θ_r is the residual water content at the wilting point [m^3/m^3];
θ_s is the saturated water content [m^3/m^3];
ϕ' is the friction angle [°];
β is the slope angle [°];
H_{ss} is the depth of interest [m];
γ is the unit weight of the soil [kN/m^3].

The different soil layers can be characterized by different parameters. The

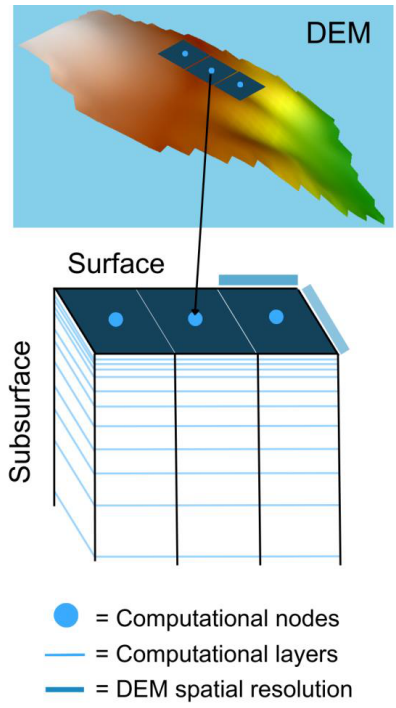

Figure 4.3: Schematic representation of the CRITERIA-3D computation domain

time-varying suction stress is determined based on the hydrological outputs (volumetric water content and soil-water potential). The soil strength parameters are: the effective cohesion (c'), the friction angle (ϕ'). The bulk density is converted to soil unit weight (γ). These parameters can be user-defined, otherwise CRITERIA-3D can assign them based on the soil texture, using empirical pedotransfer functions. Specifically, parameters' values were derived from García-Gaines and Frankestein (2015) [217], based on soil classes from the Unified Soil Classification System (USCS, [218]) associated with those from the United States Department of Agriculture (USDA, [219,220]). The texture-derived values of these parameters are considered to be highly approximative and their use is recommended only if there is lack of experimental data or no available data in literature. The root cohesion (c_r) must be selected by the user. If the maximum root cohesion is available as derived by literature studies or field measurements, it could be inserted as a crop parameter and it will be associated to the soil layer with the maximum root density. Then, the value will be reduced based on the real presence of roots in the other soil layers.

4.3 Test slope at Montuè

The CRITERIA-3D model has been validated based on field data acquired on a test slope, which is located in Montuè, Northern Apennines, Italy (Figure 4.4). A monitoring station has collected meteorological and soil data since 2012 [58, 161]. A sketch of the monitoring station and the installed sensors is provided in Figure 4.5.

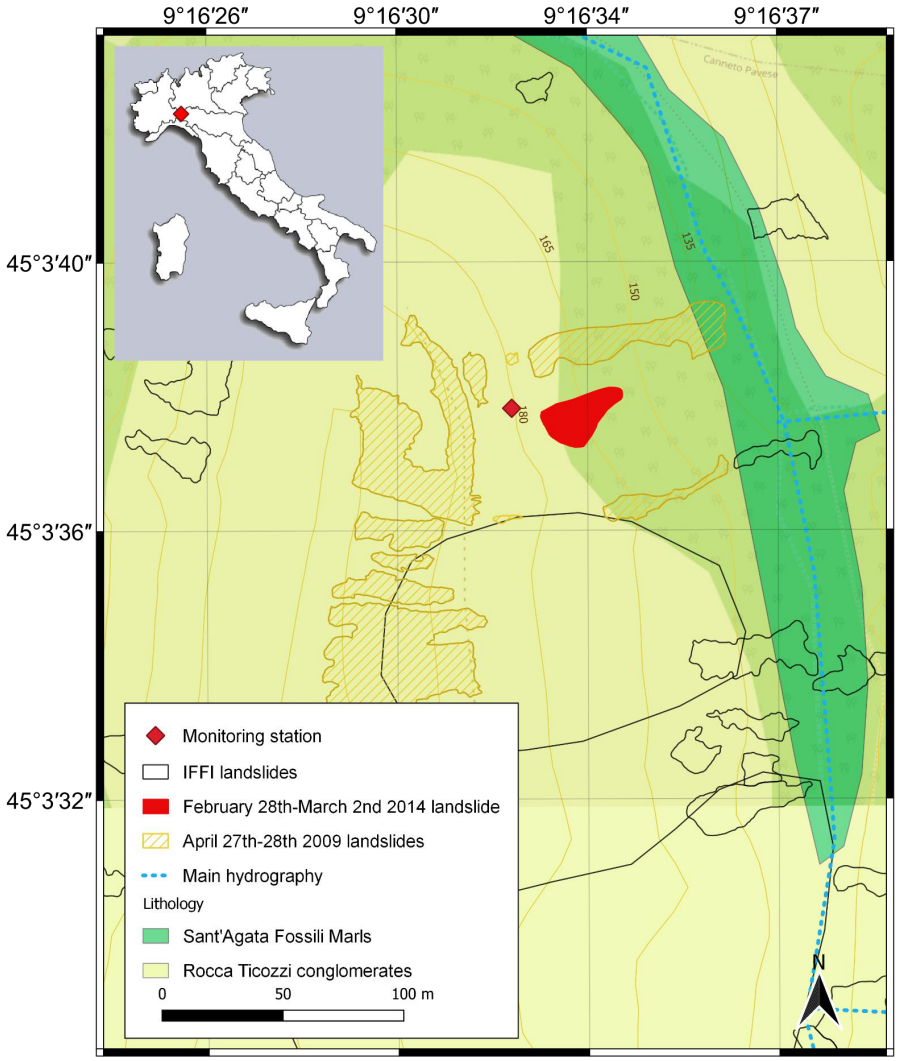

Figure 4.4: Study area of CRITERIA-3D validation

The integrated monitoring station includes a rain-gauge, a thermo-hygrometer, an anemometer, a net radiometer, and a barometer, as meteorological sen-

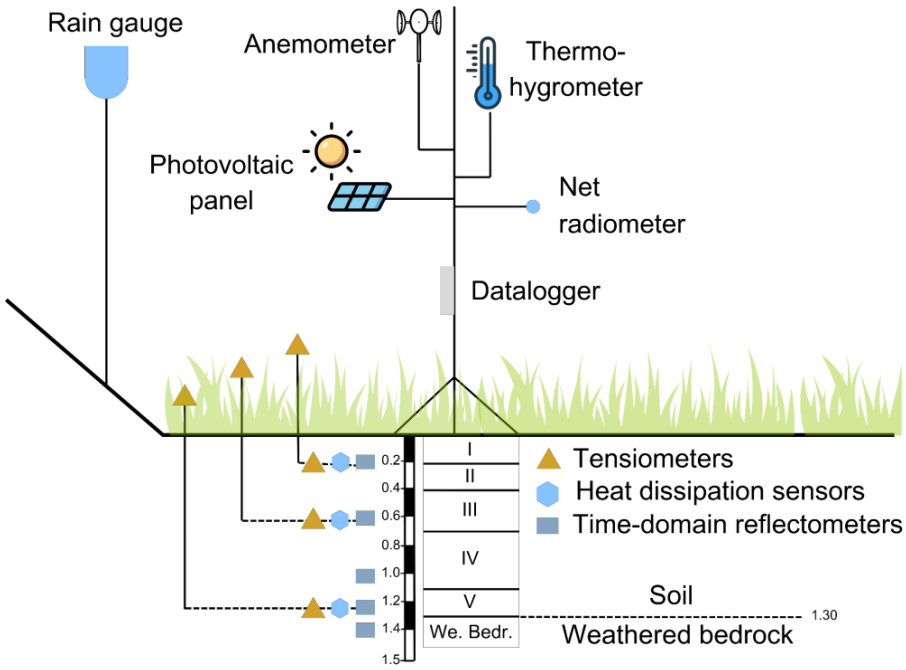

Figure 4.5: The monitoring station

sors. Moreover, six time-domain reflectometer probes with a multiplexer are installed at 20, 40, 60, 100, 120, and 140 cm to measure soil water content, while three tensiometers and three heat dissipation sensors are installed at 20, 60, and 120 cm from the ground level to measure the pore water pressure. Specific information about the installed sensors are provided by Bordoni et al. (2015) [58] and by Sannino et al. (2024) [123]. The first documented shallow landslides in the area surrounding the test slope occurred in 2009, due to a rainfall of 160 mm in 62 h [58]. After that event, the monitoring station was installed. A new shallow landslide occurred on the test slope, a few meters away from the monitoring station, between 28 February and 2 March 2014, at a depth of 100 cm, due to a rainfall event of 68.9 mm in 42 h [58].

4.4 Model application

4.4.1 Soil layers' parametrization

In this section, the parameters used to apply CRITERIA-3D in the case study of Montuè are described in detail. The soil layers are the same used in the CRITERIA-1D model simulation [123] since the test site was the

same. The values assumed for both mechanical and hydrological parameters, based on field experimental campaigns, are listed in Table 4.1 and Table 4.2, respectively. In particular, to compute the water potential and the equivalent degree of saturation, CRITERIA-3D uses the modified van Genuchten–Mualem formulation proposed by Ippisch et al. (2006) [154]. The hydraulic conductivity function is calculated through the approach presented by Mualem (1976) [221]. The parameters needed for the soil-water retention curves are: the curve fitting parameters α, n, m, and the air entry value h_e, which characterizes the transition between saturated and unsaturated regime. These parameters are estimated based on the soil texture and the fitting values, when provided. It is assumed that the soil layers are the same, keeping their constant thickness, everywhere along the slope.

Table 4.1: CRITERIA-3D mechanical parameters at Montuè test site for different soil layers

Soil layer	Depth range [cm]	Coarse fragment [%]	Organic matter [%]	Sand [%]	Silt [%]	Clay [%]	Bulk density [g/cm3]	c' [kPa]	ϕ' [°]
I	0-22	0	1.44	16.6	58	25.4	1.559	0	31
II	22-42	0	1.36	11.9	59.9	28.2	1.534	0	31
III	42-70	0	1.03	16.0	53.9	30.1	1.495	0	33
IV	70-110	0	0.88	12.6	57.9	29.5	1.518	0	33
V	110-130	0	0.62	7.7	65.8	26.5	1.418	29	26
We. Bedr.	130-145	0	0.2	75	25	0	1.532	29	26

Table 4.2: CRITERIA-3D hydrological parameters at Montuè test site for different soil layers

Soil layer	Depth range [cm]	θ_r [m^3/m^3]	θ_s [m^3/m^3]	K_{sat} [m/s]	h_e [kPa]	α [kPa^{-1}]	n [-]	m [-]
I	0-22	0.00	0.40	7E-07	2.6	0.049	1.279	0.218
II	22-42	0.01	0.41	2E-07	3.1	0.049	1.290	0.225
III	42-70	0.00	0.43	2E-07	3.1	0.044	1.243	0.195
IV	70-110	0.00	0.42	3E-07	3.1	0.104	1.310	0.237
V	110-130	0.04	0.46	3E-07	2.6	0.049	1.263	0.208
We. Bedr.	130-145	0.01	0.42	2E-07	1.0	0.034	1.329	0.247

As already discussed, in CRITERIA-3D soil hydrological anisotropy is simulated through the ratio between the horizontal hydraulic conductivity and the vertical hydraulic conductivity. In simulations related to the Montuè test site this ratio has been set equal to 4. This ratio is applied both at unsaturated and saturated hydraulic conductivities, and, due to the lack of more accurate data, it was calibrated according to field water content data and simulation outputs. The considered simulation period spans from 1st January 2012 to

30th April 2014. In this way, a period of at least one year before the landslide occurrence could be simulated, in order to reproduce a reliable soil moisture condition at the date of the landslide. Indeed, the landslide was triggered at an unspecified time during the rainfall event that occurred between 28th February and 2nd March 2014. By observing the field data, it was evident that the soil at Montuè underwent the formation of desiccation cracks during the previous dry season (summer) in 2013, evidenced by an uprising of soil water content at 40 and 60 cm of depth without a corresponding increase of water content in the upper and lower layers [123]. The parameters chosen to simulate the soil cracking formation, based on field water content and pore water pressure records, are listed in Table 4.3. The upper and lower bounds

Table 4.3: Soil cracking parameters

Maximum soil crack depth	60 cm
Minimum voids for cracks formation initiation	15 %
Voids for cracks formation ending	20 %
Maximum soil percentage covered by cracks	5 %

of void percentage were chosen in order to represent a range of moisture below the field capacity water content (i.e., the soil water content when all the micropores are filled) and higher than the wilting point water content (i.e., when the residual water is immobilized by the soil particles). This simplification, in absence of more detailed data, was adopted also according to the field observations [161]. Some authors highlighted that crack develops until a steady-state development stage, and the crack opening, intended as the soil volume occupied by cracks, varies from 0 to approximately 5 % [210]. The value of 5 % as maximum soil percentage covered by cracks was selected also according to literature data for vegetated soils and soils reinforced with vegetation fibers (e.g. [198, 222, 223]). The soil crack percentage is converted in a positive flux of 0.5 mm/day assigned firstly to nodes at 60 cm of depth and to the above nodes up to the surface, only if the fine fraction, defined as the percentage of total clay and silt content related to the coarse fragments content, is more than 50 %; this threshold was chosen to represent the fact that the soil crackings only form when the soil is fine-textured enough, even if the voids percentage is between 15 % and 20 %. Since at the Montuè test site this threshold is overpassed (Table 4.1), soil cracks are considered to have formed up to 60 cm of depth.

4.4.2 Land use and vegetation parametrization

The land use at the test site was derived from aerial photographs of 2009 (when other landslides occurred) and 2014, assuming that the 2009 coverage was valid for the whole simulation period, in absence of more detailed data. By observing the satellite photographs, three land uses were detected: a bare soil corresponding to a trail, a shrubland, and a young woodland. The 2014 landslide occurred in the woodland zone, just behind the transition between the two land uses (Figure 4.6). It is evident that some vegetation has grown around the monitoring station after 2009. Figure 4.7 reports the landslide scar, the monitoring station, and the output points chosen to validate the model outputs. More precisely, a point was chosen to represent the monitoring station (MS) and the other 5 points represent the landslide (points L1, L2, L3, L4 and L5).

Figure 4.6: Land use at Montuè case study

The 1-m DEM is considered to best represent the real topography of the test slope. It was realized through LIDAR data acquired in 2008 and 2010 by the

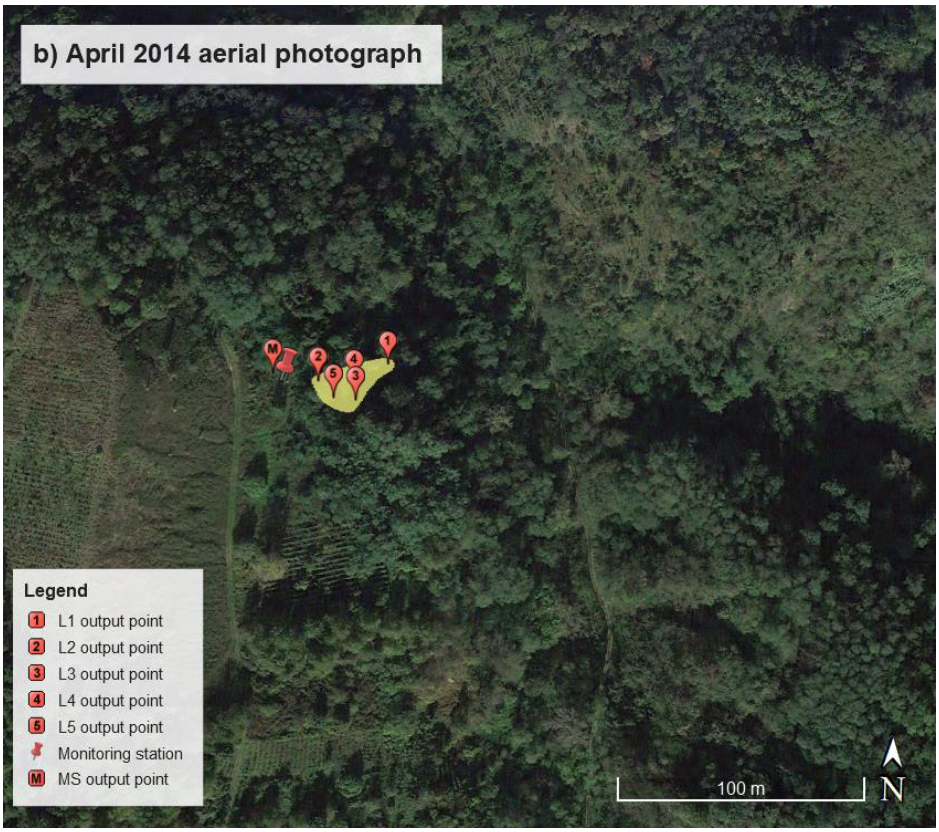

Figure 4.7: Location of the monitoring station, landslide and output points at Montuè case study

Italian Ministry for Environment, Land, and Sea.
The selected computational area has an extension of 14,547 m^2 and has been subdivided according to the real land use. As it will be explained in the following, this starting DEM has been resampled, in order to test the sensitivity of the simulation in relation to different DEM spatial resolutions. The different types of vegetation and land use present were parameterized through the values listed in Table 4.4. Figures 4.8 and 4.9 report a comparison between the difference in LAI development, evaporation and transpiration activities over the 2014, i.e. the year when the landslide occurred, for the two chosen land uses.

Table 4.4: Soil land use and crop parameters at Montuè test site

	Shrubland	Woodland	Road
LAI min [-]	0.5	1.0	-
LAI max [-]	3.0	4.0	-
Depth of first roots (RD_0) [m]	0.05	0.05	-
Maximum root depth (RD_{max}) [m]	1.4	1.45	-
Lower thermal threshold [°C]	3	0	-
Upper thermal threshold [°C]	35	35	-
Degree days phase 1	1000	2500	-
Degree days phase 2	1000	1000	-
$K_{c\ max}$	1	1	-
LAI curve factor a	4.1	4.1	-
LAI curve factor b	-0.014	-0.014	-
Root architecture shape	cardioid	cardioid	-
Root shape deformation factor [-]	0.0	0.0	-
$\psi_{\ leaf}$ [kPa]	1470.96	1569.02	-
C_r [kPa]	-	-	-
Roughness [$s/m^{1/3}$]	0.05	0.1	0.03
Pond depth [m]	0.006	0.006	0.003

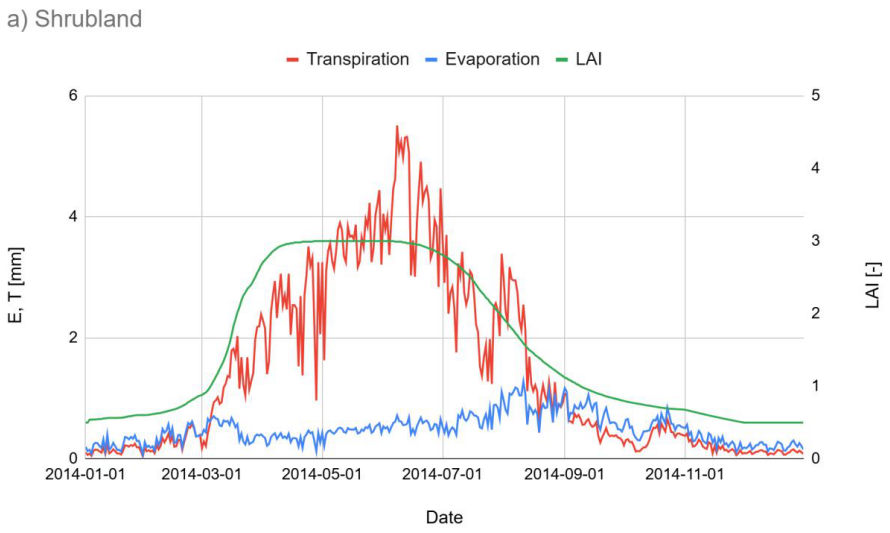

Figure 4.8: Leaf Area Index (LAI, green line), transpiration (T, red line), evaporation (E, blue line) development over the landslide year 2014 of the shrubland land use

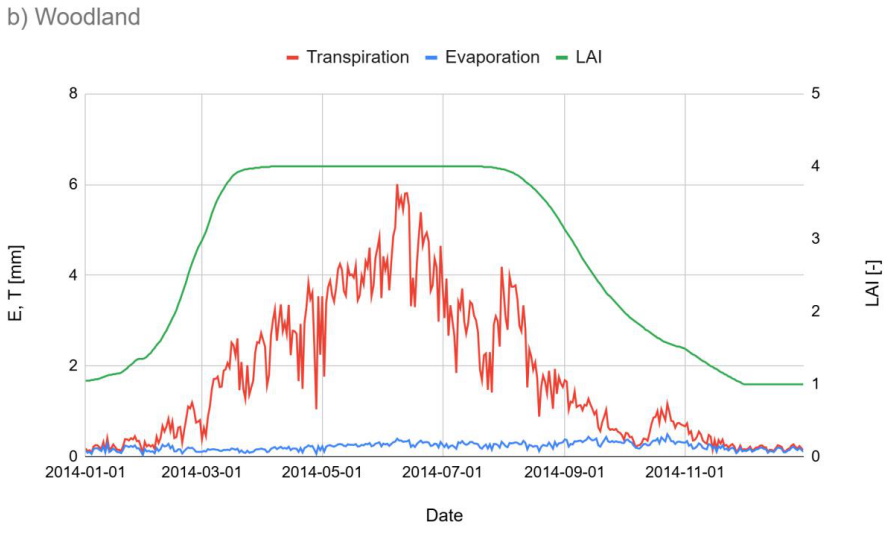

Figure 4.9: Leaf Area Index (LAI, green line), transpiration (T, red line), evaporation (E, blue line) development over the landslide year 2014 of the woodland land use

4.4.3 Model settings

In order to test the model performance, different analyses habìve been carried out by changing the DEM spatial resolution. The starting DEM with a resolution of 1 m was resampled through the algorithm saga:resampling by QGIS, deriving DEMs with spatial resolutions of 2 m, 5 m, and 10 m. The analyses were conducted keeping constant values of all other input parameters (i.e., the meteorological records, soil and crop parameters) and the same output control points. The aim was to test whether the CRITERIA-3D model is sensitive to different input resolutions. As represented in Figure 6b, six output control points were selected: one represents the position of the monitoring station (point 'MS'), which has been used to validate both water content and water potential simulations; four out of other five points are positioned along the scar contour and one point is in the middle of the 2014 landslide (points named 'L' followed by numbers). Hourly results related to the vertical positions where sensors are installed (namely, at 20, 40, 60, 100, 120, and 140 cm of depth) have been analyzed individually and also averaged, in order to obtain mean values related to the whole soil profile. Field hourly data related to the same depths have been also averaged for comparison. Hourly slope stability analyses were conducted using the different DEMs, and FoS was calculated at selected computational depths (namely, at 1, 3, 5, 10, 20, 60, 100 and 120 cm); however, only the hourly outputs related to representative depths of 10, 60 and 100 cm will be presented in the following section.

4.5 Results and discussion

4.5.1 Hydrological results

As already stated, different depths were selected for the hydrological computation and results were averaged. For the sake of conciseness, Figure 4.10 shows the comparison between the mean values of both observed and computed soil water content. Figure 4.11 shows the comparison between the values of observed and computed water potential at 60 cm of depth, which is the depth with less missing values in the field measurement series. The R_2 values reported in Table 4.5 and in Table 4.6 are related to the comparison between modeled and observed values of the volumetric water content (VWC) and the water potential (WP), respectively, at the investigated depths for different DEM resolutions. Specifically, the values correspond to the output point called 'MS' (Figure 4.7).

Table 4.5: Comparison between modeled and observed values of volumetric water content (VWC), at different depths and with different DEMs, in terms of R^2 at the output point 'MS'

DEM resolution	20 cm of depth	40 cm of depth	60 cm of depth	100 cm of depth	120 cm of depth	140 cm of depth	Whole profile 0-145 cm
1m	0.911	0.915	0.898	0.918	0.839	0.918	0.941
2m	0.918	0.921	0.900	0.918	0.839	0.915	0.944
5m	0.916	0.920	0.901	0.919	0.838	0.915	0.945
10m	0.917	0.919	0.899	0.917	0.839	0.915	0.943

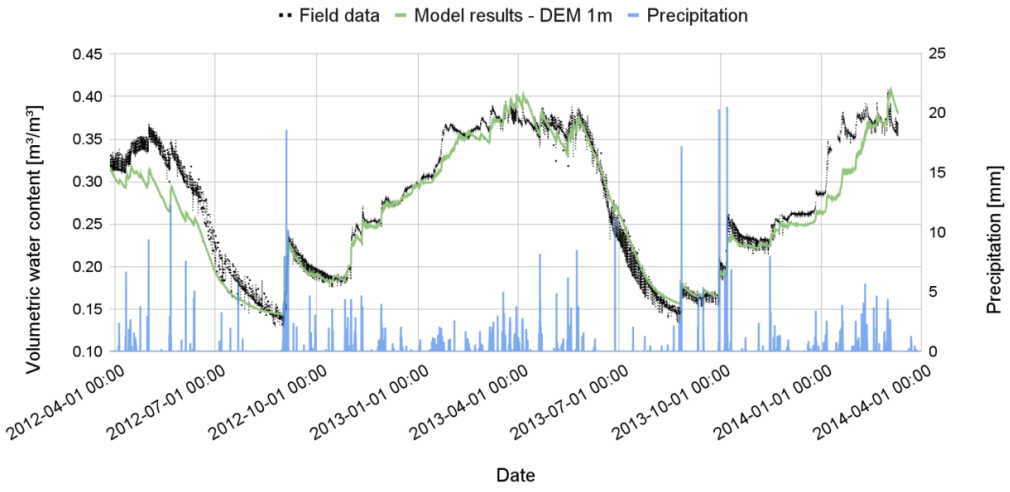

Figure 4.10: Comparison between mean values of simulated and observed water content for the whole soil profile (0-145 cm) using the 1m-DEM

Table 4.6: Comparison between modeled and observed values of water potential (WP), at different depths and with different DEMs, in terms of R^2 at point 'MS'

DEM resolution	R_2 observed vs simulated soil water potential at 20 cm	R_2 observed vs simulated soil water potential at 60 cm	R_2 observed vs simulated soil water potential at 120 cm
1m	0.691	0.880	0.803
2m	0.705	0.885	0.810
5m	0.700	0.882	0.806
10m	0.707	0.887	0.811

The different DEM spatial resolutions considered seem not to have a significant impact on the soil water content and soil water potential simulations.

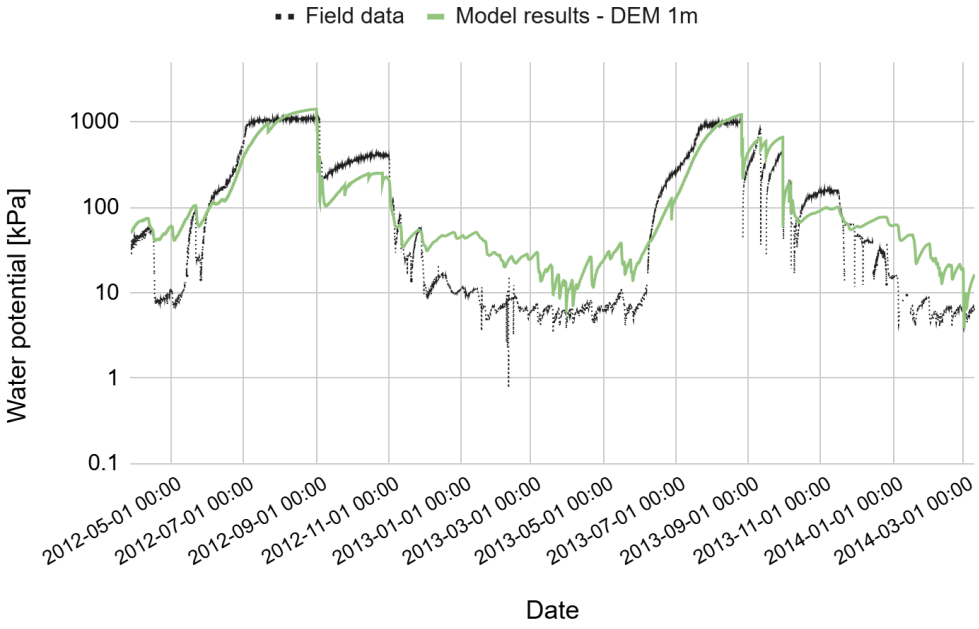

Figure 4.11: Comparison between simulated and observed water potential at depth of 60 cm using the 1m-DEM

This is maybe due to the limited spatial extent of the whole computational domain. The simulation conceiving the soil water potential obtained through a coarser DEM resolution has the best performance at all the considered depths (Table 4.6). For what concerns the soil water content, results' accuracy changes depending on the considered depth, and it is not possible to declare which DEM provided the best results. If the whole averaged soil water content is considered, the 5m-DEM seems to provide the most accurate simulation, although only little differences are present among the different simulations. Figures 4.12 and 4.13 report the model results in terms of time-varying hydrological maps related to the test slope. In particular, Table 4.12 reports the output in terms of volumetric water content, and Figure 4.13 reports the output in terms of water potential. The maps refer to two different time instants, which are representative of the states before and after the landslide occurrence, respectively. The first selected time is at 6 a.m. on 1 March 2014, i.e. one day before the triggering of the landslide, as detected by CRITERIA-3D; the second selected time is at 6 a.m. on 2 March 2014, i.e. when the instability reaches 100 cm of depth, based on the model simulation, as it will be explained in the following section on FoS. The maps, which have been derived using the 1m-DEM for computation, report the re-

sults corresponding to the representative depths of 30, 60, 100, and 140 cm, even though similar results are available for all the different computational depths.
As shown in Figures 4.12 and 4.13, for what concerns the hydrological conditions during the landslide occurrence, the maps related to the most superficial layers appear to be more homogeneous than those related to higher depths. In fact, soil water accumulates more in the hollow portions of the slope, which can be easily recognized in the maps as the slope area beneath the landslide scar and the area located some meters away from it. At the border of the computational domain, some pixels are also computed as saturated (nil or positive values of WP, Figure 4.13) and a slight concave area is also present there. The effects on hydrology exerted by the surface topography appear to be well captured by the three-dimensional model. By looking at the hydrological output maps, it could be assumed that the landslide has occurred because of the saturation of the soil profile down to 100 cm of depth. The water seeping downward and the lateral subsurface processes provoke the saturation of the hollows, and the shallower layers seem to saturate earlier in time, as they have a high moisture level while the underlying layers still don't (Figure 4.12). More precisely, the infiltration process seems to be slowed down in the soil layer III (Tables 4.1, 4.2 and Figure 4.5), which develops between 42 and 70 cm of depth. The depth of 60 cm belongs to this layer, and it is slightly more wet than the layer at 40 cm.

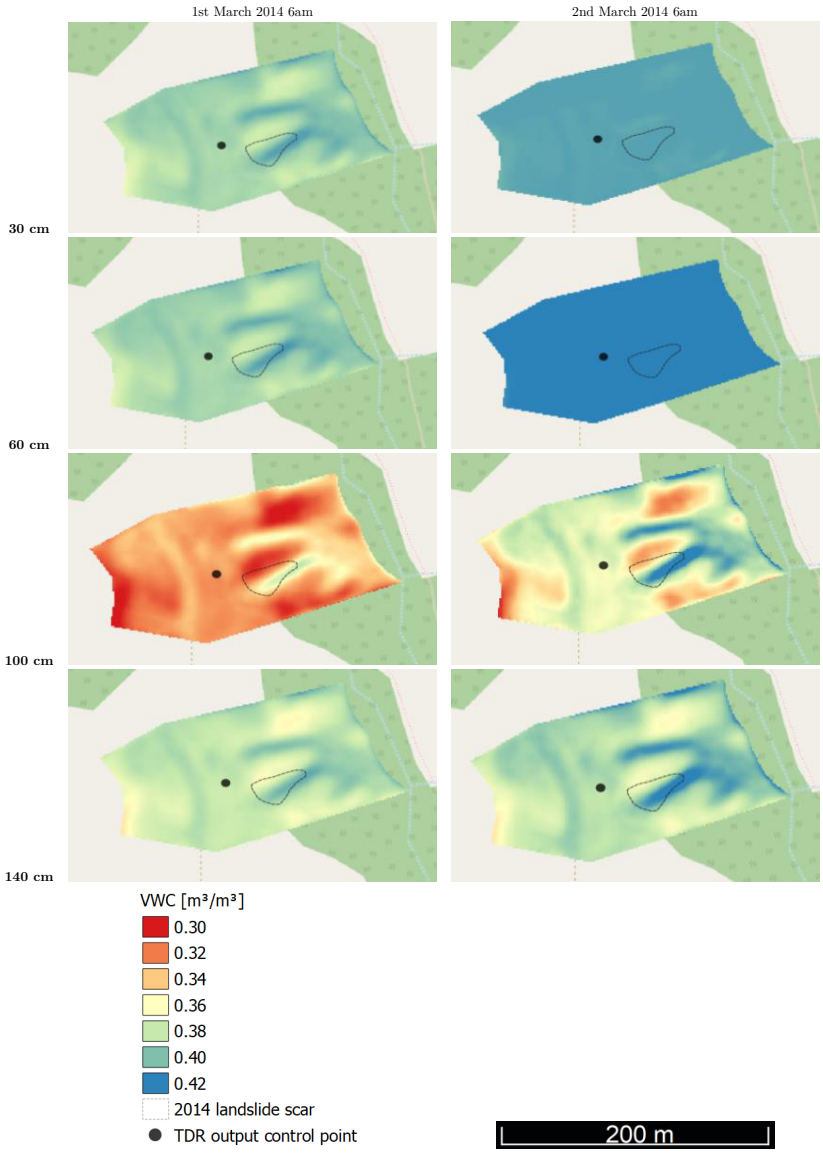

Figure 4.12: Volumetric water content output maps before (1st March 2014) and during the landslide occurrence (2nd March 2014) at different depths

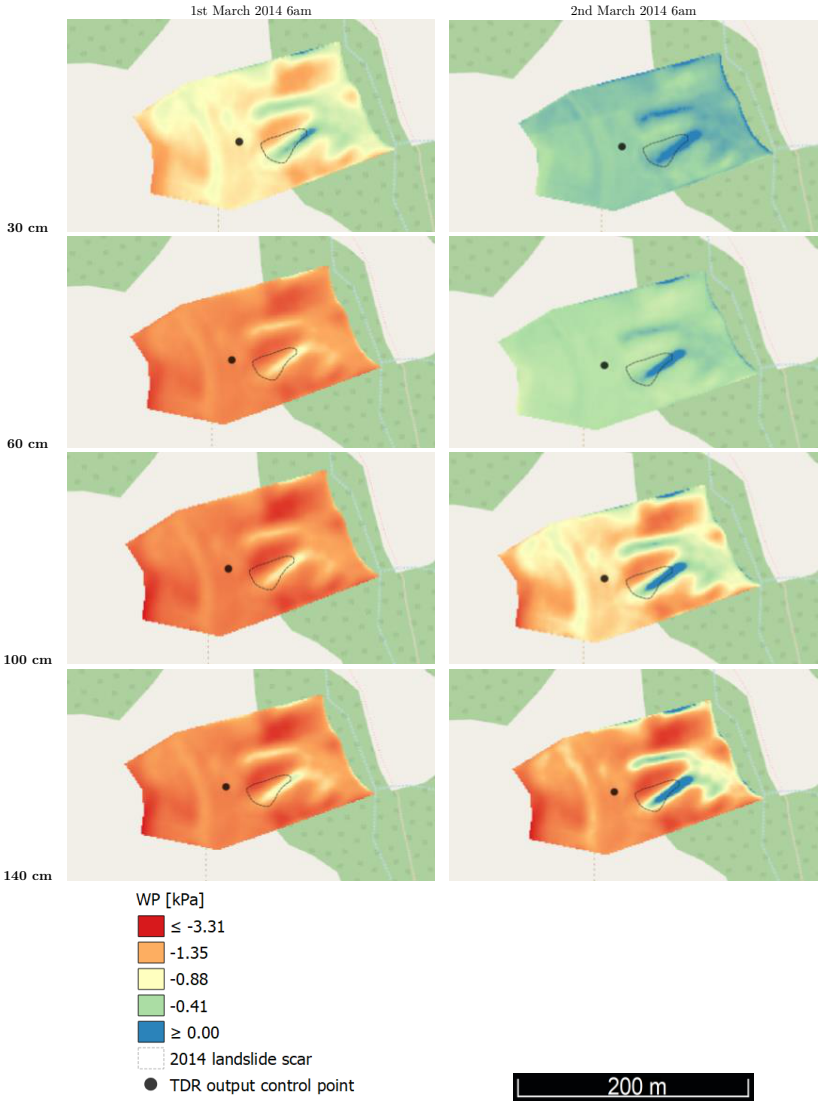

Figure 4.13: Water potential output maps before (1st March 2014) and during the landslide occurrence (2nd March 2014) at different depths

4.5.2 Slope stability analysis

Figure 4.14 shows the trend of the Factor of Safety (FoS) in the analyzed time span, calculated at three different depths, i.e. at 20, 60, and 100 cm, respectively, assuming different DEM resolutions. It can be noticed that the unstable condition (FoS < 1) at 100 cm of depth, which is represented by the blue line in the graphs, is detected at a spatial resolution of 1m, 2m, and 5m on the expected date of 2 March 2014. Indeed, 100 cm was the field observed depth of the failure surface [123]. Instead, when using the 10 m resolution DEM, the landslide is not detected by the model, as the FoS at 100 cm of depth never drops below one. On the other hand, FoS at 20 cm of depth (green line in the figures contained in Figure 4.14) becomes lower than one several times, evidencing a sensitivity of the shallow soil layer to different rainfall events occurring during the wet season after winter, when the soil is nearly saturated.

Figure 4.15 reports the resulting maps for the Factor of Safety obtained through the computational domain derived from different DEM resolutions. The maps refer to two different dates: 1 March 2014 at 6 a.m., i.e. one day before the landslide modeled occurrence, and 2 March 2014 at 6 a.m., i.e. when the unstable condition (FoS < 1) is reached at 100 cm of depth, which is the field observed depth of the failure surface. As it could be observed from Figure 4.15, the landslide is appropriately detected when adopting a DEM spatial resolution of 1, 2, and 5 m. Instead, using the DEM resolution of 10 m appears not satisfactory. This may be due to the attenuated effect of slope angles due to the topography simplification when reducing the DEM spatial resolution. Moreover, enlarging the DEM input resolution modifies the local detail of the input hydrological parameters, and so the instability conditions that may develop in a point of the domain could not be well represented, although the model responses to mesh variations can be complex and scale-dependent [199, 224, 225]. In all the simulations, except for the one with the 10 m DEM, at the border of the spatial domain some pixels are wrongly detected as unstable. This is due to the presence of a small depression, where infiltrated water accumulates. The topography effect is clearly visible in all the simulations, as the Factor of Safety (and thus, the water content) simulation clearly highlights the differences in hollow and caves present over the test slope.

It could be argued that the unstable pixels (the red ones in Figure 4.15) only partially overlap the landslide scar. It can be observed that the proposed model adopts a simplified stability analysis where mechanical aspects such as the propagation of the instability due to deformations and movement of unstable portions of soils are neglected. Nonetheless, the results appear

satisfactory in that the landslide-related hazard is appropriately assessed in both space and time. Figure 4.16 reports the model outcomes in terms of time-varying maps of Factor of Safety (FoS) calculated at different depths. FoS maps are shown referring to: a) different time steps, before and during the landslide occurrence, namely, 28 February 2014 (11 p.m.), 1 March 2014 (6 a.m.), and 2 March 2014 (6 a.m.); b) different depths, namely, 10, 30, 60, 100, and 140 cm of depth; c) 1-m spatial resolution DEM only. It can be seen that the landslide (FoS < 1) is correctly predicted in the expected position, involving soil layers down to 100 cm of depth. One day before the landslide, some pixels at 30 cm of depth are detected as unstable in the landslide body and at the border of the domain. Field data to corroborate whether some surficial processes like this have effectively occurred are not available. However, at the current model development, considering the lack of detailed data, obtaining very shallow soil portions detected as unstable is not considered as relevant for the shallow landslide prediction.
As it can be observed in Figure 4.16, during the landslide (2 March 2014 at 6 a.m.), not only the landslide scar and other shallow portions of the domain are detected as unstable at 30 cm of depth, but also some parts at the border of the computational domain and where a second hollow is present. The right border of the domain also corresponds to the lowest portion of the slope. Further studies will analyze in detail these outcomes in order to relate them to other processes such as erosion and to detect if such results can provide further information for land management purposes. However, as positioned at the border of the computational domain, such outcomes can be overlooked.

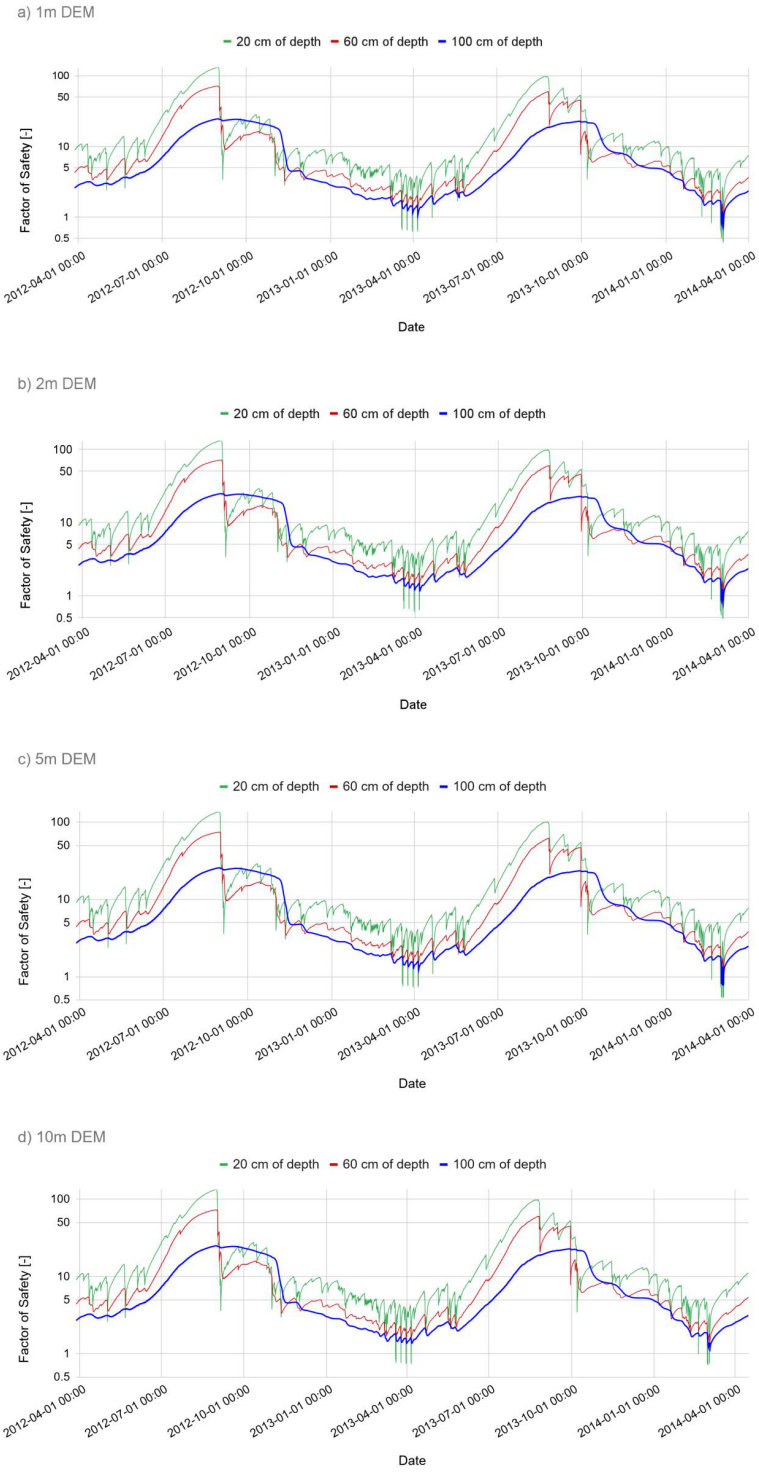

Figure 4.14: Hourly Factor of Safety for different DEM spatial resolutions: 1m, 2m, 5m and 10m. The dates are in format YYYY-MM-DD hh:mm.

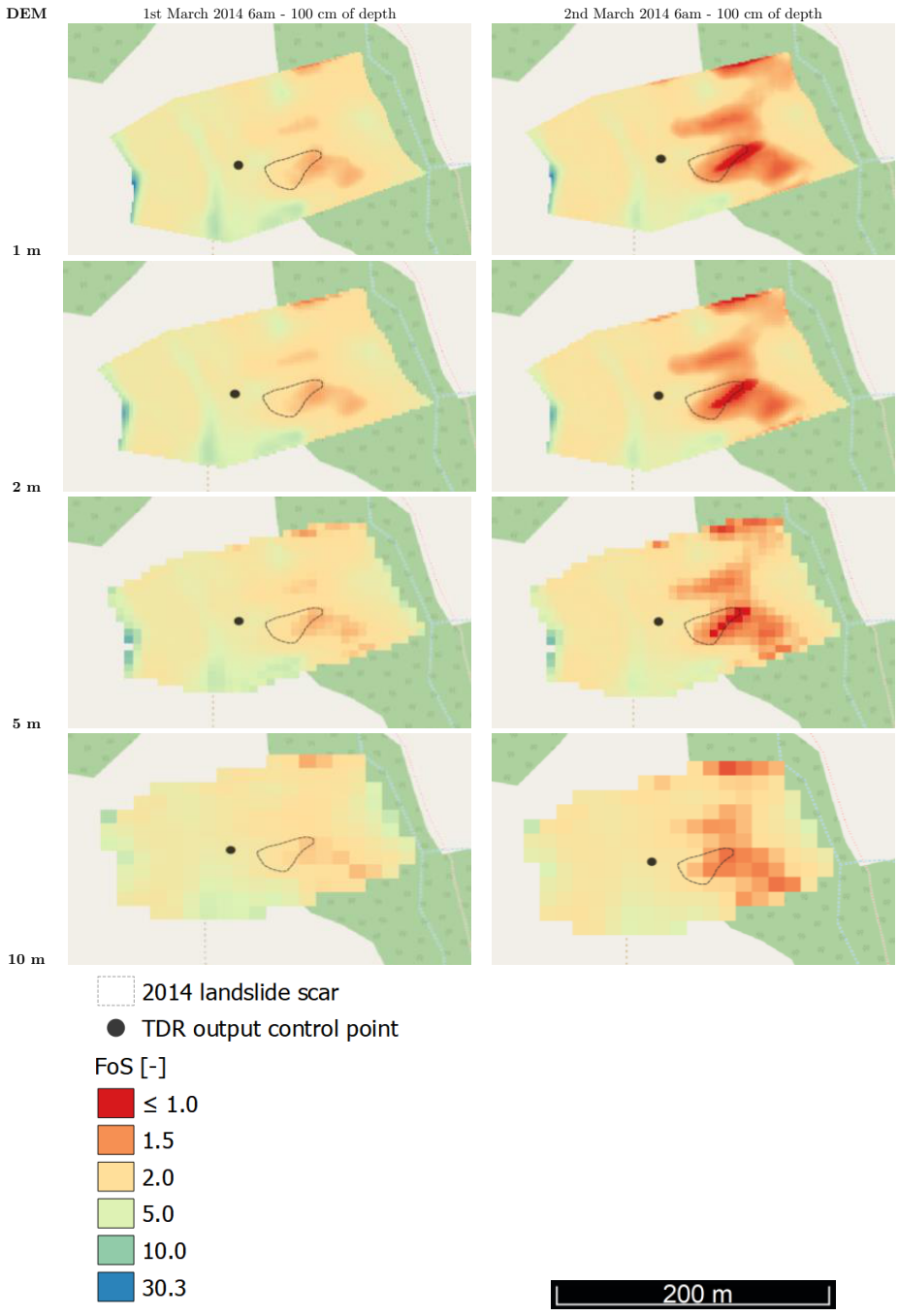

Figure 4.15: Factor of Safety maps at 100 cm of depth for the different spatial resolutions before and after the 2014 landslide

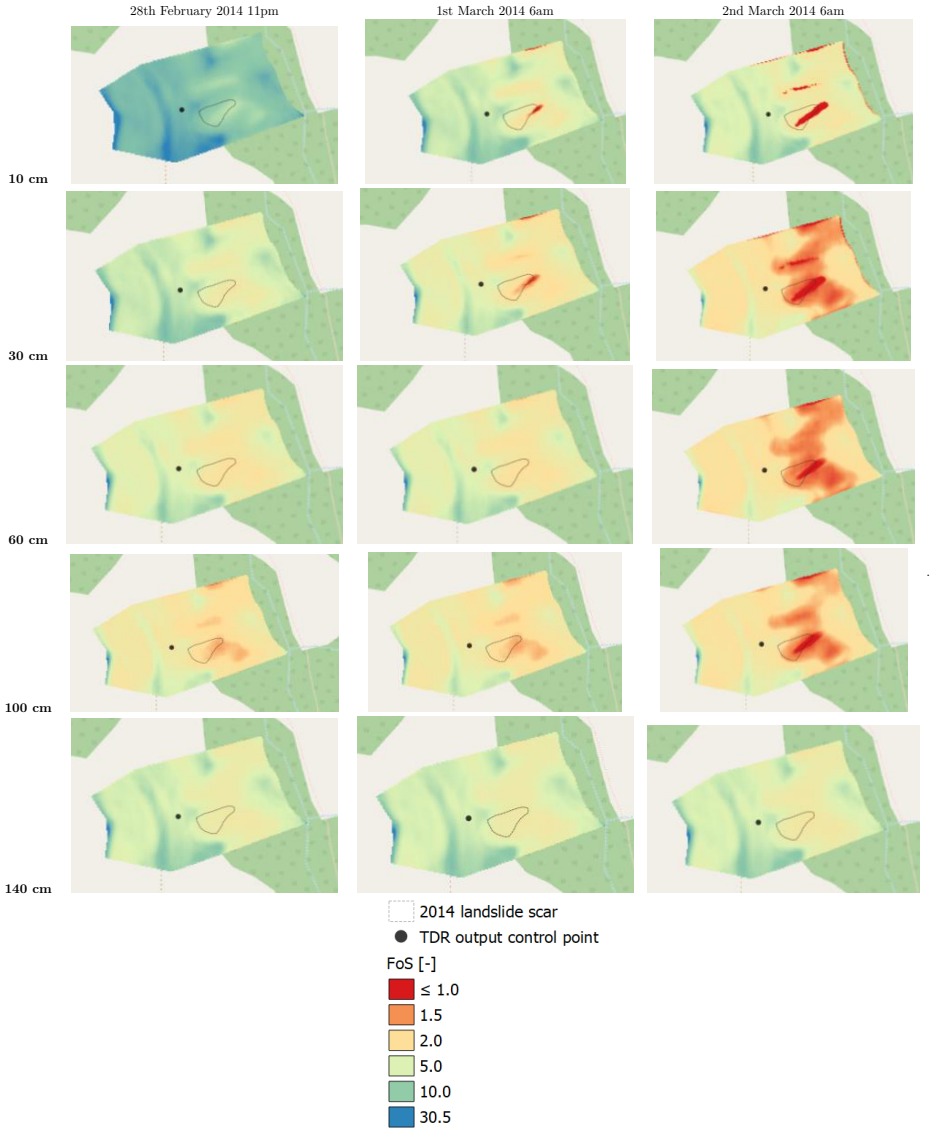

Figure 4.16: Factor of Safety maps at different depths with 1m-DEM before and after the 2014 landslide

4.6 Conclusions

In the presented research, a 3D agro-hydrological model was extended and tested as a predictive tool for rainfall-induced shallow landslides. Although designed for agronomic applications, results showed that the three-dimensional model is suitable for stability analyses in semi-natural environments. The model has been validated on a test slope where a shallow landslide occurred on 2 March 2014, during a field monitoring campaign. Results showed that, although reducing the spatial resolution of the computational mesh, in this application the hydrology simulation outcome did not significantly differ, neither for soil water content nor for soil water potential. However, an effect was observed in terms of slope stability, since the landslide occurrence was appropriately predicted only using a DEM spatial resolution of 1m, 2m, and 5 m. The landslide prediction was satisfactory in terms of time. As regards the prediction accuracy in terms of position, some differences have been observed by comparing maps and specific control points. If on the one hand FoS maps appear rather satisfactory, the FoS computation at the output control points returned values below one - thus indicating instability - only in the lowest point of the real landslide scar ('L1' output point in Figure 4.7). Such an outcome could be expected. The CRITERIA-3D model does not comprise bonds between adjacent blocks, and when an element fails the surrounding ones can keep the equilibrium until suction-induced reinforcement is lost. Moreover, as the subsurface hydrological processes are driven by water potential gradients, points at lower altitudes in the domain are those through which the water moves, inducing the corresponding soil blocks to become more close to instability. Such an outcome must be kept in mind when applying the CRITERIA-3D model in other real case studies, especially where the topography is highly complex, defining multiple slope stability output control points. Future developments will include the addition of a density map that will allow differentiating areas inside the same land use based on the real presence of vegetation. In fact, vegetation effects - and more particularly, the root density distribution - could be another factor discriminating among the different spatial resolutions to be adopted. By adding a density map, the vegetation-related effect on soil hydrology will be either reduced or increased based on the effective presence of plants. The possibility of including soil depth maps, i.e. differentiating the soil layer thickness in different zones, will also be addressed, implementing an algorithm able to consider the soil layers' thickness based on the topography and real soil depth. In fact, it is known that the soil depth distribution follows the topography, allowing deeper soil to be present in areas where the slope is less pronounced. Moreover, the relations among topography, soil depth, soil moisture, transpiration

rates and plant species' distribution at the hillslope scale can affect the soil water balance, defining spatial and temporal patterns [226]. Actually, in the CRITERIA-3D model this aspect is not included and also the vegetation is allowed to have the same root maximum depth everywhere. Including an heterogeneous soil depth could help the stability simulations in being more accurate. Another aspect that will be further explored is the behavior of the soil cracking conceptual model in relation to the different soil textural classes. The present research was related to a relatively small test area. The application of the proposed model to areas wider than a single slope are already ongoing.

Chapter 5

Application of CRITERIA-3D on a wide area

In this chapter the CRITERIA-3D model is applied over a wide area. The test area is located in Monteleone, Roncofreddo municipality (FC), in the Emilia-Romagna region. The area, which extends for approximately 57 ha, comprises an urban center and differentiated land use. It was hit by an extreme rainfall event in May 2023. The aim of the analysis was not only to test the CRITERIA-3D over an area larger than that used in Chapter 4, but also testing whether the assumptions adopted to handle different land uses were appropriate. Moreover, this application is intended as exploratory for future developments of CRITERIA-3D as a predictive tool, in response to extreme events as well.
With regard to territorial characterization, areas occupied by paved roads are considered to be completely impermeable, and the hydraulic conductivity is imposed equal to zero as surface boundary condition. Other artificial surfaces such as buildings, urban settlements, minor country roads and similar, are assigned with an infiltration rate reduced of one order of magnitude with respect to that of the underlying soil, in order to consider some heterogeneity in the artificial agglomerates, where water can partially infiltrate.
In the selected area many landslides were triggered by an extreme climatic event that occurred in Emilia Romagna region in May 2023. The landslide inventory dataset at regional scale, designated to aid the Commission for Reconstruction in implementing the recovery phase of the natural disaster [16], includes a total of 80 997 polygons, testifying the impact that such an extreme event had on the Emilia-Romagna region. The database was used to back-analyze the occurred landslides and validate the FoS computation.

5.1 Case study

As already stated, the selected area is called Monteleone, in the municipality of Roncofreddo, province of Forlì-Cesena, in the Emilia-Romagna region (Figure 5.1). Monteleone belongs to a geographical area known as "Romagna".

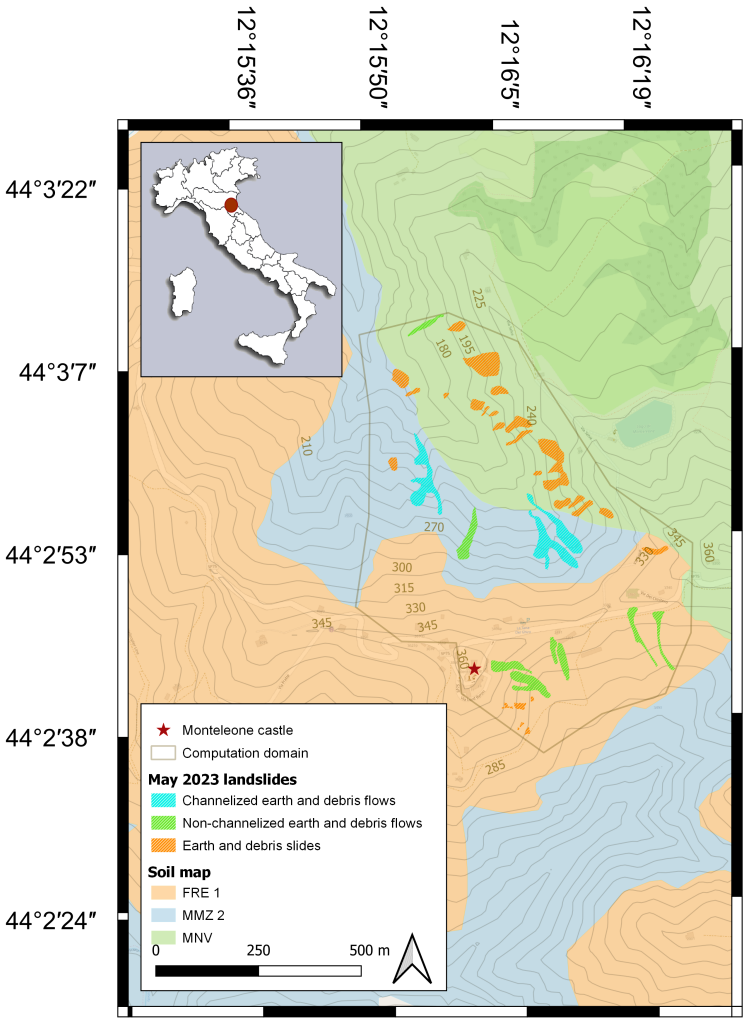

Figure 5.1: Test area of Monteleone

In May 2023, two exceptional rainfall events occurred in the test area. During the first one, on May 1-3, 200 mm of rainfall in 48 hours were recorded. The second one, only two weeks later, on May 16-17, provoked a precipitation of 230 mm in 48-hours. The return period for the combined effect of these two extreme events far surpassed 500 years [167] (Figure 5.2). During

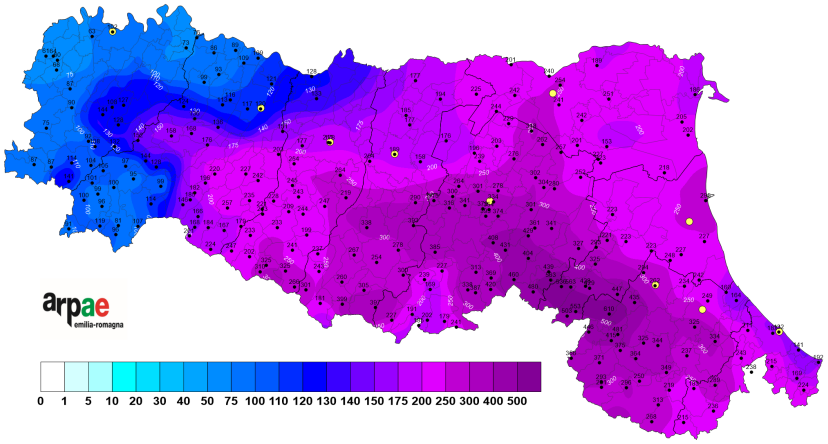

Figure 5.2: Rainfall map of the two combined rainfall events occurred in May 2023. Yellow dots are the main cities of Emilia-Romagna region, the black dots are the monitoring stations with the corresponding amount of cumulated rainfall registered from 1st May to 17th May 2023.

these events, the territory of Romagna was hit by several landslides, some of which blocking roads, isolating entire villages, and some others happening very close to people properties, constituting a high source of hazard. The total estimated damage of the two events surpasses 9 billion of euros [16]. Due to the exceptionality of the event and the high density of landslides, precise information on the exact occurrence time is scarce. However, in the Monteleone test area, from local citizens' interview, it is known that the majority of the landslides were triggered during the second event, in the night between 16 and 17 May. As only two weeks were passed since the previous 1-3 May heavy precipitations, soils were still in a moist condition, and the new rainfall inputs likely provoked the total soil strength loss.
As represented in Figure 5.1, different types of landslides occurred in the test area; namely, a) channelized earth and debris flows; b) non-channelized earth and debris flows and c) earth and debris slides. Although the infinite slope scheme, adopted for the stability analysis in the CRITERIA-3D model, may not be suitable for all the possible failure modes [20], it is here applied considering all the types of rainfall-induced shallow landslides occurred in the test area.

5.2 Model settings

The computational mesh was derived by a DEM with spatial resolution of 5mx5m. This resolution was deemed effective based on the validation re-

ported in Chapter 4. The simulation period of Monteleone case study spans from 1st January 2023 to 18th May 2023. A dry initial soil condition at the start of the simulation was manually imposed, based on the rainfall recorded in 2022, which had been a particularly dry year. The hourly input meteorological time series were derived from records of the monitoring network of the Regional Agency for Environmental Protection of Emilia-Romagna region (Arpae). They have been spatially interpolated through the automatic procedure of the CRITERIA-3D model, using the Inverse Distance Weighted (IDW) method.
With regard to the land use, the 2020 map provided by the Emilia-Romagna region was used as a base, accounting for the detail provided by the first classification level of Corine Land Cover (CLC). The resulting land use in the Monteleone study area, reshaped after visual control and manual redrawing based on aerial photographs, is constituted by: a) artificial surfaces (urban areas); b) agricultural areas, mainly represented by woody cultivations such as grapevine, olives and orchards; c) forests, represented by deciduous woodlands; d) bare soils; e) impermeable roads. The land units with the relative crops and hydrological parameters are listed in Table 5.1 and are represented in Figure 5.3, where the 2023 landslide scars are also evident.

Table 5.1: Land use of the Monteleone test case

Land use	Vegetation	Roughness [s/m$^{1/3}$]	Pond depth [m]	Root depth (initial-max) [m]	LAI min-max [-]
Urban	Bare soil	0.03	0.002	-	-
Road	Bare soil	0.015	0.001		
Bare soil	Bare soil	0.035	0.003	-	-
Forest	Broadleaf	0.1	0.005	0.1-2.0	1.0 - 4.0
Agricultural	Orchard/Grapevine	0.05	0.003	0.1-1.5	0 - 2.5

The soil map used to run the simulations is derived from the Emilia-Romagna region database; at the selected extent, the map contains three different soils, whose parameters are listed in Table 5.2.
Although not directly measured in field or in laboratory, soil horizons in Table 5.2 are attributed with mechanical parameters c' and ϕ'. The listed values are derived through the rules used by CRITERIA-3D, which are based on the classification provided by Garcìa-Gaines and Frankenstein (2015) [217]. The authors' classification links each USDA textural class with a USCS class [218], assigning fixed mechanical parameters. As already mentioned, one simulation was conducted considering the real land use (LU); instead, the second simulation adopted bare soils (BS) all over the domain, except for urban areas and paved roads. Moreover, it was decided to test the model sensitivity with respect to the value of the soil effective cohesion: two simulations as-

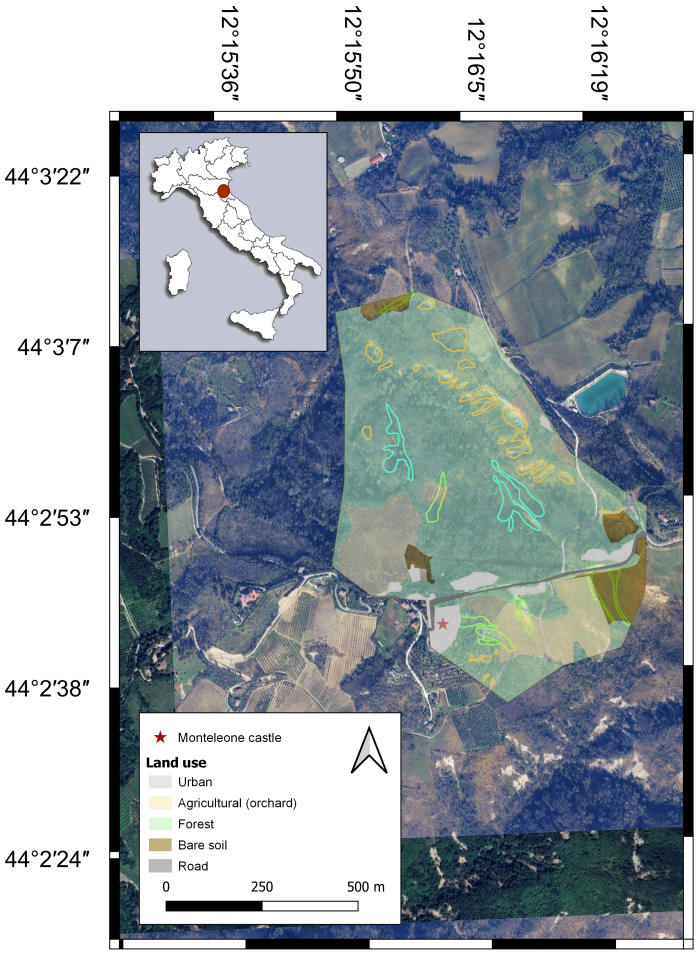

Figure 5.3: Land use at Monteleone case study

sume the values of effective cohesion (c') and friction angle (ϕ') as estimated by CRITERIA-3D (YC); instead, in the further two simulations, the effective cohesion is set equal to zero everywhere except for the horizon V of MNV soil (NC) (Table 5.2), as it has a finer texture with respect to the overlaying horizons and is assumed slightly cemented. This assumption is supported by laboratory analyses performed on similar soils [58]. Instead, assuming a nil value of effective cohesion for all other soils, is due to the following reasons: a) triaxial test results on similar soils [58, 227]; b) precautionary slope stability analysis; c) lack of specific laboratory tests.
It is known that the suction stress considered in FoS computation is a consistent way to account for the soil moisture effects on the overall stability [228]. In fact, when the soil approaches saturated conditions, the suction stress

Table 5.2: Soils characteristics at Monteleone case study. YC=Yes Cohesion cases, NC=No Cohesion cases

Soil	Horizon	Depth range (cm)	USDA Texture	γ (kN/m^3)	K_{sat} (m/s)	c'-YC (kPa)	c'-NC (kPa)	ϕ' (°)
FRE1	I	0-60	Silt loam	15.0	3.3E-07	0	0	33
FRE1	II	60-87	Loam	15.0	8.9E-07	5	0	28
FRE1	III	87-107	Silt Loam	14.9	3.9E-07	5	0	28
FRE1	IV	107-120	Silt Loam	17.6	5.8E-08	5	0	28
MMZ2	I	0-20	Loam	13.5	1.1E-06	5	0	28
MMZ2	II	20-50	Loam	14.7	1.1E-06	0	0	34
MMZ2	III	50-60	Loam	15.7	6.0E-07	5	0	28
MNV	I	0-45	Sandy Clay Loam	15.5	5.9E-07	0	0	33
MNV	II	45-65	Sandy Clay Loam	14.7	1.6E-06	0	0	33
MNV	III	65-105	Sandy Clay Loam	15.4	1.0E-06	0	0	33
MNV	IV	105-120	Sandy Clay Loam	15.6	9.1E-07	0	0	32
MNV	V	120-130	Clay Loam	16.7	7.6E-08	20	20	27

drops to zero, provoking a reduction in the overall stability, quantified in that a term of the FoS equation becomes nil (see Equation 3.10). Table 5.3 lists the 4 simulated cases, while Table 5.2 reports the soil parameters adopted in the four scenarios. The soil names reported in Table 5.2 are the same reported in Figure 5.1 and correspond to those adopted in the soil map of the Emilia Romagna region.

Table 5.3: Simulations run for the Monteleone case study

Case	Land use	Soil cohesion
LU-YC	All 5 classes	Estimated by CRITERIA-3D
LU-NC	All 5 classes	Cohesionless soils
BS-YC	Bare soil, Urban, Road	Estimated by CRITERIA-3D
BS-NC	Bare soil, Urban, Road	Cohesionless soils

5.3 Results and discussion

In this section the model outcomes in terms of FoS are presented. As no sensors of soil moisture are installed in the analyzed area, the output validation has been conducted by comparing the model results with the really occurred landslides. FoS maps were produced and values minor than 1 - indicating instability - were compared with the polygons of landslides occurred in May 2023 [16]. To compare the results, it was assumed that the

landslides have been triggered in the night between 16 and 17 May, although not precise information is available about landslide triggering timing. The FoS maps that will be presented in this section were obtained graphing the lowest value of FoS along the vertical profile starting from the slope surface. If different soils are present, the slip surface depth may vary in space, and from a practical point of view knowing where a landslide will be triggered, neglecting its precise depth, was considered sufficient to quantify the model accuracy. However, through CRITERIA-3D, maps of FoS at specific depths can be obtained, as already done in the application presented in Chapter 4, also for wide areas. Figures 5.4 and 5.5 show the outcomes of the four cases listed in Table 5.3. Figure 5.4 represents the FoS at 7am of May 17th derived adopting the values of soil effective cohesion as attributed by CRITERIA-3D; Figure 5.5 shows the FoS for the same moment, obtained setting a nil soil effective cohesion, as explained in the previous section. Through these comparisons, the effectiveness of involving the presence of vegetation in an heavy precipitation event was assessed.

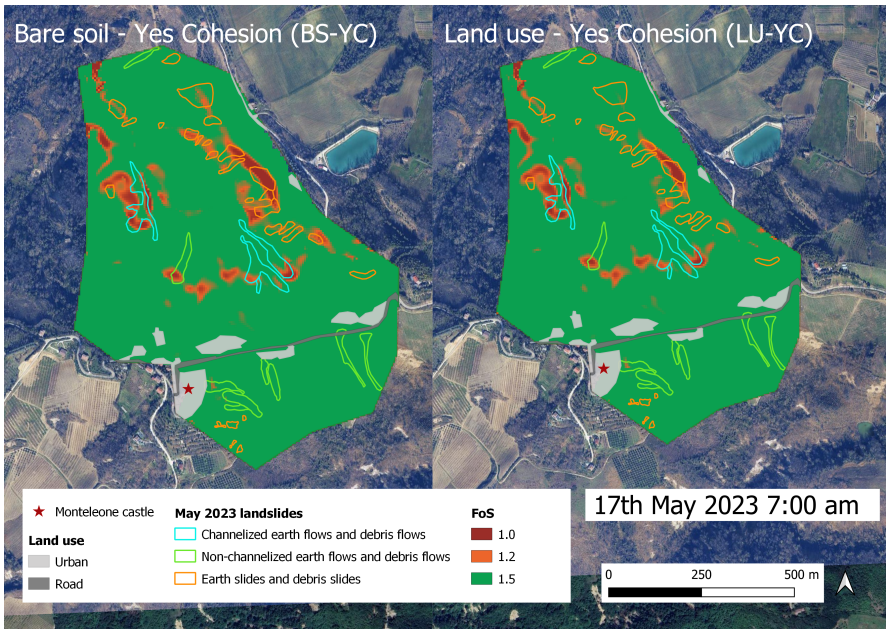

Figure 5.4: Comparison between simulations adopting bare soil and real land use. Monteleone case study - 17th May 2023 at 7 am - with soil effective cohesion

It can be argued that the simulations with and without vegetation are barely the same, thus suggesting that there is no valuable meaning of modeling transient vegetation effects on slope stability at large scale in this specific case. However, this outcome is a further evidence of the exceptional nature

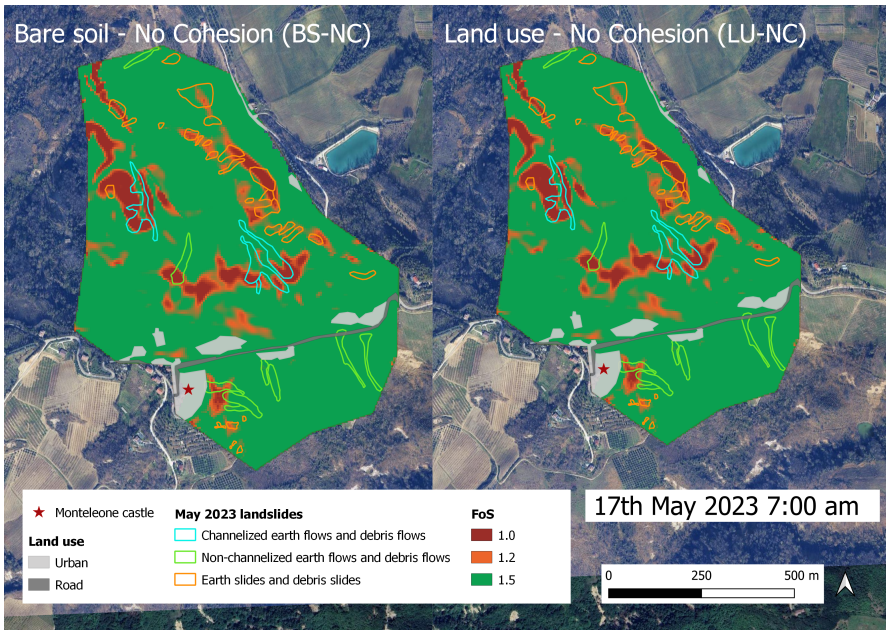

Figure 5.5: Comparison between simulations adopting bare soil and real land use. Monteleone case study - 17th May 2023 at 7 am - without soil effective cohesion

of the rainfall events occurred between 1st and 17th May 2023 in the Emilia-Romagna region. Such a great amount of rainfall seems to have vanished the hydrological reinforcement exerted by roots and canopies. Differently, an evident difference in the predictions is obtained when the soil effective cohesion is set to zero, suggesting that the estimated values of effective cohesion were not adequate.

To derive the accuracy rate of the CRITERIA-3D model quantitatively, the ROC curve analysis method is adopted [227, 229–231]. To build the ROC curve, different indicators were firstly defined: true positive (TP) coverage is the extent of the unstable areas detected by CRITERIA-3D that correspond to the landslide database polygons [%]; on the contrary, the simulated unstable areas outside the observed polygon are counted as false positive (FP) [%]. If a pixel belongs to an observed landslides scar, but CRITERIA-3D did not detect it as unstable, the correspondent area is classified as false negative (FN) [%]; all other stable pixels outside the landslide correspond to the total true negative (TN) area [%]. The TP and FN quantities are referred to the total area of landslide scars (46 200 m^2), instead the FP and TN are obtained as a ratio over the area that did not experience landslides (518 725 m^2). Table 5.4 reports the resulting percentages of this quantitative analysis.

Table 5.4: Landslides prediction accuracy rates for the Monteleone case study

Simulation	True positive	False positive	False negative	True negative
BS-YC	5.62 %	0.42 %	94.38 %	99.58 %
LU-YC	3.13 %	0.10 %	96.87 %	99.9 %
BS-NC	13.0 %	2.9 %	87 %	97.1 %
LU-NC	13.53 %	3.03 %	86.5 %	96.97 %

In the ROC analysis, TP rate measures the sensitivity of the model, indicating the number of correct predictions; whereas the specificity, which is represented by the TN rate, indicates the number of false positives. In Figure 5.6 the ROC curves obtained by varying the FoS values of the four different scenarios are represented. The quantification of the model accuracy is obtained deriving the Area Under the Curve (AUC), that is listed in Table 5.5.

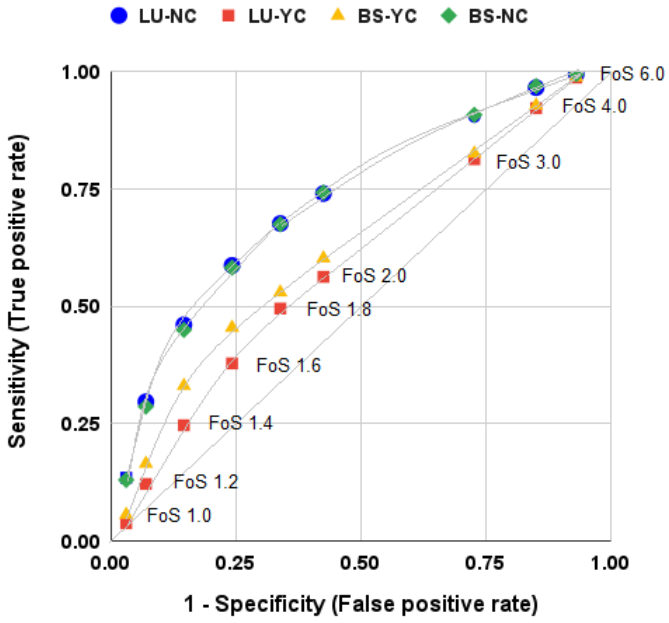

Figure 5.6: Comparison among ROC curves for the four simulations of Monteleone case study

By the ROC curve and AUC analysis, it is evident that the accuracy of the model slightly increases when no effective cohesion is considered. However,

Table 5.5: AUC of the four analyzed cases

Simulation	AUC
BS-YC	0.633
LU-YC	0.626
BS-NC	0.653
LU-NC	0.653

the obtained AUC values are not satisfactory if compared to other models in the literature [227, 230, 232, 233]. However, the ROC curve method was here applied considering the polygons as reported in the inventory, including the whole landslide body, i.e. both the source and accumulation areas. It is arguable that the ROC curve and AUC analysis may not be the most adequate method due to the mechanical simplifications adopted in the CRITERIA-3D model. At the current level of development, the proposed distributed model seems more suitable to model the main scarp and, more precisely, the landslide crown areas instead of the whole mapped landslide area. Notwithstanding the limitations of the ROC analysis for the proposed model, it was decided to apply it considering the entire scars, in order to avoid artifacts in the quantitative accuracy evaluation.

Chapter 6

Concluding remarks and future perspectives

The aim of this thesis was to incorporate the transient modeling of vegetation effects in slope stability analysis for rainfall-induced shallow landslides. The research project started from an agro-hydrological model, in both its unidimensional and three-dimensional versions, namely, CRITERIA-1D and CRITERIA-3D, developed by the Hydro-Meteo-Climate Service of the Regional Agency for the Environment Protection and Energy of the Emilia-Romagna region (Arpae-SIMC) [123, 150, 153, 156]. The models were extended in order to incorporate a simplified slope stability analysis based on the Factor of Safety computation, adopting the infinite slope scheme. The hydrological and mechanical behavior of unsaturated soil is taken into account through the derivation of transient values of water potential and water content, unified in the concept of suction stress [74, 228], which quantifies the effects of capillary forces on the overall stability, becoming null when the soil is saturated. The vegetation dynamic modeling is ensured by the use of the Growing Degree Days (GDD), a well established method in agronomic applications [183]. The phenological stage of the plant is obtained through the transient derivation of the Leaf Area Index (LAI), based on the actual phenological stage of the plant. Moreover, the daily or hourly evapotranspiration activity, dependent on the actual soil water content, modifies the soil moisture content at each time step, thus deriving with strong physical basis the real vegetation behavior in relation to the general soil water balance. All the transient modeling of vegetation effects is based on real meteorological input conditions, represented by daily precipitation and minimum and maximum air temperature (CRITERIA-1D) or hourly precipitation, average air temperature, solar radiation, wind intensity and air humidity (CRITERIA-3D) time series.

This thesis has shown that involving dynamic activity of plants in assessing the antecedent soil moisture condition in relation to precipitation events reduces the overestimation of landslides in time (see Chapter 3). The application of the three-dimensional version on a test slope where both field hydrological measurements and soil laboratory tests were available, confirms the ability of the model to reproduce the observed landslides both in time and in space (Chapter 4). Nonetheless, when the rainfall is exceptionally intense, there are no significant quantitative differences in stability assessments during the extreme event if vegetation effects are considered or not (see Chapter 5). However, further applications of the CRITERIA-3D model in the Romagna area will assess more in detail if differences are encountered when considering different types of land management or land use. The application shown in Chapter 5 of this thesis only considered few months of simulation. By comparing the applications of Chapters 3 and 4, at the test slope of Montuè, and Chapter 5, at the Monteleone test area, it can be outlined that replacing specific laboratory measurements of soil mechanical parameters such as the effective cohesion with estimated values based on other variables, such as the soil texture, appears not appropriate. Nonetheless, considering that only public available data have been used as input, the application of Monteleone can be considered rather satisfactory. Statistical treatment of soil shear strength input parameters are necessary when enlarging the width of the application area, and in this sense further experimental campaigns are needed to train and validate any statistical model at territorial scale. Despite the simplifications adopted in the slope stability computation, CRITERIA-3D model showed to be effective in relation to different types of landslides. Further developments will include the model refinement in order to assess the possibility to develop a Landslide Early Warning System (LEWS) for civil protection purposes.
Suggestions for further studies are thereby:

- to optimize the code performance, exploring whether its parallelization is feasible;
- to better manage the land use, by introducing density maps upon which defining areas with more and less presence of vegetation;
- to parametrize the soil cracking model for different soil textures;
- to validate the model at territorial scale, by using more reliable values of soil shear strength parameters, based on laboratory tests;
- to quantify the probability of landslide occurrence based on a statistical assessment of soil shear strength parameters' value.

References

[1] MG Persichillo, M Bordoni, and C Meisina. The role of land use changes in the distribution of shallow landslides. *Science of the total environment*, 574:924–937, 2017.

[2] D Tiranti, G Nicolò, and AR Gaeta. Shallow landslides predisposing and triggering factors in developing a regional early warning system. *Landslides*, 16:235–251, 2019.

[3] F Guzzetti, SL Gariano, S Peruccacci, MT Brunetti, I Marchesini, M Rossi, and M Melillo. Geographical landslide early warning systems. *Earth-Science Reviews*, 200:102973, 2020.

[4] R Greco and L Pagano. Basic features of the predictive tools of early warning systems for water-related natural hazards: examples for shallow landslides. *Natural Hazards and Earth System Sciences*, 17(12):2213–2227, 2017.

[5] A Stumpf, JP Malet, and C Delacourt. Correlation of satellite image time-series for the detection and monitoring of slow-moving landslides. *Remote sensing of environment*, 189:40–55, 2017.

[6] S Fiolleau, S Uhlemann, S Wielandt, and B Dafflon. Understanding slow-moving landslide triggering processes using low-cost passive seismic and inclinometer monitoring. *Journal of Applied Geophysics*, 215:105090, 2023.

[7] M Tondo, M Mulas, G Ciccarese, G Marcato, G Bossi, D Tonidandel, V Mair, and A Corsini. Detecting Recent Dynamics in Large-Scale Landslides via the Digital Image Correlation of Airborne Optic and LiDAR Datasets: Test Sites in South Tyrol (Italy). *Remote Sensing*, 15(12):2971, 2023.

[8] TA Bogaard and R Greco. Invited perspectives: Hydrological perspectives on precipitation intensity-duration thresholds for landslide initia-

tion: proposing hydro-meteorological thresholds. *Natural Hazards and Earth System Sciences*, 18(1):31–39, 2018.

[9] C Vennari, SL Gariano, L Antronico, MT Brunetti, G Iovine, S Peruccacci, O Terranova, and F Guzzetti. Rainfall thresholds for shallow landslide occurrence in Calabria, southern Italy. *Natural Hazards and Earth System Sciences*, 14(2):317–330, 2014.

[10] JW Godt, RL Baum, WZ Savage, D Salciarini, WH Schulz, and EL Harp. Transient deterministic shallow landslide modeling: requirements for susceptibility and hazard assessments in a GIS framework. *Engineering Geology*, 102(3-4):214–226, 2008.

[11] P Sudani and KA Patil. Evaluating the significance of saturation in shallow landslide failure: saturated–unsaturated soil perspective. *Multiscale and Multidisciplinary Modeling, Experiments and Design*, 6(4):591–601, 2023.

[12] H Rahardjo, Y Kim, and A Satyanaga. Role of unsaturated soil mechanics in geotechnical engineering. *International Journal of Geo-Engineering*, 10:1–23, 2019.

[13] R Rosso, MC Rulli, and G Vannucchi. A physically based model for the hydrologic control on shallow landsliding. *Water Resources Research*, 42(6), 2006.

[14] TT Viet, G Lee, TM Thu, and HU An. Effect of digital elevation model resolution on shallow landslide modeling using TRIGRS. *Natural Hazards Review*, 18(2):04016011, 2017.

[15] H Lee, K Calvin, D Dasgupta, G Krinner, A Mukherji, P Thorne, C Trisos, J Romero, P Aldunce, K Barrett, et al. *Climate change 2023: synthesis report. Contribution of working groups I, II and III to the sixth assessment report of the intergovernmental panel on climate change*. The Australian National University, 2023.

[16] M Berti, M Pizziolo, M Scaroni, M Generali, V Critelli, M Mulas, M Tondo, F Lelli, C Fabbiani, F Ronchetti, et al. RER2023: the landslide inventory dataset of the May 2023 Emilia-Romagna event. *Earth System Science Data Discussions*, 2024:1–24, 2024.

[17] G Sannino, M Bordoni, M Bittelli, C Meisina, F Tomei, and R Valentino. Deterministic Physically Based Distributed Models for Rainfall-Induced Shallow Landslides. *Geosciences*, 14(10):255, 2024.

[18] A Ali, J Huang, AV Lyamin, SW Sloan, DV Griffiths, MJ Cassidy, and JH Li. Simplified quantitative risk assessment of rainfall-induced landslides modelled by infinite slopes. *Engineering Geology*, 179:102–116, 2014.

[19] DG Milledge, DV Griffiths, SN Lane, and J Warburton. Limits on the validity of infinite length assumptions for modelling shallow landslides. *Earth Surface Processes and Landforms*, 37(11):1158–1166, 2012.

[20] M Lora, M Camporese, PA Troch, and P Salandin. Rainfall-triggered shallow landslides: infiltration dynamics in a physical hillslope model. *Hydrological Processes*, 30(18):3239–3251, 2016.

[21] A DiBiagio, V Capobianco, A Oen, and LM Tallaksen. State-of-the-art: parametrization of hydrological and mechanical reinforcement effects of vegetation in slope stability models for shallow landslides. *Landslides*, 21(10):2417–2446, 2024.

[22] I Murgia, F Giadrossich, Z Mao, D Cohen, GF Capra, and M Schwarz. Modeling shallow landslides and root reinforcement: A review. *Ecological Engineering*, 181:106671, 2022.

[23] Z Mao. Root reinforcement models: Classification, criticism and perspectives. *Plant and Soil*, 472(1):17–28, 2022.

[24] A Lausch, O Bastian, S Klotz, PJ Leitão, A Jung, D Rocchini, ME Schaepman, AK Skidmore, L Tischendorf, and S Knapp. Understanding and assessing vegetation health by in situ species and remote-sensing approaches. *Methods in ecology and evolution*, 9(8):1799–1809, 2018.

[25] F Cotecchia, F Santaloia, P Lollino, C Vitone, G Pedone, and O Bottiglieri. From a phenomenological to a geomechanical approach to landslide hazard analysis. *European Journal of Environmental and Civil Engineering*, 20(9):1004–1031, 2016.

[26] MJ Crozier. Deciphering the effect of climate change on landslide activity: A review. *Geomorphology*, 124(3-4):260–267, 2010.

[27] SL Gariano and F Guzzetti. Landslides in a changing climate. *Earth-science reviews*, 162:227–252, 2016.

[28] M Polemio, O Petrucci, et al. Rainfall as a landslide triggering factor an overview of recent international research. *Landslides in research, theory and practice*, 2000.

[29] P Reichenbach, M Rossi, BD Malamud, M Mihir, and F Guzzetti. A review of statistically-based landslide susceptibility models. *Earth-science reviews*, 180:60–91, 2018.

[30] F Guzzetti, A Carrara, M Cardinali, and P Reichenbach. Landslide hazard evaluation: a review of current techniques and their application in a multi-scale study, Central Italy. *Geomorphology*, 31(1-4):181–216, 1999.

[31] Z Fang, Y Wang, C van Westen, and L Lombardo. Landslide hazard spatiotemporal prediction based on data-driven models: Estimating where, when and how large landslide may be. *International Journal of Applied Earth Observation and Geoinformation*, 126:103631, 2024.

[32] GB Crosta and P Frattini. Distributed modelling of shallow landslides triggered by intense rainfall. *Natural Hazards and Earth System Sciences*, 3(1/2):81–93, 2003.

[33] A Kyriou, KG Nikolakopoulos, and IK Koukouvelas. Timely and low-cost remote sensing practices for the assessment of landslide activity in the service of hazard management. *Remote Sensing*, 14(19):4745, 2022.

[34] KG Nikolakopoulos, A Kyriou, Ioannis K Koukouvelas, N Tomaras, and E Lyros. UAV, GNSS, and InSAR data analyses for landslide monitoring in a mountainous village in western greece. *Remote Sensing*, 15(11):2870, 2023.

[35] KG Nikolakopoulos, A Kyriou, and Ioannis K Koukouvelas. UAV, GNSS, and GIS for the Rapid Assessment of Multi-Occurrence Landslides. *Geosciences*, 14(6):160, 2024.

[36] V Tsironi, A Ganas, I Karamitros, E Efstathiou, I Koukouvelas, and E Sokos. Kinematics of active landslides in Achaia (Peloponnese, Greece) through InSAR time series analysis and relation to rainfall patterns. *Remote Sensing*, 14(4):844, 2022.

[37] Y Li and W Duan. Decoding vegetation's role in landslide susceptibility mapping: An integrated review of techniques and future directions. *Biogeotechnics*, page 100056, 2023.

[38] S Raia, M Alvioli, M Rossi, RL Baum, JW Godt, and F Guzzetti. Improving predictive power of physically based rainfall-induced shallow landslide models: a probabilistic approach. *Geoscientific Model Development*, 7(2):495–514, 2014.

[39] G Scaringi, X Fan, Q Xu, C Liu, C Ouyang, G Domènech, F Yang, and L Dai. Some considerations on the use of numerical methods to simulate past landslides and possible new failures: the case of the recent xinmo landslide (Sichuan, China). *Landslides*, 15:1359–1375, 2018.

[40] R Greco, P Marino, and TA Bogaard. Recent advancements of landslide hydrology. *Wiley Interdisciplinary Reviews: Water*, 10(6):e1675, 2023.

[41] J Lu, Q Zhang, AD Werner, Y Li, S Jiang, and Z Tan. Root-induced changes of soil hydraulic properties–a review. *Journal of Hydrology*, 589:125203, 2020.

[42] JJ Ni, AK Leung, and CWW Ng. Modelling effects of root growth and decay on soil water retention and permeability. *Canadian Geotechnical Journal*, 56(7):1049–1055, 2019.

[43] T de Jesús Arce-Mojica, U Nehren, K Sudmeier-Rieux, PJ Miranda, and D Anhuf. Nature-based solutions (NbS) for reducing the risk of shallow landslides: Where do we stand? *International journal of disaster risk reduction*, 41:101293, 2019.

[44] M Vicarelli, K Sudmeier-Rieux, A Alsadadi, A Shrestha, S Schütze, M Kang, Ma Leue, D Wasielewski, and J Mysiak. On the cost-effectiveness of nature-based solutions for reducing disaster risk. *Science of The Total Environment*, page 174524, 2024.

[45] SK Vanapalli, DG Fredlund, DE Pufahl, and AW Clifton. Model for the prediction of shear strength with respect to soil suction. *Canadian geotechnical journal*, 33(3):379–392, 1996.

[46] SL Kuriakose, VG Jetten, CJ Van Westen, G Sankar, and LPH Van Beek. Pore water pressure as a trigger of shallow landslides in the Western Ghats of Kerala, India: some preliminary observations from an experimental catchment. *Physical geography*, 29(4):374–386, 2008.

[47] Q Ran, Y Hong, W Li, and J Gao. A modelling study of rainfall-induced shallow landslide mechanisms under different rainfall characteristics. *Journal of Hydrology*, 563:790–801, 2018.

[48] JP McKenna, PM Santi, X Amblard, and J Negri. Effects of soil-engineering properties on the failure mode of shallow landslides. *Landslides*, 9:215–228, 2012.

[49] N Gofar and H Rahardjo. Saturated and unsaturated stability analysis of slope subjected to rainfall infiltration. In *MATEC Web of Conferences*, volume 101, page 05004. EDP Sciences, 2017.

[50] EJ Gabet and SM Mudd. The mobilization of debris flows from shallow landslides. *Geomorphology*, 74(1-4):207–218, 2006.

[51] RM Iverson, ME Reid, and RG LaHusen. Debris-flow mobilization from landslides. *Annual Review of Earth and Planetary Sciences*, 25(1):85–138, 1997.

[52] AM Ridley. Soil suction—what it is and how to successfully measure it. In *FMGM 2015: Proceedings of the Ninth Symposium on Field Measurements in Geomechanics*, pages 27–46. Australian Centre for Geomechanics, 2015.

[53] DG Fredlund. Unsaturated soil mechanics in engineering practice. *Journal of geotechnical and geoenvironmental engineering*, 132(3):286–321, 2006.

[54] M Bittelli, R Valentino, F Salvatorelli, and PR Pisa. Monitoring soil-water and displacement conditions leading to landslide occurrence in partially saturated clays. *Geomorphology*, 173:161–173, 2012.

[55] JW Godt, RL Baum, and N Lu. Landsliding in partially saturated materials. *Geophysical research letters*, 36(2), 2009.

[56] Y Mualem. A new model for predicting the hydraulic conductivity of unsaturated porous media. *Water resources research*, 12(3):513–522, 1976.

[57] MT Van Genuchten. A closed-form equation for predicting the hydraulic conductivity of unsaturated soils. *Soil science society of America journal*, 44(5):892–898, 1980.

[58] M Bordoni, C Meisina, R Valentino, N Lu, M Bittelli, and S Chersich. Hydrological factors affecting rainfall-induced shallow landslides: from the field monitoring to a simplified slope stability analysis. *Engineering Geology*, 193:19–37, 2015.

[59] AK Leung, A Garg, and CWW Ng. Effects of plant roots on soil-water retention and induced suction in vegetated soil. *Engineering Geology*, 193:183–197, 2015.

[60] MW Farthing and FL Ogden. Numerical solution of Richards' equation: A review of advances and challenges. *Soil Science Society of America Journal*, 81(6):1257–1269, 2017.

[61] Y Zha, J Yang, J Zeng, CHM Tso, W Zeng, and L Shi. Review of numerical solution of Richardson–Richards equation for variably saturated flow in soils. *Wiley Interdisciplinary Reviews: Water*, 6(5):e1364, 2019.

[62] R Cockett, LJ Heagy, and E Haber. Efficient 3D inversions using the Richards equation. *Computers & Geosciences*, 116:91–102, 2018.

[63] H Rahardjo, K Chatterjea, EC Leong, and JY Wang. Effect of hydraulic anisotropy on soil-water characteristic curve. *Soils and Foundations*, 56(2):228–239, 2016.

[64] Y Jin, B Zhang, A Thimm, and H Zepp. Anisotropy of soil hydraulic properties along arable slopes. 2008.

[65] A Ali, J Huang, AV Lyamin, SW Sloan, and MJ Cassidy. Boundary effects of rainfall-induced landslides. *Computers and Geotechnics*, 61:341–354, 2014.

[66] H Liu, TW Lei, J Zhao, CP Yuan, YT Fan, and LQ Qu. Effects of rainfall intensity and antecedent soil water content on soil infiltrability under rainfall conditions using the run off-on-out method. *Journal of Hydrology*, 396(1-2):24–32, 2011.

[67] E Tabacchi, L Lambs, H Guilloy, A Planty-Tabacchi, E Muller, and H Decamps. Impacts of riparian vegetation on hydrological processes. *Hydrological processes*, 14(16-17):2959–2976, 2000.

[68] HH Gerke. Preferential flow descriptions for structured soils. *Journal of Plant Nutrition and Soil Science*, 169(3):382–400, 2006.

[69] L Montrasio, R Valentino, and GL Losi. Rainfall infiltration in a shallow soil: a numerical simulation of the double-porosity effect. *Electronic Journal of Geotechnical Engineering*, 16:1387–1403, 2011.

[70] W Shao, Z Yang, J Ni, Y Su, W Nie, and X Ma. Comparison of single-and dual-permeability models in simulating the unsaturated hydro-mechanical behavior in a rainfall-triggered landslide. *Landslides*, 15:2449–2464, 2018.

[71] WJ Rawls, DL Brakensiek, and N Miller. Green-Ampt infiltration parameters from soils data. *Journal of hydraulic engineering*, 109(1):62–70, 1983.

[72] SE Cho. Prediction of shallow landslide by surficial stability analysis considering rainfall infiltration. *Engineering Geology*, 231:126–138, 2017.

[73] S Xiao, T Dai, and S Li. Review and Comparative Analysis of Factor of Safety Definitions in Slope Stability. *Geotechnical and Geological Engineering*, pages 1–21, 2024.

[74] N Lu and J Godt. Infinite slope stability under steady unsaturated seepage conditions. *Water resources research*, 44(11), 2008.

[75] W Liu, Z Yang, and S He. Modeling the landslide-generated debris flow from formation to propagation and run-out by considering the effect of vegetation. *Landslides*, 18:43–58, 2021.

[76] EB Masi, V Tofani, G Rossi, S Cuomo, W Wu, D Salciarini, E Caporali, and F Catani. Effects of roots cohesion on regional distributed slope stability modelling. *Catena*, 222:106853, 2023.

[77] EB Masi, S Segoni, and V Tofani. Root reinforcement in slope stability models: a review. *Geosciences*, 11(5):212, 2021.

[78] GB Bischetti, EA Chiaradia, T Epis, and E Morlotti. Root cohesion of forest species in the Italian Alps. *Plant and soil*, 324:71–89, 2009.

[79] JJ Ni, AK Leung, CWW Ng, and W Shao. Modelling hydro-mechanical reinforcements of plants to slope stability. *Computers and Geotechnics*, 95:99–109, 2018.

[80] EM Schmaltz and M Mergili. Integration of root systems into a GIS-based slip surface model: computational experiments in a generic hillslope environment. *Landslides*, 15:1561–1575, 2018.

[81] F Giadrossich, D Cohen, M Schwarz, A Ganga, R Marrosu, M Pirastru, and GF Capra. Large roots dominate the contribution of trees to slope stability. *Earth Surface Processes and Landforms*, 44(8):1602–1609, 2019.

[82] LJ Waldron. The shear resistance of root-permeated homogeneous and stratified soil. *Soil Science Society of America Journal*, 41(5):843–849, 1977.

[83] TH Wu, WP McKinnell III, and DN Swanston. Strength of tree roots and landslides on Prince of Wales Island, Alaska. *Canadian Geotechnical Journal*, 16(1):19–33, 1979.

[84] N Pollen and A Simon. Estimating the mechanical effects of riparian vegetation on stream bank stability using a fiber bundle model. *Water Resources Research*, 41(7), 2005.

[85] D Cohen, M Schwarz, and D Or. An analytical fiber bundle model for pullout mechanics of root bundles. *Journal of Geophysical Research: Earth Surface*, 116(F3), 2011.

[86] M Schwarz, D Cohen, and D Or. Root-soil mechanical interactions during pullout and failure of root bundles. *Journal of Geophysical Research: Earth Surface*, 115(F4), 2010.

[87] M Schwarz, F Giadrossich, and D Cohen. Modeling root reinforcement using a root-failure Weibull survival function. *Hydrology and Earth System Sciences*, 17(11):4367–4377, 2013.

[88] M Schwarz, P Lehmann, and D Or. Quantifying lateral root reinforcement in steep slopes–from a bundle of roots to tree stands. *Earth Surface Processes and Landforms: The Journal of the British Geomorphological Research Group*, 35(3):354–367, 2010.

[89] C Moos, P Bebi, F Graf, J Mattli, C Rickli, and M Schwarz. How does forest structure affect root reinforcement and susceptibility to shallow landslides? *Earth Surface Processes and Landforms*, 41(7):951–960, 2016.

[90] NG Patil and SK Singh. Pedotransfer functions for estimating soil hydraulic properties: A review. *Pedosphere*, 26(4):417–430, 2016.

[91] V Meena, S Kumari, and V Shankar. Physically based modelling techniques for landslide susceptibility analysis: A comparison. In *IOP Conference Series: Earth and Environmental Science*, volume 1032, page 012033. IOP Publishing, 2022.

[92] DR Montgomery and WE Dietrich. A physically based model for the topographic control on shallow landsliding. *Water Resources Research*, 30(4):1153–1171, 1994.

[93] EM O'loughlin. Prediction of surface saturation zones in natural catchments by topographic analysis. *Water Resources Research*, 22(5):794–804, 1986.

[94] W Wu and RC Sidle. A distributed slope stability model for steep forested basins. *Water Resources Research*, 31(8):2097–2110, 1995.

[95] T Takasao and M Shiiba. Incorporation of the effect of concentration of flow into the kinematic wave equations and its applications to runoff system lumping. *Journal of Hydrology*, 102(1-4):301–322, 1988.

[96] A Burton and JC Bathurst. Physically based modelling of shallow landslide sediment yield at a catchment scale. *Environmental Geology*, 35:89–99, 1998.

[97] J Ewen, G Parkin, and PE O'Connell. SHETRAN: distributed river basin flow and transport modeling system. *Journal of Hydrologic Engineering*, 5(3):250–258, 2000.

[98] MB Abbott, JC Bathurst, JA Cunge, PE O'Connell, and J Rasmussen. An introduction to the European Hydrological System—Systeme Hydrologique Europeen,"SHE", 1: History and philosophy of a physically-based, distributed modelling system. *Journal of Hydrology*, 87(1-2):45–59, 1986.

[99] RM Iverson. Landslide triggering by rain infiltration. *Water Resources Research*, 36(7):1897–1910, 2000.

[100] P Frattini, G Crosta, and R Sosio. Approaches for defining thresholds and return periods for rainfall-triggered shallow landslides. *Hydrological Processes: An International Journal*, 23(10):1444–1460, 2009.

[101] RL Baum, WZ Savage, and JW Godt. *TRIGRS: a Fortran program for transient rainfall infiltration and grid-based regional slope-stability analysis, version 2.0*. US Geological Survey Reston, VA, USA, 2008.

[102] R Srivastava and TCJ Yeh. Analytical solutions for one-dimensional, transient infiltration toward the water table in homogeneous and layered soils. *Water Resources Research*, 27(5):753–762, 1991.

[103] N Saadatkhah, MH Tehrani, S Mansor, Z Khuzaimah, A Kassim, and R Saadatkhah. Impact assessment of land cover changes on the runoff changes on the extreme flood events in the Kelantan River basin. *Arabian Journal of Geosciences*, 9:1–17, 2016.

[104] M Alvioli and RL Baum. Parallelization of the TRIGRS model for rainfall-induced landslides using the message passing interface. *Environmental Modelling & Software*, 81:122–135, 2016.

[105] L Montrasio and R Valentino. A model for triggering mechanisms of shallow landslides. *Natural Hazards and Earth System Sciences*, 8(5):1149–1159, 2008.

[106] L Montrasio, R Valentino, A Corina, L Rossi, and R Rudari. A prototype system for space–time assessment of rainfall-induced shallow landslides in Italy. *Natural hazards*, 74:1263–1290, 2014.

[107] L Montrasio, MPA Gatto, and C Miodini. The role of plants in the prevention of soil-slip: The G-SLIP model and its application on territorial scale through G-XSLIP platform. *Landslides*, 20(6):1149–1165, 2023.

[108] G Capparelli and P Versace. FLaIR and SUSHI: two mathematical models for early warning of landslides induced by rainfall. *Landslides*, 8:67–79, 2011.

[109] C Lepore, E Arnone, LV Noto, G Sivandran, and RL Bras. Physically based modeling of rainfall-triggered landslides: a case study in the Luquillo forest, Puerto Rico. *Hydrology and Earth System Sciences*, 17(9):3371–3387, 2013.

[110] E Arnone, D Caracciolo, LV Noto, F Preti, and RL Bras. Modeling the hydrological and mechanical effect of roots on shallow landslides. *Water Resources Research*, 52(11):8590–8612, 2016.

[111] VY Ivanov, RL Bras, and ER Vivoni. Vegetation-hydrology dynamics in complex terrain of semiarid areas: 2. Energy-water controls of vegetation spatiotemporal dynamics and topographic niches of favorability. *Water Resources Research*, 44(3), 2008.

[112] DG Milledge, D Bellugi, JA McKean, AL Densmore, and WE Dietrich. A multidimensional stability model for predicting shallow landslide size and shape across landscapes. *Journal of Geophysical Research: Earth Surface*, 119(11):2481–2504, 2014.

[113] A Cislaghi, EA Chiaradia, and GB Bischetti. Including root reinforcement variability in a probabilistic 3D stability model. *Earth Surface Processes and Landforms*, 42(12):1789–1806, 2017.

[114] D Cohen and M Schwarz. Tree-root control of shallow landslides. *Earth Surface Dynamics*, 5(3):451–477, 2017.

[115] JJ Lizárraga, P Frattini, GB Crosta, and G Buscarnera. Regional-scale modelling of shallow landslides with different initiation mechanisms: sliding versus liquefaction. *Engineering geology*, 228:346–356, 2017.

[116] G Buscarnera and C Di Prisco. Soil stability and flow slides in unsaturated shallow slopes: Can saturation events trigger liquefaction processes? *Géotechnique*, 63(10):801–817, 2013.

[117] JJ Lizárraga and G Buscarnera. Safety factors to detect flowslides and slips in unsaturated shallow slopes. *Géotechnique*, 68(5):442–450, 2018.

[118] M Abdollahi, F Vahedifard, and FT Tracy. Post-wildfire stability of unsaturated hillslopes against rainfall-triggered landslides. *Earth's Future*, 11(3):e2022EF003213, 2023.

[119] FT Tracy and F Vahedifard. Analytical solution for coupled hydro-mechanical modeling of infiltration in unsaturated soils. *Journal of Hydrology*, 612:128198, 2022.

[120] EP Glenn, AR Huete, PL Nagler, and SG Nelson. Relationship between remotely-sensed vegetation indices, canopy attributes and plant physiological processes: What vegetation indices can and cannot tell us about the landscape. *Sensors*, 8(4):2136–2160, 2008.

[121] T Lann, H Bao, H Lan, H Zheng, and C Yan. Hydro-mechanical effects of vegetation on slope stability: A review. *Science of the Total Environment*, page 171691, 2024.

[122] EM Schmaltz, LPH Van Beek, TA Bogaard, S Kraushaar, S Steger, and T Glade. Strategies to improve the explanatory power of a dynamic slope stability model by enhancing land cover parameterisation and model complexity. *Earth Surface Processes and Landforms*, 44(6):1259–1273, 2019.

[123] G Sannino, F Tomei, M Bittelli, M Bordoni, C Meisina, and R Valentino. Implementation of a slope stability method in the CRITERIA-1D agro-hydrological modeling scheme. *Landslides*, 21:2597—-2616, 2024.

[124] RT Pack, DG Tarboton, and CN Goodwin. The SINMAP approach to terrain stability mapping. In *D. Moore and O. Hungr (eds), 8th Congress of the International Association of Engineering Geology*, pages 1157—-66.

[125] S Simoni, F Zanotti, G Bertoldi, and R Rigon. Modelling the probability of occurrence of shallow landslides and channelized debris flows using GEOtop-FS. *Hydrological Processes: An International Journal*, 22(4):532–545, 2008.

[126] G Rossi, F Catani, L Leoni, S Segoni, and V Tofani. HIRESSS: a physically based slope stability simulator for HPC applications. *Natural Hazards and Earth System Sciences*, 13(1):151–166, 2013.

[127] FB van Zadelhoff, A Albaba, D Cohen, C Phillips, B Schaefli, LKA Dorren, and M Schwarz. Introducing SlideforMap; a probabilistic finite slope approach for modelling shallow landslide probability in forested situations. *Natural Hazards and Earth System Sciences Discussions*, 2021:1–33, 2021.

[128] V Medina, M Hürlimann, Z Guo, A Lloret, and J Vaunat. Fast physically-based model for rainfall-induced landslide susceptibility assessment at regional scale. *Catena*, 201:105213, 2021.

[129] C Iadanza, A Trigila, and F Napolitano. Identification and characterization of rainfall events responsible for triggering of debris flows and shallow landslides. *Journal of Hydrology*, 541:230–245, 2016.

[130] R Tufano, G Formetta, D Calcaterra, and P De Vita. Hydrological control of soil thickness spatial variability on the initiation of rainfall-induced shallow landslides using a three-dimensional model. *Landslides*, 18(10):3367–3380, 2021.

[131] TA Bogaard and R Greco. Landslide hydrology: from hydrology to pore pressure. *Wiley Interdisciplinary Reviews: Water*, 3(3):439–459, 2016.

[132] T Kavzoglu, I Colkesen, and EK Sahin. Machine learning techniques in landslide susceptibility mapping: a survey and a case study. *Landslides: Theory, Practice and Modelling*, pages 283–301, 2019.

[133] P Lima, S Steger, T Glade, and FG Murillo-García. Literature review and bibliometric analysis on data-driven assessment of landslide susceptibility. *Journal of Mountain Science*, 19(6):1670–1698, 2022.

[134] M Bordoni, V Vivaldi, L Lucchelli, L Ciabatta, L Brocca, JP Galve, and C Meisina. Development of a data-driven model for spatial and temporal shallow landslide probability of occurrence at catchment scale. *Landslides*, 18:1209–1229, 2021.

[135] M Durmaz, M Hürlimann, N Huvaj, and V Medina. Comparison of different hydrological and stability assumptions for physically-based modeling of shallow landslides. *Engineering Geology*, 323:107237, 2023.

[136] SD Pardeshi, SE Autade, and SS Pardeshi. Landslide hazard assessment: recent trends and techniques. *SpringerPlus*, 2:523, 2013.

[137] E Gioia, G Speranza, M Ferretti, JW Godt, RL Baum, and F Marincioni. Application of a process-based shallow landslide hazard model over a broad area in Central Italy. *Landslides*, 13:1197–1214, 2016.

[138] A Bronstert and EJ Plate. Modelling of runoff generation and soil moisture dynamics for hillslopes and micro-catchments. *Journal of Hydrology*, 198(1-4):177–195, 1997.

[139] M Minacapilli, M Iovino, and G D'Urso. A distributed agro-hydrological model for irrigation water demand assessment. *Agricultural Water Management*, 95(2):123–132, 2008.

[140] JC van Dam, P Groenendijk, RFA Hendriks, and JG Kroes. Advances of modeling water flow in variably saturated soils with SWAP. *Vadose Zone Journal*, 7(2):640–653, 2008.

[141] L Montrasio and R Valentino. Modelling rainfall-induced shallow landslides at different scales using SLIP-Part I. *Procedia Engineering*, 158:476–481, 2016.

[142] JC Bathurst, CI Bovolo, and F Cisneros. Modelling the effect of forest cover on shallow landslides at the river basin scale. *Ecological Engineering*, 36(3):317–327, 2010.

[143] H Guo, C Qu, L Liu, Q Zhang, and Y Liu. Reliability analysis of vegetated slope considering spatial variability of soil and root properties. *Computers and Geotechnics*, 169:106257, 2024.

[144] H Guo, CWW Ng, and Q Zhang. Three-dimensional numerical analysis of plant-soil hydraulic interactions on pore water pressure of vegetated slope under different rainfall patterns. *Journal of Rock Mechanics and Geotechnical Engineering*, 2024.

[145] CWW Ng, A Leung, and J Ni. *Plant-soil slope interaction*. CRC Press of Taylor and Francis Group, 2019. ISBN: 978-1-138-19755-8. 206.

[146] CWW Ng, Q Zhang, J Ni, and Z Li. A new three-dimensional theoretical model for analysing the stability of vegetated slopes with different root architectures and planting patterns. *Computers and Geotechnics*, 130:103912, 2021.

[147] CWW Ng, H Guo, J Ni, Q Zhang, and Z Chen. Effects of soil–plant-biochar interactions on water retention and slope stability under various rainfall patterns. *Landslides*, 19(6):1379–1390, 2022.

[148] J Ni, AK Leung, and CWW Ng. Unsaturated hydraulic properties of vegetated soil under single and mixed planting conditions. *Géotechnique*, 69(6):554–559, 2019.

[149] P Campi, F Modugno, A Navarro, F Tomei, G Villani, and M Mastrorilli. Evapotranspiration simulated by CRITERIA and AquaCrop models in stony soils. *Italian Journal of Agronomy*, 10(2):67–73, 2015.

[150] F Tomei, G Antolini, G Villani, M Bittelli, and G Sannino. CRITERIA-1D technical manual. Arpae Emilia-Romagna - Hydro-Meteo-Climate Service, 2024. https://github.com/ARPA-SIMC/CRITERIA1D/blob/master/DOC/CRITERIA1D_technical_manual.pdf. Accessed 29 Jan 2024.

[151] CWW Ng, JJ Ni, and AK Leung. Effects of plant growth and spacing on soil hydrological changes: a field study. *Géotechnique*, 70(10):867–881, 2020.

[152] JJ Ni, S Bordoloi, W Shao, A Garg, G Xu, and AK Sarmah. Two-year evaluation of hydraulic properties of biochar-amended vegetated soil for application in landfill cover system. *Science of the Total Environment*, 712:136486, 2020.

[153] M Bittelli, F Tomei, A Pistocchi, M Flury, J Boll, ES Brooks, and G Antolini. Development and testing of a physically based, three-dimensional model of surface and subsurface hydrology. *Advances in Water Resources*, 33(1):106–122, 2010.

[154] O Ippisch, H-J Vogel, and P Bastian. Validity limits for the van Genuchten–Mualem model and implications for parameter estimation and numerical simulation. *Advances in Water Resources*, 29(12):1780–1789, 2006.

[155] GH Hargreaves and ZA Samani. Reference crop evapotranspiration from temperature. *Applied Engineering in Agriculture*, 1(2):96–99, 1985.

[156] G Antolini, F Tomei, F Dottori, V Marletto, M Van Soetendael, and M Bittelli. CRITERIA technical manual. Arpae Emilia-Romagna - Hydro-Meteo-Climate Service, 2016. https://www.arpae.it/it/temi-ambientali/meteo/scopri-di-piu/strumenti-di-modellistica/criteria/criteria_2016_technical-manual.pdf. Accessed 20 Jan 2024.

[157] DJ Varnes. Slope movements: types and processes. In *Landslide Analysis and Control, National Academy of Sciences, Special Report 176*, pages 11–33. Schuster, R.L., Krizek, R.J. (Eds.), Transportation Research Board, Washington D.C., 1978.

[158] C Cronkite-Ratcliff, KM Schmidt, and C Wirion. Comparing root cohesion estimates from three models at a shallow landslide in the Oregon Coast Range. *GeoHazards*, 3(3):428–451, 2022.

[159] AL Flint, GS Campbell, KM Ellett, and C Calissendorff. Calibration and temperature correction of heat dissipation matric potential sensors. *Soil Science Society of America Journal*, 66(5):1439–1445, 2002.

[160] IUSS Working Group WRB. World reference base for soil resources 2006, first update 2007, 2007. World Soil Resources Reports No. 103. FAO, Rome. https://www.fao.org/fileadmin/templates/nr/images/resou rces/pdf_documents/wrb2007_red.pdf.

[161] M Bordoni, M Bittelli, R Valentino, V Vivaldi, and C Meisina. Observations on soil-atmosphere interactions after long-term monitoring at two sample sites subjected to shallow landslides. *Bulletin of Engineering Geology and the Environment*, 80(10):7467–7491, 2021.

[162] M Bordoni, V Vivaldi, A Giarola, R Valentino, M Bittelli, and C Meisina. Comparison between mechanical and hydrological reinforcement effects of cultivated plants on shallow slope stability. *Science of the Total Environment*, 912:168999, 2024.

[163] A Stokes, GB Douglas, T Fourcaud, F Giadrossich, C Gillies, T Hubble, JH Kim, KW Loades, Z Mao, IR McIvor, et al. Ecological mitigation of hillslope instability: ten key issues facing researchers and practitioners. *Plant and Soil*, 377:1–23, 2014.

[164] M Bordoni, M Bittelli, R Valentino, S Chersich, and C Meisina. Improving the estimation of complete field soil water characteristic curves through field monitoring data. *Journal of Hydrology*, 552:283–305, 2017.

[165] Driessen PM. The water balance of the soil. In: van Keulen H, Wolf J (eds) Modelling of agricultural production: weather, soils and crops., 1986. Pudoc, pp 76–116. https://edepot.wur.nl/172091 (9022008584).

[166] M Tosi. Root tensile strength relationships and their slope stability implications of three shrub species in the Northern Apennines (Italy). *Geomorphology*, 87(4):268–283, 2007.

[167] A Brath, N Casagli, M Marani, P Mercogliano, and R Motta. Rapporto della Commissione tecnico-scientifica istituita con deliberazione della Giunta Regionale n. 984/2023 e determinazione dirigenziale 14641/2023, al fine di analizzare gli eventi meteorologici estremi del mese di maggio 2023, Regione Emilia-Romagna, 12 dicembre 2023, 2023. https://www. regione. emilia-romagna. it/urp/servizie-strumenti/novita-editoriali/rapporto-della-commissionetecnico-scientifica-istituita-al-fine-di-analizzare-gli-eventimeteorologici-estremi-del-mese-di-maggio-2023.

[168] GG Anagnostopoulos, S Fatichi, and P Burlando. An advanced process-based distributed model for the investigation of rainfall-induced landslides: The effect of process representation and boundary conditions. *Water Resources Research*, 51(9):7501–7523, 2015.

[169] D Tiranti and D Rabuffetti. Estimation of rainfall thresholds triggering shallow landslides for an operational warning system implementation. *Landslides*, 7:471–481, 2010.

[170] MN Papa, V Medina, F Ciervo, and A Bateman. Derivation of critical rainfall thresholds for shallow landslides as a tool for debris flow early warning systems. *Hydrology and Earth System Sciences*, 17(10):4095–4107, 2013.

[171] M Bordoni, B Corradini, L Lucchelli, R Valentino, M Bittelli, V Vivaldi, and C Meisina. Empirical and physically based thresholds for the occurrence of shallow landslides in a prone area of Northern Italian Apennines. *Water*, 11(12):2653, 2019.

[172] SC Oliveira, JL Zêzere, S Lajas, and R Melo. Combination of statistical and physically based methods to assess shallow slide susceptibility at the basin scale. *Natural Hazards and Earth System Sciences*, 17(7):1091–1109, 2017.

[173] JY Park, SR Lee, DH Lee, YT Kim, and JS Lee. A regional-scale landslide early warning methodology applying statistical and physically based approaches in sequence. *Engineering Geology*, 260:105193, 2019.

[174] IT Hwang, HJ Park, and JH Lee. Probabilistic analysis of rainfall-induced shallow landslide susceptibility using a physically based model and the bootstrap method. *Landslides*, 20(4):829–844, 2023.

[175] DG Fredlund. Slope stability analysis incorporating the effect of soil suction. *Slope stability*, pages 113–144, 1987.

[176] JW Godt, B Şener-Kaya, N Lu, and RL Baum. Stability of infinite slopes under transient partially saturated seepage conditions. *Water Resources Research*, 48(5), 2012.

[177] DG Toll, SDN Lourenço, J Mendes, D Gallipoli, FD Evans, CE Augarde, YuJ Cui, AM Tang, JC Rojas, L Pagano, et al. Soil suction monitoring for landslides and slopes. *Quarterly Journal of Engineering Geology and Hydrogeology*, 44(1):23–33, 2011.

[178] A Gonzalez-Ollauri and SB Mickovski. Hydrological effect of vegetation against rainfall-induced landslides. *Journal of Hydrology*, 549:374–387, 2017.

[179] J Zhang, H Qiu, B Tang, D Yang, Y Liu, Z Liu, B Ye, W Zhou, and Y Zhu. Accelerating effect of vegetation on the instability of rainfall-induced shallow landslides. *Remote Sensing*, 14(22):5743, 2022.

[180] J Corominas, C van Westen, P Frattini, L Cascini, JP Malet, S Fotopoulou, F Catani, M Van Den Eeckhaut, O Mavrouli, F Agliardi, et al. Recommendations for the quantitative analysis of landslide risk. *Bulletin of engineering geology and the environment*, 73:209–263, 2014.

[181] NF Fernandes, RF Guimarães, RAT Gomes, BC Vieira, DR Montgomery, and H Greenberg. Topographic controls of landslides in Rio de Janeiro: field evidence and modeling. *Catena*, 55(2):163–181, 2004.

[182] Y Hong, R Adler, and G Huffman. Evaluation of the potential of NASA multi-satellite precipitation analysis in global landslide hazard assessment. *Geophysical Research Letters*, 33(22), 2006.

[183] GS McMaster and WW Wilhelm. Growing degree-days: one equation, two interpretations. *Agricultural and Forest Meteorology*, 87(4):291–300, 1997.

[184] A Wypych, A Sulikowska, Z Ustrnul, and D Czekierda. Variability of growing degree days in Poland in response to ongoing climate changes in Europe. *International Journal of Biometeorology*, 61:49–59, 2017.

[185] A Gonzalez-Ollauri and SB Mickovski. Plant-soil reinforcement response under different soil hydrological regimes. *Geoderma*, 285:141–150, 2017.

[186] JC Van Dam and RA Feddes. Numerical simulation of infiltration, evaporation and shallow groundwater levels with the Richards equation. *Journal of Hydrology*, 233(1-4):72–85, 2000.

[187] IM Young, JW Crawford, and C Rappoldt. New methods and models for characterising structural heterogeneity of soil. *Soil and Tillage Research*, 61(1-2):33–45, 2001.

[188] X Zuo, X Zhao, H Zhao, T Zhang, Y Guo, Y Li, and Y Huang. Spatial heterogeneity of soil properties and vegetation–soil relationships following vegetation restoration of mobile dunes in Horqin Sandy Land, Northern China. *Plant and soil*, 318:153–167, 2009.

[189] F Hagedorn and M Bundt. The age of preferential flow paths. *Geoderma*, 108(1-2):119–132, 2002.

[190] H Peron, T Hueckel, L Laloui, and LB Hu. Fundamentals of desiccation cracking of fine-grained soils: experimental characterisation and mechanisms identification. *Canadian Geotechnical Journal*, 46(10):1177–1201, 2009.

[191] S Krisnanto, H Rahardjo, DG Fredlund, and EC Leong. Mapping of cracked soils and lateral water flow characteristics through a network of cracks. *Engineering Geology*, 172:12–25, 2014.

[192] Ryan D Stewart and MRA Najm. Field measurements of soil cracks. *Soil Science Society of America Journal*, 84(5):1462–1476, 2020.

[193] JM Zhang, Y Luo, Z Zhou, L Chong, C Victor, and YF Zhang. Effects of preferential flow induced by desiccation cracks on slope stability. *Engineering Geology*, 288:106164, 2021.

[194] Y Luo, J Zhang, Z Zhou, JP Aguilar-Lopez, R Greco, and TA Bogaard. Effects of dynamic changes of desiccation cracks on preferential flow: experimental investigation and numerical modeling. *Hydrology and Earth System Sciences*, 27(3):783–808, 2023.

[195] CS Tang, C Zhu, Q Cheng, H Zeng, JJ Xu, BG Tian, and B Shi. Desiccation cracking of soils: A review of investigation approaches, underlying mechanisms, and influencing factors. *Earth-Science Reviews*, 216:103586, 2021.

[196] CS Tang, B Shi, C Liu, L Gao, and HI Inyang. Experimental investigation of the desiccation cracking behavior of soil layers during drying. *Journal of Materials in Civil Engineering*, 23(6):873–878, 2011.

[197] DG Fredlund. *Soil mechanics for unsaturated soils*. New York USA: John Wiley & Sons Inc, 1993.

[198] E Safari, MJ Ghazizade, MA Abduli, and B Gatmiri. Variation of crack intensity factor in three compacted clay liners exposed to annual cycle of atmospheric conditions with and without geotextile cover. *Waste Management*, 34(8):1408–1415, 2014.

[199] RJ Hardy, PD Bates, and MG Anderson. The importance of spatial resolution in hydraulic models for floodplain environments. *Journal of Hydrology*, 216(1-2):124–136, 1999.

[200] AS Cotter, I Chaubey, TA Costello, TS Soerens, and MA Nelson. Water quality model output uncertainty as affected by spatial resolution of input data 1. *JAWRA Journal of the American Water Resources Association*, 39(4):977–986, 2003.

[201] Y Mualem. Anisotropy of unsaturated soils. *Soil Science Society of America Journal*, 48(3):505–509, 1984.

[202] S Assouline and D Or. Anisotropy factor of saturated and unsaturated soils. *Water resources research*, 42(12), 2006.

[203] CT Petersen, A Trautner, and S Hansen. Spatio-temporal variation of anisotropy of saturated hydraulic conductivity in a tilled sandy loam soil. *Soil and Tillage Research*, 100(1-2):108–113, 2008.

[204] V Bagarello, S Sferlazza, and A Sgroi. Testing laboratory methods to determine the anisotropy of saturated hydraulic conductivity in a sandy–loam soil. *Geoderma*, 154(1-2):52–58, 2009.

[205] ES Brooks. *Distributed hydrologic modeling of the eastern Palouse*. PhD thesis, University of Idaho, 2003.

[206] ES Brooks, J Boll, and PA McDaniel. Distributed and integrated response of a geographic information system-based hydrologic model in the eastern Palouse region, Idaho. *Hydrological Processes: An International Journal*, 21(1):110–122, 2007.

[207] GE Liston and M Sturm. A snow-transport model for complex terrain. *Journal of Glaciology*, 44(148):498–516, 1998.

[208] Q Cheng, CS Tang, H Zeng, C Zhu, N An, and B Shi. Effects of microstructure on desiccation cracking of a compacted soil. *Engineering Geology*, 265:105418, 2020.

[209] N Yesiller, CJ Miller, G Inci, and K Yaldo. Desiccation and cracking behavior of three compacted landfill liner soils. *Engineering Geology*, 57(1-2):105–121, 2000.

[210] JH Li, LM Zhang, and X Li. Soil-water characteristic curve and permeability function for unsaturated cracked soil. *Canadian Geotechnical Journal*, 48(7):1010–1031, 2011.

[211] JT Ritchie and DS Nesmith. Temperature and crop development. *Modeling Plant and Soil Systems*, 31:5–29, 1991.

[212] DL Trudgill, A Honek, D Li, and NM van Straalen. Thermal time–concepts and utility. *Annals of Applied Biology*, 146(1):1–14, 2005.

[213] E Guerra, F Ventura, and RL Snyder. Crop coefficients: A literature review. *Journal of Irrigation and Drainage Engineering*, 142(3):06015006, 2016.

[214] PM Driessen and NT Konijn. *Land-use systems analysis*. WAU and Interdisciplinary Research (INRES), 1992.

[215] J Doorenbos and AH Kassam. Yield response to water. *Irrigation and drainage paper*, 33:257, 1979.

[216] RG Allen, M Smith, LS Pereira, and A Perrier. An update for the calculation of reference evapotranspiration. *ICID bulletin*, 43(2):35–92, 1994.

[217] RA García-Gaines and S Frankenstein. USCS and the USDA soil classification system: Development of a mapping scheme, 2015. https://usace.contentdm.oclc.org/digital/api/collection/p266001coll1/id/3757/download.

[218] A Casagrande. Classification and identification of soils. *Transactions of the American Society of Civil Engineers*, 113(1):901–930, 1948.

[219] CE Kellogg. *Soil survey manual*. Number 274. US Department of Agriculture, 1937.

[220] C Ditzler, K Scheffe, and HC Monger. Soil survey manual. 2017.

[221] Y Mualem. A new model for predicting the hydraulic conductivity of unsaturated porous media. *Water Resources Research*, 12(3):513–522, 1976.

[222] H Trabelsi, M Chebbi, H Guiras, M Jamei, and EE Romero Morales. Stabilization of clayey soil using fibre reinforcement. In *Unsaturated Soils: UNSAT 2018: The 7th International Conference on Unsaturated Soils*, pages 545–550. The Hong Kong University of Science and Technology (HKUST), 2018.

[223] IW Wardhana, MA Budihardjo, T Istirokhatun, and N Ikhlas. Desiccation cracks behaviour of leachate in bentonite-zeolite composite liner. In *IOP Conference Series: Earth and Environmental Science*, volume 894, page 012043. IOP Publishing, 2021.

[224] JM Schoorl, MPW Sonneveld, and A Veldkamp. Three-dimensional landscape process modelling: the effect of dem resolution. *Earth Surface Processes and Landforms: The Journal of the British Geomorphological Research Group*, 25(9):1025–1034, 2000.

[225] P Tarolli and G Dalla Fontana. Hillslope-to-valley transition morphology: New opportunities from high resolution DTMs. *Geomorphology*, 113(1-2):47–56, 2009.

[226] HJ Tromp-van Meerveld and JJ McDonnell. On the interrelations between topography, soil depth, soil moisture, transpiration rates and species distribution at the hillslope scale. *Advances in Water Resources*, 29(2):293–310, 2006.

[227] L Montrasio, R Valentino, and GL Losi. Towards a real-time susceptibility assessment of rainfall-induced shallow landslides on a regional

scale. *Natural Hazards and Earth System Sciences*, 11(7):1927–1947, 2011.

[228] N Lu and WJ Likos. Origin of cohesion and its dependence on saturation for granular media. In *Poromechanics V: Proceedings of the Fifth Biot Conference on Poromechanics*, pages 1669–1675, 2013.

[229] T Fawcett. An introduction to ROC analysis. *Pattern recognition letters*, 27(8):861–874, 2006.

[230] D Zizioli, C Meisina, R Valentino, and L Montrasio. Comparison between different approaches to modeling shallow landslide susceptibility: a case history in Oltrepo Pavese, Northern Italy. *Natural Hazards and Earth System Sciences*, 13(3):559–573, 2013.

[231] V Vakhshoori and M Zare. Is the ROC curve a reliable tool to compare the validity of landslide susceptibility maps? *Geomatics, Natural Hazards and Risk*, 9(1):249–266, 2018.

[232] I Cantarino, MA Carrion, F Goerlich, and V Martinez Ibañez. A ROC analysis-based classification method for landslide susceptibility maps. *Landslides*, 16:265–282, 2019.

[233] PV Gorsevski, PE Gessler, RB Foltz, and WJ Elliot. Spatial prediction of landslide hazard using logistic regression and ROC analysis. *Transactions in GIS*, 10(3):395–415, 2006.

La borsa di dottorato è stata cofinanziata con risorse del
Programma Operativo Nazionale Ricerca e Innovazione 2014-2020, risorse FSE REACT-EU
Azione IV.4 “Dottorati e contratti di ricerca su tematiche dell’innovazione”
e Azione IV.5 “Dottorati su tematiche Green”